

DETERMINATION OF THE SENSE OF SHEAR USING THE ORIENTATION OF SHEAR BAND FOLIATION IN MYLONITES: FIELD EVIDENCE FROM THE KEBAN COMPLEX, EASTERN TURKEY

Gültekin SAVCI*

ABSTRACT. — The structural features of the northern part of the Bitlis suture zone of the Alpine-Himalayan orogenic belt (Turkey) show intense internal deformations. The variable lithology and microstructural features of the high strain zones commonly found in the Keban complex are characterized by mylonitic texture. The Keban complex were formed in ancient continental margin sedimentary sequences of the northern branch of the Neo-Tethys. Single sets of shear band foliations occur within mylonite zones composed of strongly foliated phyllitic psammites. Two well defined microscopic criteria, the tails of the augen structures and smaller scale shear zones which were formed between the relatively undeformed pod shaped aggregates, are used to deduce the sense of shear in a lithologically inhomogeneous brittle-ductile shear zone of the Keban complex. The sense of shear determined in this way from the anastomosing part of the shear zone is then applied to the orientation of shear band foliation in the same shear zone. This microscopic evaluation of the structures suggests that the acute angle between the shear band foliation and the mylonitic foliation points in the shear direction as proposed by earlier research which were based on experimental studies. Therefore, the determination of sense the of shearing in the field using the orientation of shear band foliations in mylonites is suggested.

INTRODUCTION

The importance of shear band structures has become increasingly recognized in recent studies of ductile shear zones (e.g. Cobbold, 1977a, b; Platt and Vissers, 1980; White et al., 1980; Simpson and Schmid, 1983). Shear band foliation is a microstructure commonly found in mylonites. It is a small scale open crenulation cleavage and occurs at a low angle (typically less than 45°) to the enveloping surface of the older foliation (mylonitic foliation) defined by the average grain shape fabric (Fig. 1) (Platt, 1979; Platt and Vissers, 1980; White, 1979; White et al., 1980; Gapais and White, 1982). Shear band foliation has been intensively studied in pelitic mylonites (phyllonites) (Sibson, 1977; Bell, 1978; Platt, 1979; White, 1979; White et al., 1980), in phyllites (Platt and Vissers, 1980), in quartz mylonite (Berthe et al., 1979b; Gapais and White, 1982), and in quartz-feldspathic mylonite (Gapais, 1979; Simpson, 1984), within the past few years. White (1979) discusses field and microstructural observations of shear band foliations in the light of experimental studies on high strain deformation of metals and concludes that the foliation resembles shear bands which form during the high strain deformation of metals, particularly during rolling.

The spacing between bands is observed to be about 280 μm by Gapais and White (1982) for quartz mylonite from the Hercynian belt of Brittany in France. They measured the width of the bands at about 600 μm Platt and Vissers (1980) measured the spacing between bands from 2 cm to 20 cm for phyllitic mylonite from the Vanoise massif in the French Penninic Alps. According to Berthe et al. (1979a,b), White (1979), Platt and Vissers (1980), White et al. (1980), and Gapais and White (1982), shear bands develop during the late stage of the same deformation that produced the mylonitic foliation. Shear bands are believed to develop at relatively low temperatures when the rock no longer is capable of homogeneously accommodating the bulk deformation at the imposed strain rate, so that the bulk deformation is accommodated by deformation in the shear bands (Gapais

and White, 1982, p. 13), an explanation similar to that given by other researchers (e.g. Berthe et al., 1979a,b; Platt, 1979; White, 1979; Platt and Vissers, 1980; White et al., 1980; Passchier, 1982; Simpson, 1984).

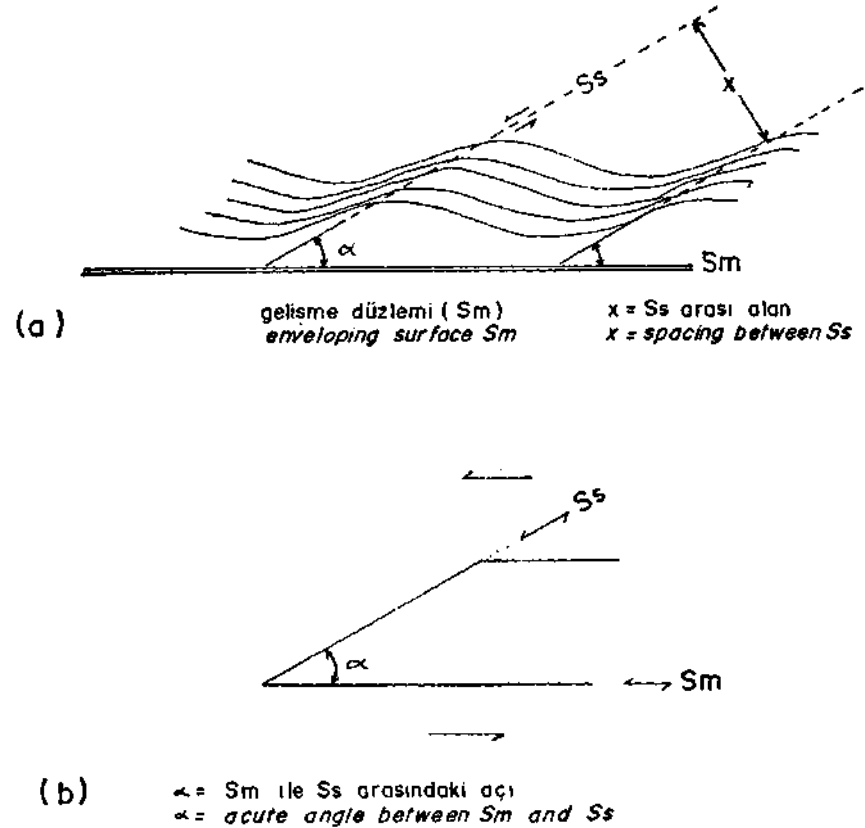


Fig. 1 - a - Geometry of shear band foliation (modified after Platt and Vissers, 1980, fig. 9); b - The acute angle between shear band foliation (S_s) and mylonitic foliation (S_m) points in the shear direction (data compiled from White et al., 1980; Simpson and Schmid, 1983).

Platt (1979), Platt and Vissers (1980), and Passchier (1982) referred to shear band foliation found in mylonites as «extensional crenulation cleavage». Platt and Vissers (1980, p. 397) described extensional crenulation cleavage as «sets of small scale ductile shear bands along the limbs of very open microfolds in the foliation. The sense of movement on the shear bands is such as to cause a component of extension along the older foliation».

Usually two sets of shear bands may develop at a low angle (less than 45°) to the mylonitic foliation (Platt and Vissers, 1980; White et al., 1980). In the light of experimental studies White et al. (1980, p. 178 and 186) proposed that if only one set of shear bands is formed in a mylonitic rock, the acute angle between the shear band foliation and the mylonitic foliation always points in the shear direction. Similar results were obtained by Simpson and Schmid (1983). Platt and Vissers (1980, p. 407-410) invoke that two sets of shear band foliations may form as a consequence of symmetric

coaxial progressive deformation. They also note that a single set of shear bands probably develops as a result of asymmetric coaxial or noncoaxial progressive deformations.

Let us consider a small square of mylonitic rock with a mylonitic foliation undergoing a coaxial progressive deformation where the principal directions of the incremental strain are parallel to the principal directions of the total strain at each instant during the progressive deformation (Fig. 2a and b). In progressive deformation, the principal incremental strain and the total strain are defined by principal stretches (i.e. S^I : principal directions of incremental stretch, S^T : principal directions of total stretch) (Means, 1976, p. 226). In the case of symmetric coaxial progressive deformation, where the direction of maximum incremental stretch (S_1^I) and the direction of maximum total stretch (S_1^T) are both parallel to the mylonitic foliation at each instant, two conjugate sets of shear bands may initiate at a low angle (45° or less) to the pre-existing mylonitic foliation (Fig. 2a), as stated by Platt and Vissers (1980). At each instant during a coaxial progressive deformation the axes of the incremental and total strain ellipses (or ellipsoids) correspond to each other (Figs. 2a and b). This suggests that during the symmetric coaxial progressive deformation both sets of the shear bands will rotate toward the direction of maximum principal stretches (S_1^I and S_1^T) and the mylonitic foliation (S_m) with same rate, and they will remain active throughout this progressive deformation history. Platt and Vissers (1980, p. 407) assert that «simultaneous activity of both sets will be difficult: they will probably have to alternate, or operate on different scales».

During an asymmetric coaxial progressive deformation where the direction of maximum incremental stretch (S_1^I) and the direction of maximum total stretch (S_1^T) are both oblique to the mylonitic foliation (S_m), two sets of shear bands asymmetric with respect to the mylonitic foliation may form (Platt and Vissers, 1980) (Fig. 2b). In Fig. 2b, the acute angle between the first set of the shear bands and the mylonitic foliation is greater than the acute angle between the second set and the mylonitic foliation. With the coaxial progressive deformation, these shear band foliations will rotate toward the direction of maximum principal stretches (S_1^I and S_1^T) with same rate. The acute angle between shear bands (both 1 and 2 in Fig. 2b) and the mylonitic foliation decreases with the rotation. The second set becomes parallel to the mylonitic foliation first. At this instant, the second set may probably become inactive, because it requires a reverse slip direction on the mylonitic foliation (Fig. 2b) (Platt and Vissers, 1980). The first set of the shear bands therefore remains active as a single set of shear bands.

An example of a noncoaxial progressive deformation where the principal directions of the incremental stretch (S^I) are not parallel to the principal directions of the total stretch (S^T) at any instant during the progressive deformation is shown in Fig. 2c. At each instant during the noncoaxial progressive deformation the axes of the incremental and total strain ellipses (or ellipsoids) do not correspond to one another. Therefore at each instant during the noncoaxial progressive deformation the two conjugate sets of shear bands will rotate toward the direction of maximum incremental stretch (S_1^I) with different rates. In this case, simple shearing is assumed to be parallel to the S_m combined with flattening parallel to S_3^I (Fig. 2c). The second set of the shear bands shown in Fig. 2c will rotate with a greater rate than the first one. The second shear band that rotates faster will become inactive when it reaches the point where it is nearly parallel to the mylonitic foliation. The first set becomes dominant and remains active (Platt and Vissers, 1980) in the same sense of shear direction implied for the whole rock body undergoing the progressive deformation.

While the above review focuses mostly on the shear band foliation developed in pelitic, quartzitic, and quartzofeldspathic mylonites, this paper is concerned with a detailed description of shear band structures within phyllitic psammities and calcareous mylonites within a 15 m wide brittle-ductile shear zone in the Keban metamorphic complex of Eastern Turkey. This study shows field evidence to determine the sense of shear using the orientation of shear band foliation in high strain rocks. The results of microstructural studies on shear band foliation are compared with the interpretation of White et al. (1980) and Simpson and Schmid (1983) for deducing the sense of shear in high strain rocks displaying one set of shear band foliation.

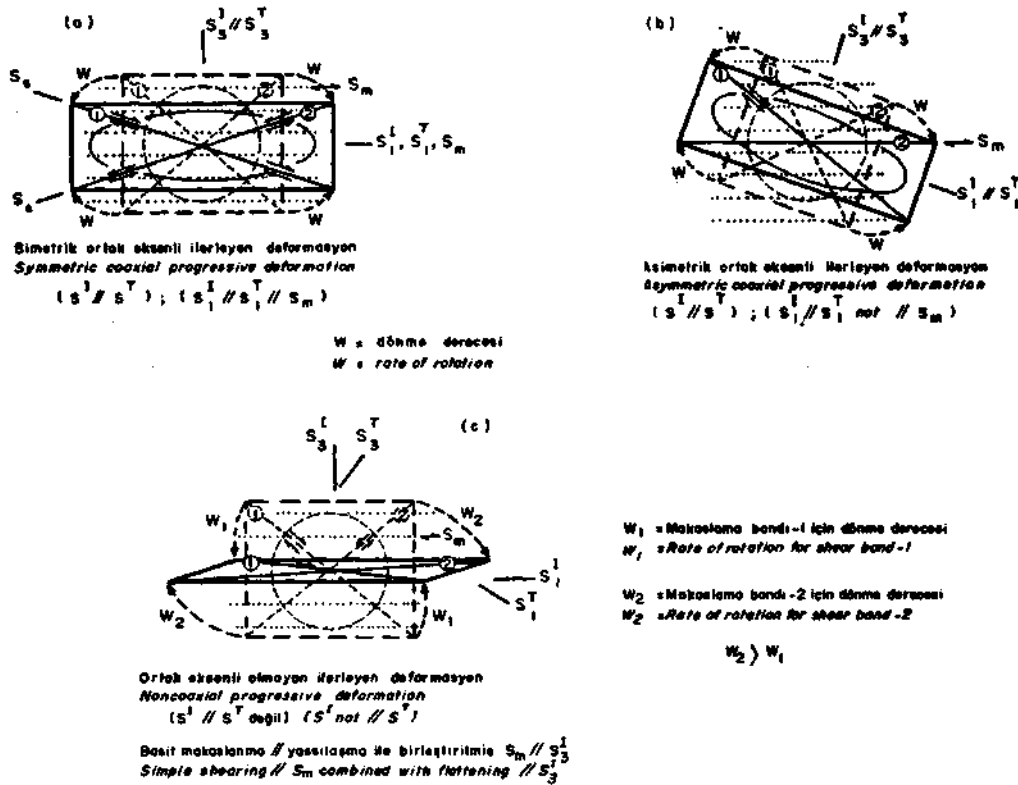


Fig. 2 - Shear band development.

a - Symmetric coaxial progressive deformation where the direction of S_1^I , the direction of S_1^T , and S_m are all parallel to one another; b - Asymmetric coaxial progressive deformation where S_1^I and S_1^T are parallel to each other in each instant but oblique to S_m . S_m is assumed to be a passive marker during the formation of S_s ; c - Noncoaxial progressive deformation where the S_1^I , S_1^T , and S_m are all oblique to one another. S_1^I - Direction of maximum incremental stretch; S_1^T - Direction of maximum total stretch; S_3^I - Direction of minimum incremental stretch; S_3^T - Direction of minimum total stretch; S_m - Mylonitic foliation; S_s - Shear band foliation (see text for discussion) (cf. Platt and Vissers (1980, Fig. 11) and White (1979, Fig. 2)).

GEOLOGICAL OUTLINE OF THE KEBAN METAMORPHIC COMPLEX

The Keban metamorphics are complexly deformed, and form the most northerly structural slice within the Bitlis suture zone of the Alpine-Himalayan orogenic belt in Eastern Turkey (Fig. 3). They are tectonically intercalated between the Mesozoic Munzur limestone and the Maastrichtian ophiolites of the Ovacik unit (Özgül et al., 1978) in the north, and the Campanian-Maastrichtian Elazığ volcanic island arc complex (Hempton and Savcı, 1982) in the south (Fig. 3a). Three main lithological units are distinguished in the Keban metamorphic complex. They are marble, phyllitic psammite and limestone units. The contacts between these units are all folded thrusts (Fig. 3b) or brittle-ductile shear zones in the sense of Ramsay (1980).

The marble unit is composed of calcite crystals which comprise 95-98 % of the rock. In between the calcite crystals, there are some muscovite (1-2 %) and epidote (2-3 %) crystals. The marble unit also locally shows 1 to 50 m thick amphibolite interlayers around the Pertek area (Perinfeke, 1979).

The phyllitic psammites are pervasively interlayered with calcschist layers which range from 1 cm to 20 cm in thickness. The phyllitic psammite is a dark gray, fine grained rock consisting of 75-80 % quartz, 10-15 % muscovite-sericite, 5 % iron-oxide, 4 % chlorite, 4 % calcite, 2 % epidote, and very rare graphite and plagioclase. The calcschist interlayers are composed of 40-45 % calcite, 25-30 % quartz, 10-15 % muscovite-sericite, 10 % iron-oxide, 5 % chlorite, and very rare plagioclase feldspars. The structurally highest metamorphic unit consists of limestones with a mineral composition: 85-95 % calcite, 2-5 % iron-oxide, 3 % quartz, 2 % plagioclase, 2-3 % epidote, and very rare muscovite.

These ancient continental margin sedimentary sequences were formed between Palaeozoic (?) and the Triassic times (Kipman, 1981), and experienced low grade greenschist metamorphism during the Jurassic to the Lower Cretaceous (Savcı, 1983). They are cut by hypabyssal syenite porphyries intruded during the late Cretaceous (Savcı, 1983). In the Keban metamorphics, at least two phases of penetrative deformation are documented. There is also evidence for one nonpenetrative deformation. For more detailed description of the geological setting and tectogenic history of the Keban metamorphic complex, the reader is referred to Savcı (1983).

MINERALOGY AND MICROSTRUCTURES OF SELECTED MYLONITES

The descriptions of fault rocks given below are from ductile deformational parts of the brittle-ductile shear zone. Figure 4 is a schematic map and cross sectional view of this northeast trending and southeast dipping brittle-ductile shear zone which contains a number of lithologies (i.e. phyllitic psammite, calcschist, and limestone).

The mylonitic body formed in the brittle-ductile shear zone (Fig. 4) shows a progressive change in its texture within 15m from northwest to southeast across the zone. To the northwest, the mylonitic rocks become much finer grained. The stage in this development of the sequence is shown in Figs. 4, 5, and 7.

The first example to be described is a highly strained calcschists of the Keban metamorphic complex. They are composed of 40-50 % quartz, 20 % muscovite-sericite-chlorite, and 20-30 % calcite. Calcite usually occurs in the form of pod shaped aggregates up to 1.5 cm. The sheared, foliated calcite-quartz-mica-chlorite rich material surrounding the remnant unshaped calcite pods define an anastomosing shear zone (Figs. 4b and 5) in the sense of Simpson (1983). The average preferred

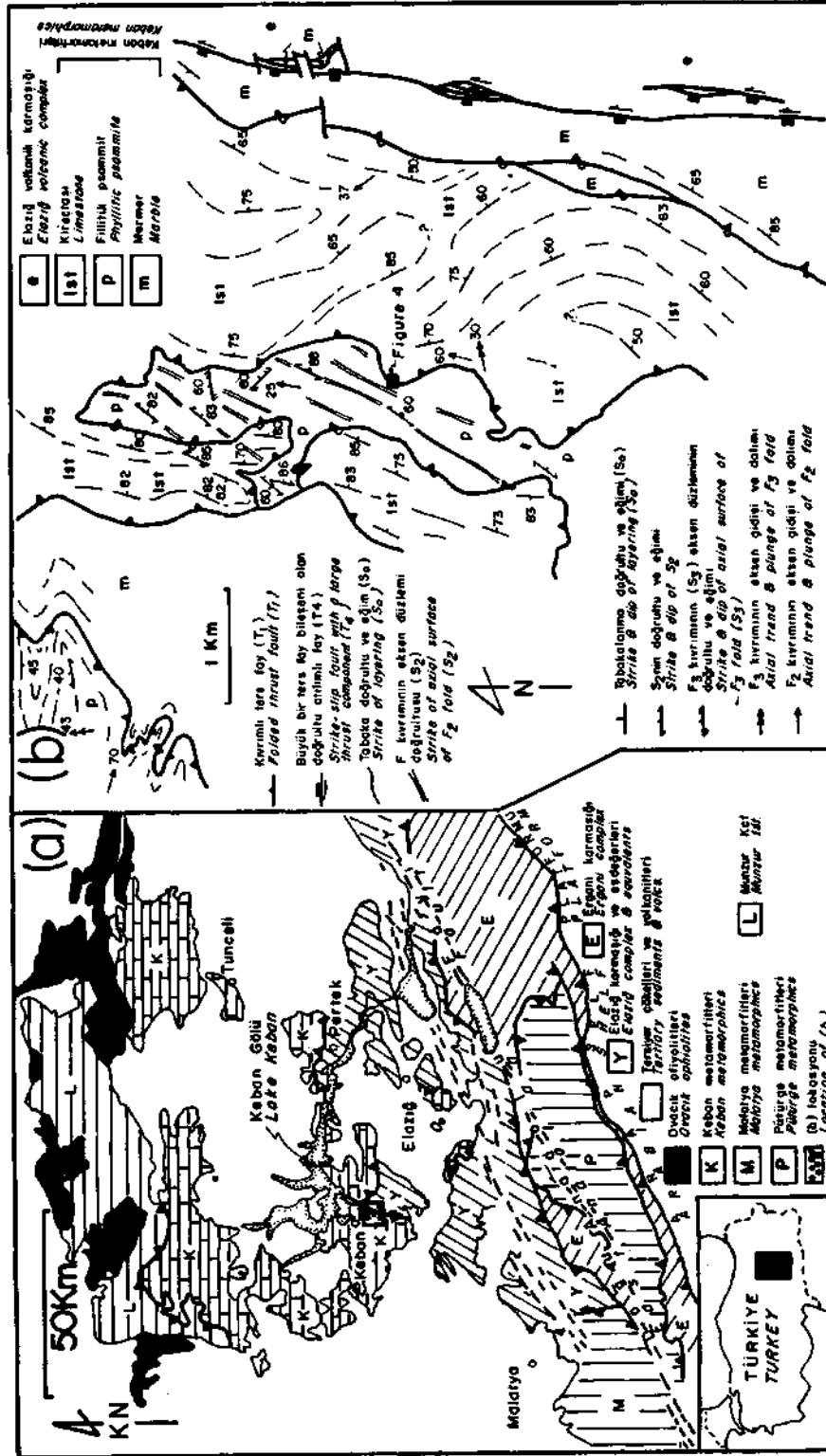


Fig. 3 a - Simplified geological map and tectonic setting of the Elazığ area, Eastern Turkey. In conjunction with the author's own observations, the map is compiled and somewhat reinterpreted from MTA (1961 a,b), Perinçek (1979), and Şengür and Yılmaz (1981); b - Simplified form surface and tectonic map of the Keban metamorphic complex, near Keban.

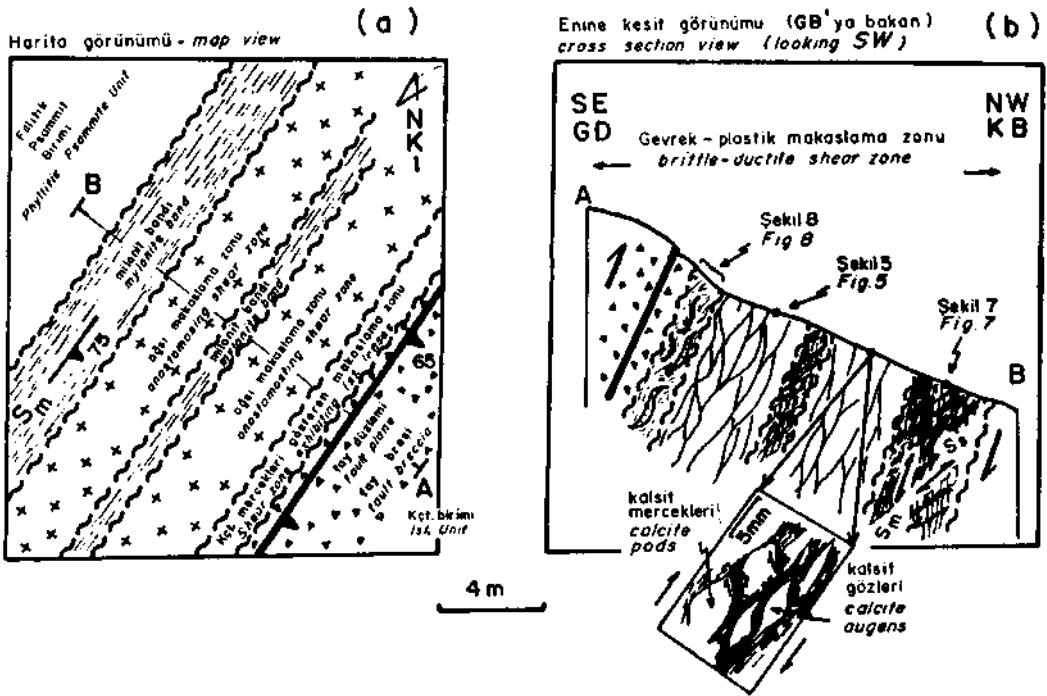


Fig. 4 - A schematic map (a) and cross section view (b) of the brittle-ductile shear zone studied.

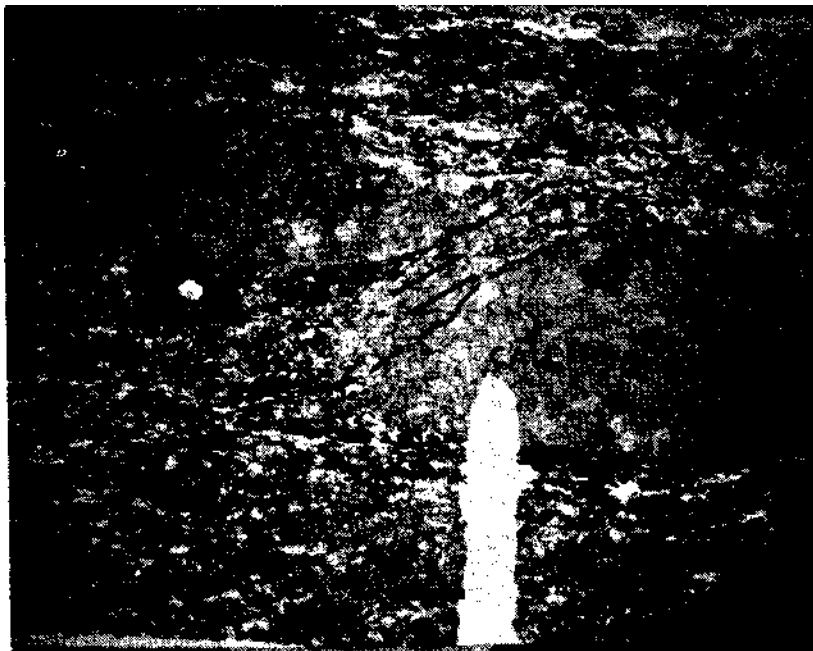


Fig. 5 - Photomicrograph of relatively unshaped calcite pods surrounded by strongly foliated ductile matrix (calcite-quartz-mica-chlorite) (polarized light; section perpendicular to the intermediate strain axis) (cf. Fig. 6b).

dimensional orientation of quartz, muscovite, sericite, and chlorite grains defines a mylonitic foliation. Simpson and Schmid (1983, p. 1282-1283) show that if the tails of the retort-shaped grains (augen) are comprised of fine grained material of the same composition as the augen material, they can then be used to deduce the shear direction. They demonstrate that these tails extend along the foliation plane in the shear direction (Fig. 6a). In this anastomosing shear zone, the tails of the calcite augen are composed of much finer grained calcite crystals. Moreover, between the calcite pods, smaller scale shear zones often occur at a low angle (30° to 35°) to the major shear zone defined by mylonitic foliation which surrounds the calcite pods and augens. As is shown in Fig. 5, the sense of displacement in this small scale shear zone between the calcite pods is southeast-over-northwest. Simpson (1983, p. 63) shows that in an anastomosing shear zone the small shear zones between the relatively undeformed pods have the same sense of displacement as that of the major shear zones surrounding the pods (Fig. 6b). Using the criteria indicated above, i.e., asymmetry of augen structures (Fig. 6a) and shear direction in small shear zones formed between relatively undeformed pods (Fig. 6b), the sense of shearing is also determined as southeast-over-northwest (Fig. 5).

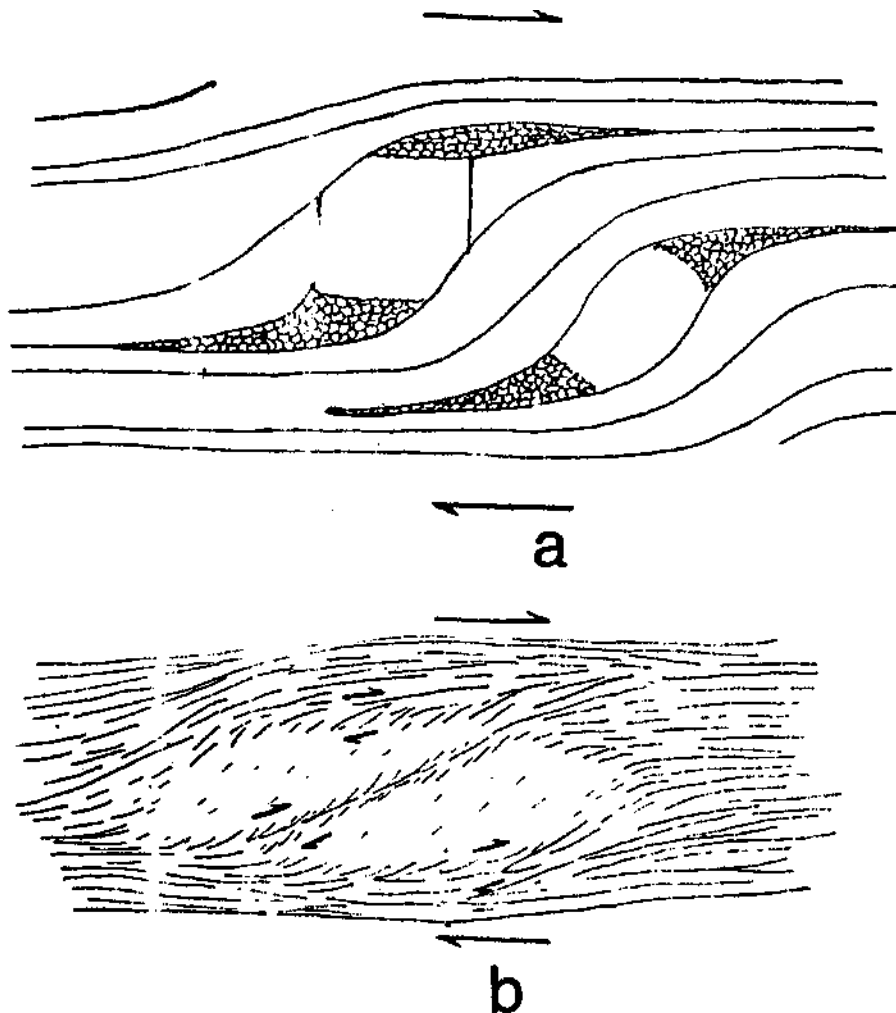


Fig. 6 a - The tails of the retort-shaped augens extend along the foliation plane in the shear direction (after Simpson and Schmid, 1983, Fig. 4); b - Small ductile shear zone between relatively undeformed pod-shaped aggregates has same sense of displacement as the major shear zones which surround the pods (after Simpson, 1983, Fig. 2a).

The second example to be described is a phyllitic psammite mylonite of the Keban metamorphic complex. It is composed of 75-85 % quartz, 10-15 % muscovite-sericite-chlorite, 5 % feldspar, 1-5 % iron-oxide, and about 1 % epidote. In these strongly foliated mylonites, the preferred dimensional orientation of quartz, feldspar, muscovite, sericite, and epidote grains or aggregates define a well developed mylonitic foliation (S_m) (Fig. 7). As readily observed in Fig. 7, this rock also shows a shear band foliation (S_s) which is about 30° oblique with respect to the mylonitic foliation. Generally, shear band foliation is defined by the preferred mineral elongation of micas. Where affected by a shear band, the mylonitic foliation trends into parallelism with the shear band boundary (Fig. 7). The spacing between bands varies from 100 to 780 μm . The width of the bands is usually 10 to 170 μm . As is mentioned in the introduction, according to White et al. (1980) and Simpson and Schmid (1983) the angular relationships between the shear band foliation (S_s) and the mylonitic foliation (S_m) define the sense of shear (Fig. 1b). Using this criterion, the direction of shearing in this mylonite determined as southeast-over-northwest as well (Fig. 7).

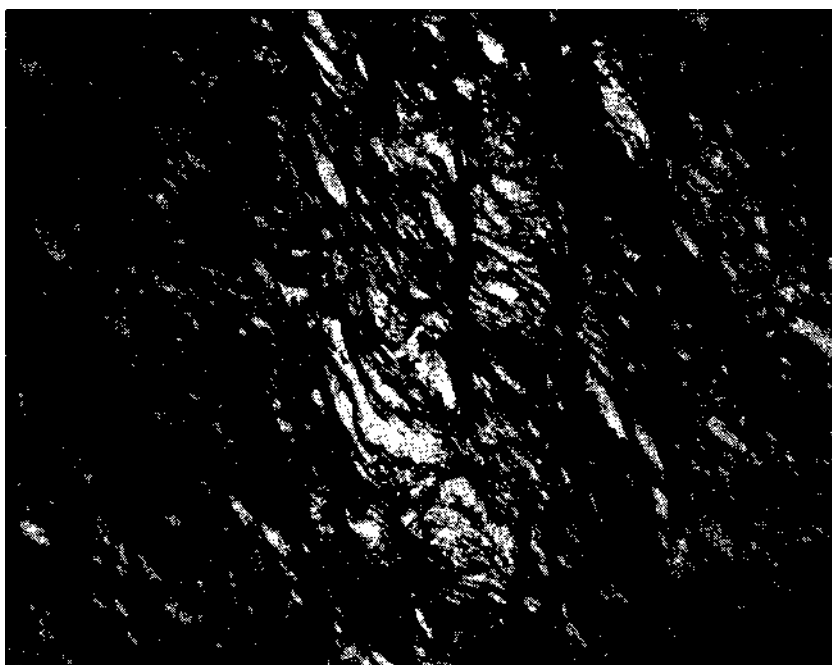


Fig. 7 - Photomicrograph of shear band structure within the phyllitic psammite - mylonite studied (polarized light; section perpendicular to the intermediate strain axis). Shear band foliation (S_s) is defined by the vertical dark zones. Within these zones mylonitic foliation (S_m) has been reoriented. White grains are mostly quartz. Dark fine-grained material is mica and chlorite. The average angle between S_m and S_s is 30° and the spacing between bands is up to 500 μm . Shear sense is southeast-over-northwest.

From the foregoing, it is concluded that the «sense of shear» observations at the microscopic scale (i.e., asymmetry of augen structures (Fig. 6a) and shear direction in small shear zones formed between relatively undeformed pods (Fig. 5)) corroborate the similar observation and conclusions based on the position of shear bands with respect to mylonitic foliation (Fig. 7). Therefore, the above result based on a field evidence is consistent with shear band interpretation of White et al. (1980) and Simpson and Schmid (1983).

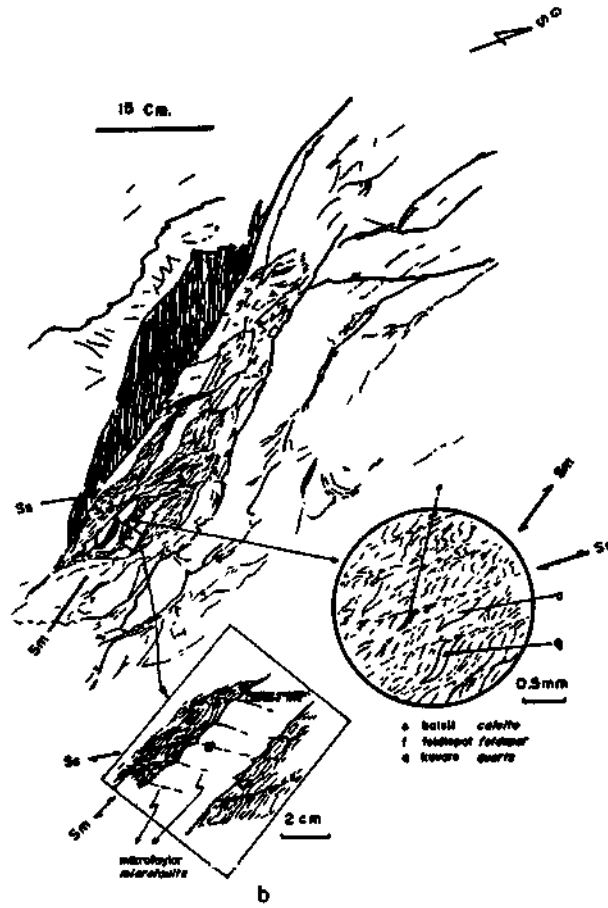
The third example studied consists of a limestone-calcschist unit within the same brittle ductile shear zone (Fig. 4). This part of the shear zone, which is about one meter thick, is characterized by limestone lenses and quartz-mica rich calcschist layers between these lenses. At an outcrop scale, mylonitic foliation is defined by long axes of relatively unshaped limestone lenses which are up to 20 cm long and 2 to 5 cm wide; by grain shapes of calcite, quartz and feldspar, and by elongation of muscovite crystals which formed between the limestone lenses in zones 1 to 4 cm thick (Fig. 8). The thin mylonitic zones are composed of 35 % quartz, 25-35 % calcite, 5-7 % feldspar and 20 % muscovite-sericite-chlorite. In these thin, strongly foliated zones, there are some small scale open crenulation cleavages occurring at a low angle (35°) to the enveloping surface of the mylonitic foliation (Fig. 8). Where affected by these open crenulation cleavages, the mylonitic foliation trends into parallelism with these crenulation boundaries. Spacing between the crenulation cleavage surfaces varies between 500 and 850 μm . These open crenulation cleavages have similar characteristics to those shown in Fig. 7 and are interpreted as shear band foliation due to their resemblance to similar features described by White (1979), White et al. (1980), and Gapais and White (1982). Based on the angular relationships between the shear band foliation and the mylonitic foliation (Fig. 1b) the sense of movement determined in this way is also southeast-over-northwest (Fig. 8). Moreover, where affected by shear bands, tips of the limestone lenses curve and trend into parallelism with shear band boundaries (Fig. 8). In the main body of limestone lenses, microfaults cut across the lenses at a high angle (58°) to the mylonitic foliation. These microfaults occur only in the limestone lenses. The sense of displacement for microfaults formed in the limestone lenses is in the same sense as the shear band foliations developed between the lenses (Fig. 8). The shear band structures are interpreted in the same way as Gapais and White (1982) in that at the same high strain-rate, the deformational mechanism was brittle in the limestone lenses and more ductile in the quartz-mica rich zones. These quartz-mica rich zones consist of strongly foliated, thin ductile shear zones between relatively little deformed limestone lenses. Therefore, the two rock types with different physical properties have quite different behavioral responses to the deformation. Brittle and ductile deformations may occur in close proximity within the same shear zone at the same time. It is concluded that when the bulk deformation cannot be accommodated by the dominant deformation process at the imposed strain rate, it is accommodated by deformation in the form of ductile shear bands in the quartz-mica rich calcschist and by deformation in the form of brittle microfaults in the limestone lenses.

CONCLUSIONS

Two well defined microscopic criteria are used to deduce the sense of shear in a lithologically inhomogeneous brittle-ductile shear zone of the Keban metamorphic complex. They are: (1) The tails of the asymmetric augen structures which extend along the foliation plane, and allow the sense of shear to be determined (Fig. 6a, Simpson and Schmid, 1983); (2) In anastomosing shear zones, the sense of shear determined in a smaller scale shear zones which were formed between the relatively undeformed pod shaped aggregates is in the same direction with the major shear zone surrounding these aggregates (Fig. 6b, Simpson, 1983). In the ductile mylonite bands found in the same shear zone (Fig. 4), the acute angle between the shear band foliation and the mylonitic foliation points in the same shear direction determined for the anastomosing shear zone showing asymmetric augen structures and relatively unshaped calcite pods (Fig. 5). This result is consistent with the sense of shearing interpretation of White et al. (1980) and Simpson and Schmid (1983) for high-strain mylonites exhibiting a single set of ductile shear band foliations. The Keban mylonites with a single set of shear band foliation may have been formed during a noncoaxial progressive deformation.



Fig. 8 a - A shear zone showing brittle deformational features (microfaults) in limestone lenses, and ductile deformational features (mylonitic foliation (S_m) and shear band foliation (S_s)) in the more ductile quartz-mica rich strongly foliated thin zones formed between the limestone lenses (cross section view).



Şek. 8b - A sketch drawn from Fig. 8a.

ACKNOWLEDGEMENTS

I am very grateful to J.F. Casey, W.D. Means, A.M.C. Şengör and W.S. Kidd for many useful comments on earlier drafts of this paper. For his encouragement and support J. Butler deserves a special mention. Field study was supported by Turkish Petroleum Company and grants from NSF EAR-7910729 and NASA NAG-524.

Manuscript received June 6, 1985

REFERENCES

- Bell, T.H., 1978, Progressive deformation and reorientation of fold axes in a ductile mylonite zone: The Woodroffe Thrust: *Tectonophysics* 44, 285-320.

- Berthe, D.; Choukroune, P. and Jegouzo, P., 1979 a, Orthogneiss, mylonite and noncoaxial deformation of granites: the example of the South Armorican shear zone: *J. Struct. Geol.*, 1, 31-42.
- ; ——— and Gapais, D., 1979 b, Orientations preferentielles du quartz et orthogneissification progressive en regime cisaillant: l' exemple du cisaillement subarmoricain: *Bull. Mineral.*, 102, 265-272.
- Cobbold, P.R., 1977 a, Description and origin of banded deformation structures. I., Regional strain, local perturbations, and deformation bands: *Can. J. Earth Sci.*, 14, 1721-1731.
- , 1977 b, Description and origin of banded deformation structures. II. Rheology and the growth of banded perturbations: *Can. J. Earth Sci.*, 14, 2510-2523.
- Gapais, D., 1979, Deformation progressive d'un quartzite dans une zone plisee (segment hercynien de Bretagne centrale): *Bull. Mineral.*, 102, 249-264.
- and White, S.H., 1982, Ductile shear bands in a naturally deformed quartzite: *Texture and Microstruct.*, 5, 1-17.
- Hempton, M.R. and Savcı, G., 1982, Elazığ volkanik karmaşığının petrolojik ve yapısal özellikleri: *Bull. Geol. Soc. Turkey.*, 25, 143-150.
- Kipman, E., 1981, Keban'ın jeolojisi ve Keban şaryajı: *İstanbul Yerbilimleri Mecm.*, 1, 75-81.
- MTA Genel Müdürlüğü, 1961 a, Geological map of Turkey, scale 1:500,000, Erzurum sheet: MTA Publ., Ankara-Turkey.
- , 1961 b, Geological map of Turkey, scale 1:500,000, Sivas sheet: MTA Publ., Ankara-Turkey.
- Means, W.D., 1976, *Stress and Strain*: Springer-Verlag, New York.
- Özgül, N.; Turşucu, A.; Özyardımcı, N.; Bingöl, İ.; Şenol, M. and Uysal, Ş., 1978, Munzurlar'ın temel jeoloji özellikleri: *Türkiye Jeol. Kur- 32. Bilimsel ve Teknik Kurultayı, Bildiri Özetleri*, 10-11.
- Passchier, C.W., 1982, Mylonitic deformation in the Saint-Barthelemy Massif, French Pyrenees, with emphasis on the genetic relationship between ultramylonite and pseudotachlyte: Ph. D. thesis, Univ. Amsterdam. *Gua Papers of Geology*, 1.
- Perinçek, D., 1979, Palu, Karabegan, Elazığ, Sivrice, Malatya alanının jeolojisi ve petrol imkanları: TPAO Rep. (unpublished), 1361, 1-33.
- Platt, J.P., 1979, Extensional crenulation cleavage: *J. Struct. Geol.*, 1, 95-96.
- and Vissers, R.L.M., 1980, Extensional structures in anisotropic rocks: *J. Struct. Geol.*, 2, 397-410.
- Ramsay, J.G., 1980, Shear zone geometry: a review: *J. Struct. Geol.*, 2, 83-99.
- Savcı, G., 1983, Structure and tectonics of the Keban Metamorphics in the northern margin of the Bitlis suture zone, SE Turkey: Unpublished M.S. thesis, S.U.N.Y. Albany.
- Şengör, A.M.C. and Yılmaz, Y., 1981, Tethyan evolution of Turkey: a plate tectonic approach.: *Tectonophysics*, 75, 181-241.
- Sibson, R.H., 1977, Fault rocks and fault mechanisms: *J. Geol. Soc. London*, 133, 191-213.
- Simpson, C., 1983, Strain and shape-fabric variations associated with ductile shear zones: *J. Struct. Geol.* 5, 61-72.
- , 1984, Borrego spring-Santa Rosa mylonite zone: a late Cretaceous west-directed thrust in southern California: *Geol.*, 12, 8-11.
- and Schmid, S.M., 1983, Some criteria to deduce the sense of movement in sheared rocks: *Bull. Geol. Soc. Am.*, 94, 1281-1288.

White, S.H., 1979, Large strain deformation: *J. Struct. Geol.*, 1, 333-339.

———; Burrows, S.E.; Carreras, J.; Shaw, N.D. and Humphreys, F.J., 1980, On mylonites in ductile shear zones: *J. Struct. Geol.*, 2, 175-187.

GEOLOGY OF THE SÖKE-SELÇUK-KUŞADASI REGION AND PETROCHEMICAL FEATURES OF THE VOLCANIC ROCKS

Tuncay ERCAN*; Umur AKAT*; Erdoğan GÜNAY** ve Yılmaz SAVAŞÇIN***

ABSTRACT.— The basement of the investigated area consists mainly of metamorphic rock units of the «coverschists» of the Menderes massive, namely Şenköy, Bafa formations and Bozdağ group with respective ages of Early-Medial Permian, Upper Permian-Lower Triassic and Middle Triassic-Upper Cretaceous. Zeytinköy formation, a flyschoid sequence of Upper Cretaceous age, overrides the basement by a tectonic contact. These are unconformably overlain by the continental Söke formation of Miocene age followed by Balatlık and Hisartepe volcanics. Quaternary is represented by colluvium and alluvium. Petrochemical work shows that the volcanics originated partly from the mantle, but mainly are of siallic origin. They are compared to other volcanic rocks of the region.

BIOSTRATIGRAPHY AND PALEONTOLOGY OF THE MEDİK-EBREME (NW MALATYA) AREA

Sefer ÖRÇEN*

ABSTRACT.— This paper deals with paleontology and biostratigraphy of the sedimentary rocks in the vicinity of Medik-Ebreme area located northwest of Malatya. The age of the formations of the area range from Upper Jurassic to the Quaternary. Horasançay formation, Upper Jurassic to Lower Cretaceous in age, consists essentially of micrites and dolomitic limestones deposited on the open shelf. The unconformably overlying Medik formation is represented by conglomerates with mudstone interbeds deposited in an alluvial fan of Paleocene age. The Medik formation is unconformably overlain by the Tohma formation, Middle-Upper Eocene in age, and consists of conglomerates, sandstones and alternations of limestones and marls deposited in lagoonal, beach and shallow marine (shelf) environments. Çavuş formation consisting of clastic limestones deposited on the shallow shelf, sits unconformably on the Tohma formation and is of Aquitanian age. This sequence is unconformably succeeded by the Ansurçay formation, Burdigalian in age, consisting mainly of clastic limestones, marls and reefal limestones. Mısırdere formation, consisting of conglomerates, sandstones and mudstones, was laid down in environments of alluvial fans and braided streams. The following biozones were defined on the basis of paleontologic data: the *Velates schmiedeli* biozone in Lower Lutetian; the *Nummulites pinfoldi* biozone in Middle Lutetian; the *Nummulites aturicus* biozone and *Nummulites perforatus* subbiozone in Upper Lutetian; the *Nummulites fabianii* biozone and *Chapmanina gassinensis* subbiozone in Lower Priabonian; the *Miogypsinoidea complanatus* biozone in Aquitanian; the *Miogypsina irregularis* biozone and *Miogypsina intermedia* biozone in Burdigalian. These biozones were matched, biostratigraphically and chronostratigraphically, with their equivalents in Turkey and in other parts of the world.

INTRODUCTION

Following an elaborate selection of the area (Fig. 1), this investigation was undertaken to solve the stratigraphic problems by means of a detailed examination of paleontologic data and understanding of biozonal relations to reach to a synthesis of paleogeography and ecology (Fig. 2).

The investigated area lies in Eastern Taurids, comprising 1:25 000 scaled map of «Malatya K 40 d₄ and K 39 c₃» covering an area of approximately 240 sq. kms.

The earliest detailed work was carried out by Ayan (1961) in the region. This work investigated the general geology and petroleum potential of the Hekimhan-Ebreme region, north of Malatya.

Akkuş (1971) carried out geologic investigations in the Darende-Balaban basin (ESE of Malatya) defining units of Mesozoic (Jurassic-Cretaceous, Upper Cretaceous) and Quaternary age. He also reports ophiolitic assemblages in addition to volcanism occurring prior to Lutetian and after Burdigalian.

Yoldaş (1972) carried out geologic investigations to understand the petroleum potential of the area north of Malatya. He studied the sedimentary rocks of Paleozoic, Mesozoic (Upper Jurassic-Lower Cretaceous, Maestrichtian) and Cenozoic (Ypresian, Lutetian, Oligocene, Lower Miocene, Upper Miocene and Quaternary) age and distinguished serpentinites and volcanic rocks consisting of trachyandesites, basalts and andesites.

Sirel (1976 a, b) defined the microfauna *Rhapydionina malatyaensis* n.sp., *Nummulites heheticus* (Kaufmann), *Fabiania cassis* (Opperheim), *Orbitolites* sp. in Lutetian rocks and *Nummulites*

fabianii (Prever), *Nummulites incrassatus* de la Harpe, *Chapmanina gassinensis* Silvestri on the overlying Bartonian rocks, sitting unconformably on Orbitoides and Siderolites bearing limestones (Maestrichtian) north of Darende (west of Malatya). The same author also defined *Nummulites aturicus* Joly and Leymerie, *Nummulites helveticus* (Kaufmann), *Fabiania cassis* (Oppenheim), *Gyroidinella magna* Le Calvez in Upper Lutetian limestones cropping out in the vicinity of Darende-Gürün; *Eoannularia conica* n.sp., *Eoannularia eocenica* Cole and Bermudez, *Chapmanina gassinensis* Silvestri, *Halkyardia minima* (Liebus) and benthonic microfauna in the upper sections including *Nummulites* cf. *fabianii* (Prever).

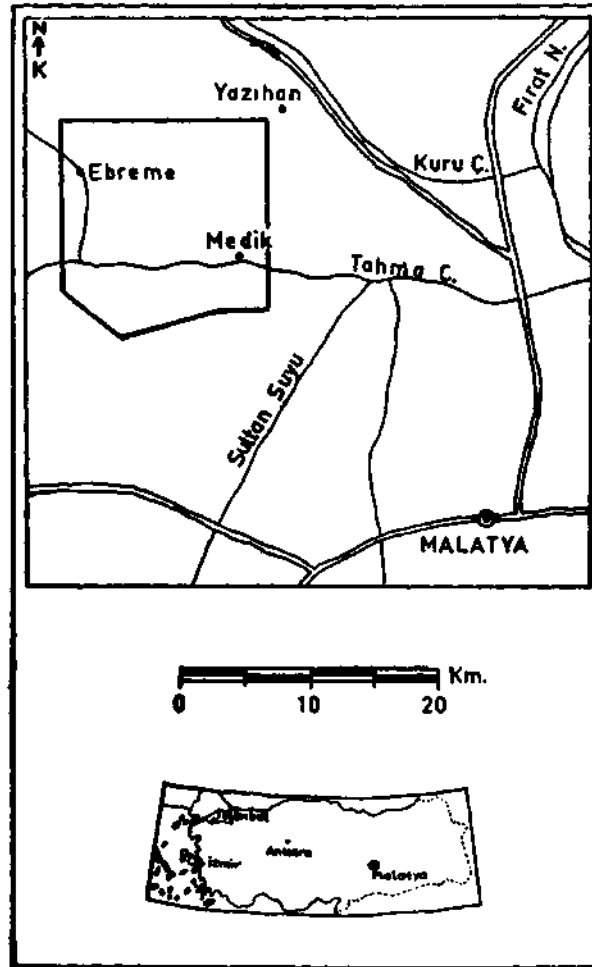


Fig. 1 - Location map of the investigated area.

Kurtman (1978) differentiated Permo-Carboniferous, Mesozoic (Jurassic-Cretaceous, Upper Cretaceous) and Cenozoic (Lutetian, Priabonian Neogene and Quaternary) units in the region in his work entitled «Geology and Tectonic Features of Gürün Region».

STRATIGRAPHY

The stratigraphy of the region is described in three sections entitled «lithostratigraphy, biostratigraphy and chronostratigraphy». Formations are nomenclated by the author except for the Horasançal fm. (Kurtman, 1978). Paleontologic data is controlled through an elaborate reconsideration of the biostratigraphy.

Lithostratigraphy

The investigated area composed of units of Upper Jurassic-Lower Cretaceous, Paleocene, Middle-Upper Eocene, Lower Miocene and Plio-Quaternary age. These units (lithostratigraphic), their stratigraphic setting and interrelations are shown in Figures 3 and 4.

Horasançal formation. — The type section crops out in the Ebreme and Saravlı creeks (Fig. 5). It consists of light gray, medium to thick bedded micrites in the lower and yellowish gray dolomitic limestones with chert interstratifications in the upper section. The lower boundary does not crop out. The upper boundary is unconformably covered by Medik and Tohma formations respectively in the southern parts of the investigated area and along Tohma valley. The thickness is 300 m.

The lower section of the micrites yields the characteristic fossils of *Valvulinella jurassica* Henson and *Clypeina jurassica* Favre (algae) indicating the age of Upper Jurassic. Dolomitic limestones comprising the upper section are unfossiliferous. Therefore, the age of the formation is considered as Upper Jurassic-Lower Cretaceous. The sedimentary features and the microfauna suggest an open shelf environment of deposition.

Medik formation. — The type locality lies approximately 2.5 km northwest of the Medik village. It consists of parallel or cross-bedded, medium to thick bedded, well-cemented, poorly sorted (angular to rounded pebbles derived from the Horasançal limestone and volcanoclastic units cropping out in the region), reddish-brown conglomerates alternating with red, thin, medium to thick bedded, parallel bedded mudstones. It sits on the Horasançal formation with an angular unconformity and is unconformably covered by the Tohma formation. Because of faulting and remaining somepart in the Medik dam, to find out exact thickness, was not possible. However, the thickness is estimated 1400 m (data obtained from the Akçadağ well of MTA).

The formation does not contain any fossils. It is considered to be Paleocene in age according to its stratigraphic setting and the pebble content. The sedimentologic parameters indicate an alluvial fan as the environment of deposition.

Tohma formation. — This formation can typically be observed along the road of Çivril village and around Çorak and Yoğunsakız districts (Figs. 6,7). The Tohma formation consists, from base to top;

- a. Zeynepoğlu member consisting of alternations of conglomerates, sandstones and mudstones,
- b. Yoğunsakız member consisting of conglomerates and sandstones followed by alternations of limestones and marls,
- c. Çorak member consisting of alternations of mudstones, sandstones and clayey limestones,
- d. Çivril member consisting of alternating marls and limestones,
- e. İriağaç member consisting of massive limestones with the lower section containing marl intercalations.

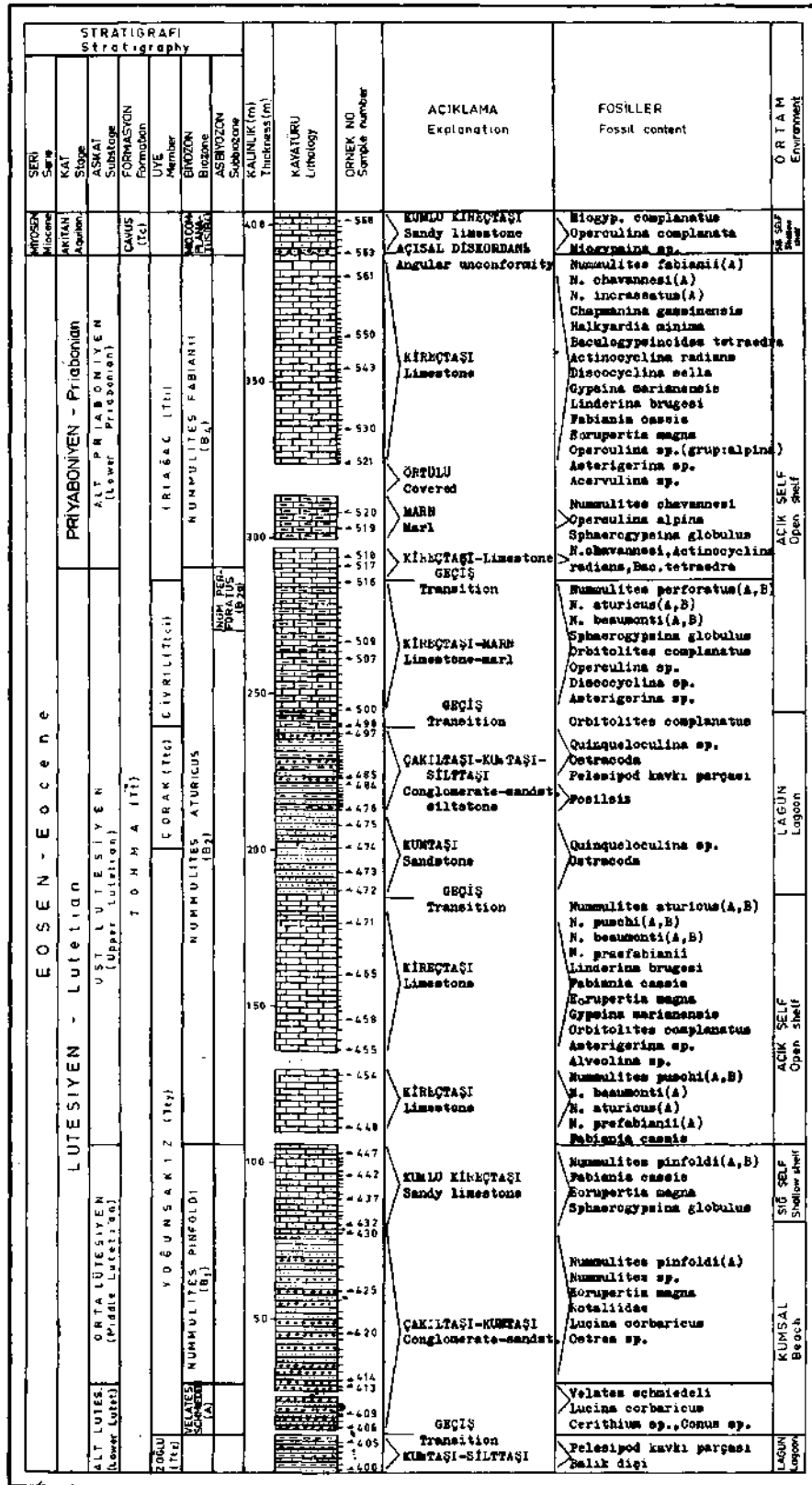


Fig. 7 - Measured stratigraphic section of Aşağıköy.

The formation lies unconformably on the Medik formation southeast of the investigated area and on the Horasaçal formation along the Tohma valley. The upper boundary is defined by the angular unconformities represented by the bases of Çavuş and Ansurçay formations. The thickness varies between 350-850 m.

The sandstone and sandy limestone alternation in the lowermost section of the Tohma formation contains a rich macrofauna of *Velates schmiedeli* Chemnitz, *Lucina corbaricus* Leymerie indicating a Lower Lutetian age. Limestones at the lower section contains a benthonic association of foraminifera of *Nummulites pinfoldi* Davies, *Orbitolites complanatus* Lamarck and *Fabiania cassis* (Oppenheim) of Middle Lutetian age. The marl-limestone alternation in the medial section is characterised by an Upper Lutetian microfauna comprising of *Nummulites aturicus* Joly and Leymerie, *Nummulites perforatus* (De Montfort), *Nummulites puschi* D'Archiac and Haime, *Nummulites praefabianii* Varentsof and Menner, *Assilina exponens* (Sowerby), *Linderina brugesi* Schlumberger. The limestones in the uppermost section contains a benthonic microfauna of Lower Priabonian age, consisting of *Nummulites fabianii* (Prever), *Nummulites incrassatus* De La Harpe, *Nummulites chavannesi* De La Harpe, *Chapmanina gassinensis* Silvestri, *Halkyardia minima* (Liebus), *Baculogypsinoides tetraedra* Gumbel. The environment of deposition of the Tohma formation is believed to be lagoonal, beach and shallow-open shelf according to the dwelling organisms and sedimentary features.

Çavuş formation. — It can typically be seen along Gendere and approximately 1 km southwest of Olukkaya peak (Fig. 6). It consists of yellow thin to medium bedded, well-cemented clastic limestones and yellowish-white, thin bedded clayey limestones as interbeds. It unconformably overlies the Tohma formation. It is unconformably overlain by the Ansurçay formation. The thickness of the unit varies between 50-100 m.

A microfauna consisting of benthonic foraminifera was determined from the collected samples: *Miogypsinoides complanatus* (Schlumberger), *Archaias kirkukensis* Henson, *Lepidocyclina* (*Nephrolepidina*) *ournoueri* (Lemoine and Douville), *Spiroclypeus margaritatus* (Schlumberger), *Operculina complanata* (Defrance) and *Miogypsina* sp. An Aquitanian age was assigned to the unit in accordance with this microfauna. It was deposited on the shallow shelf.

Ansurçay formation. — It is typically observed in Gendere and at İkiz peak (Fig. 5). It consists, from base to top, of thin to medium bedded, horizontal or cross-bedded, yellowish brown clastic limestone; gray, horizontal and medium to thick bedded and poorly cemented marls (Bortliyenli member) and yellowish white, indurated, very thick bedded to massive reefal limestones (İkiztepe member) based by a conglomerate horizon in the uppermost section, which overlies unconformably Tohma and Çavuş formations. It is unconformably covered by Mısırdere formation. The thickness of the unit is approximately 150 m.

Foraminifers obtained from the detrital limestone and marl of the Lower and Middle parts of Ansurçay formation such as *Miogypsina irregularis* (Michelotti), *Lepidocyclina* (*Nephrolepidina*) *ournoueri* (Lemoine and Douville), *Miogypsinoides* sp., *Amphistegina lessonii* d'Orbigny, *Lenticulina vortex* (Fichtel and Moll), *Sphaeroidina bulloides* d'Orbigny, *Globigerinoides* sp., *Globoquadrina* sp., *Globigerina* sp., *Flabellipecten burdigalensis* Lamarck, *Flabellipecten* cf. *solarium* Lamarck, *Clamys* cf. *scabrella* Lamarck, *Scutella* cf. *paulensis* indicate an age Burdigalian. The following microfossils have been found in the reefal limestone of the upper most level of the Ansurçay formation *Miogypsina intermedia* Droger, *Borelis melo* Fichtel and Moll, *Quinqueloculina* sp. coral, algae and pelecypoda according to these fossils Burdigalian age has been assumed for the upper most level of Ansurçay formation which has been deposited on a shallow marine, open shelf and reefal environment.

Mısırdereformation. — It can be observed typically in the northern section of Tohma stream. From base to top, it consists of reddish brown, poorly sorted, parallel bedded mudstones with thin intercalations of conglomerates followed by gray, poor to wellsorted, with eroded bottoms of bedding, parallel or cross-bedded conglomerates and yellowish gray, cross-bedded sandstones. It rests unconformably on the Ansurçay formation and is covered by recent alluvium. The thickness of the unit varies between 20–40 m.

This unit does not contain neither micro nor macrofossils. It was deposited in alluvial fans and braided streams.

Biostratigraphy

Biostratigraphic units (biozones) were observed according to the fossil content and distribution in the sediments of the area. Biozones are defined on the abundance of micro and macrofossils or according to the fauna defining a given stratigraphic horizon. «The International Stratigraphic Guides» (Hedberg, 1975) was used as a guide for distinction of the biozones.

Six benthonic foraminifera and one gastropoda biozones were defined in the Eocene-Miocene series. A biozone map was prepared to show the distribution and relations (Fig. 8).

Velates schmiedeli abundance biozone. — It is a macrofossil zone characterized by the *Velates schmiedeli* species of the Neritidae family. It occurs dominantly in the lower section of the Yoğunsakız member of the Tohma formation. It contains other macrofossils such as *Lucina corbaricus*, *Cerithium* sp., *Conus* sp., *Ostrea* sp. in addition to its typical constituent. It is dated as Lower Lutetian.

Nummulites pinfoldi abundance biozone. — It is a benthonic foraminifera biozone characterized by the *Nummulites pinfoldi* species of the Nummulitidae family. It dominates in the medial section of the Yoğunsakız member of the Tohma formation. In addition to the main component of the unit, the benthonic foraminifera species of *Orbitolites complanatus*, *Fabiania cassis*, *Eorupertia magna*, *Sphaerogypsina globulus*, *Aeolina* sp. and *Quinqueloculina* sp. are present. It is dated as Middle Lutetian.

Nummulites aturicus range biozone. — It is a benthonic foraminifera biozone characterized by the *Nummulites aturicus* species of the Nummulitidae family. The zone is limited at the base by the disappearance of *Nummulites pinfoldi* and appearance of *Nummulites aturicus*. It is limited at the top by the disappearance of *Nummulites aturicus* and appearance of *Nummulites fabianii*. It is dominant in the uppermost section of Yoğunsakız member, Çivril, Çorak members and in the lower section of İriağaç member of the Tohma formation. In addition to the main species of the biozone, the following benthonic foraminifera also occur in these units: *Nummulites perforatus*, *Nummulites beaumonti*, *Nummulites puschi*, *Nummulites praefabianii*, *Assilina exponens*, *Fabiania cassis*, *Linderina brugesii*, *Sphaerogypsina globulus*, *Asterigerina* sp., *Rhapydionina* sp., *Discorbis* sp., *Quinqueloculina* sp. A subbiozone, namely *Nummulites perforatus* abundance subbiozone, was distinguished in the uppermost section of the *Nummulites aturicus* range biozone. *Nummulites aturicus* range biozone is of Upper Lutetian age.

Nummulites fabianii range biozone. — It is a benthonic foraminifera zone characterized by the *Nummulites fabianii* species of the Nummulitidae family. The lower boundary of the biozone is limited by the disappearance of *Nummulites aturicus* and appearance of *Nummulites fabianii*. The upper limit can not be determined due to the incomplete nature of the sequence. It is dominant in the uppermost section of the İriağaç member of the Tohma formation. The benthonic foraminifera of *Nummulites chavannesi*, *Nummulites incrassatus*, *Chapmanina gassinensis*, *Halkyardia minima*, *Fabiania*

cassis, *Linderina brugesi*, *Baculogypsinoides tetraedra*, *Eorupertia magna*, *Discocyclina sella*, *Actinocyclina radians*, *Gypsina marianensis*, *Operculina alpina*, *Lituonella* sp., *Peneroplis* sp. are associated to the main species of the biozone. An abundance subbiozone characterized by the *Chapmanina gas-sinensis* in the uppermost section of the *Nummulites fabianii* range biozone. *Nummulites fabianii* range biozone is dated as Lower Priabonian.

Miogypsinoides complanatus abundance biozone. — It is a zone of benthonic foraminifera characterized by *Miogypsinoides complanatus* sp. of the Miogypsinidae family. It is dominant in the sediments of the Çavuş formation. The benthonic foraminifera of *Archaias kirkukensis*, *Lepidocyclina (Nephrolepidina) tournoueri*, *Spiroclypeus margantatus*, *Operculina complanata*, *Amphistegina lessonii*, *Miogypsina* sp., *Pararotalia* sp. are associated to the main species of the biozone. It is dated as Aquitanian.

Mwgypsina irregularis abundance biozone. — It is a benthonic foraminifera zone characterized by the *Miogypsina irregularis* species of the Miogypsinidae family. It is dominant in the sediments of the Bortliyenli member of the Ansurçay formation. The benthonic and planctonic foraminifera of *Lepidocyclina (Nephrolepidina) tournoueri*, *Amphistegina lessonii*, *Lenticulina vortex*, *Pullenia bulloides*, *Sphaeroidina bulloides*, *Miogypsinoides* sp., *Globigerinoides* sp., *Globoquadrina* sp., *Globigerina* sp. and macrofossils of *Flabellipecten burdigalensis*, *Flabellipecten* cf. *solarium*, *Chlamys* cf. *scabrella*, *Scutella* cf. *paulensis* are found in addition to the main species. It is dated as Burdigalian.

Miogypsina intermedia abundance biozone. — It is a benthonic foraminifera zone characterized by *Miogypsina intermedia* species of the Miogypsinidae family. It occurs dominantly in the İkiztepe member of the Ansurçay formation. The following foraminifera typically occur with the main component of the biozone: *Borelis melo*, *Amphistegina lessonii*, *Gypsina* sp. *Acervulina* sp. corals, bryozoa, pelecypoda and gastropoda are additionally occurring macrofossils. The age interval is defined as Upper Burdigalian.

The correlation of the defined biozones are shown in a table (Fig. 9).

Chronostratigraphy

The fossils have been valuable guides in definition of the chronostratigraphic units. Chronostratigraphic units were constructed to correspond to the biozones. The aim of this section is to define the relative ages indicated by the paleontological data yielded by the Mesozoic and Cenozoic sediments.

Era : Mesozoic

Period : Jurassic - Cretaceous

Upper Jurassic - Lower Cretaceous-series: This unit is differentiated through the benthonic microfauna comprising *Valrulinella jurassica* and *Clypeina jurassica*

Era : Cenozoic

System : Tertiary

Subsystem : Paleogene

Paleocene series: It is considered to correspond to the process of formation of the continental sediments of the Medik formation.

Eocene series: It is subdivided into subseries of Middle and Upper Eocene. The Middle Eocene subseries is represented by the Lutetian stage. The Lutetian stage is further subdivided into sub-stages of Lower Lutetian (*Velates schmiedeli* biozone), Middle Lutetian (*Nummulites pinfoldi* biozone) and Upper Lutetian (*Nummulites aturicus* biozone). Upper Eocene subseries is represented by the Priabonian (Lower Priabonian) stage.

Subsystem : Neogene

Miocene series: It is represented by the Miocene subseries. This is subdivided into substages of Aquitanian (*Miogypsinoides complanatus* biozone) and Burdigalian (*Miogypsina irregularis* and *Miogypsina intermedia* biozones).

Sediments of the Misirdere formation are considered to have been deposited during the large time interval of Pliocene and Quaternary.

The relations between lithostratigraphic, biostratigraphic and chronostratigraphic units are shown in Fig. 10.

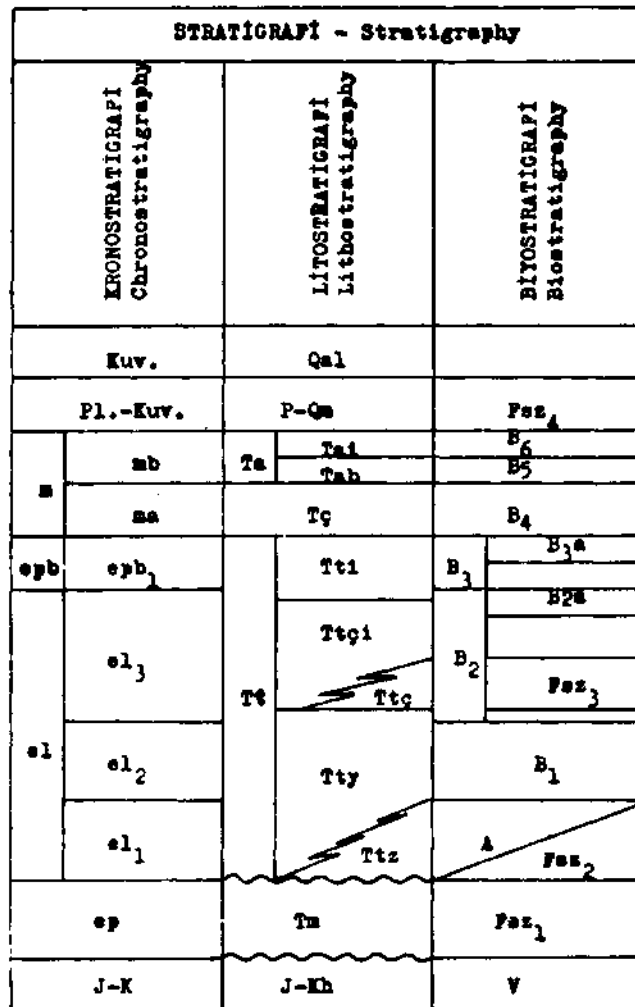


Fig. 10 - Relation between the lithostratigraphic, biostratigraphic and chronostratigraphic units defined for the investigated area. (The explanation of symbols is given in figures 3,8 and 12).

A complete harmony of correlation of the biozones, biostratigraphic and chronostratigraphic, are shown to exist (Fig. 11) with those of Turkey (İstanbul, Ankara, Denizli, Kastamonu, Malatya, Sivas, Muş regions) carried out by Dacı (1951), Dacı and Dizer (1953), Dizer (1962 a,b), Sirel and Gündüz (1976), Sirel (1976), Sakinç (1982), and Dizer (1982) and of the world (France, Italy, Greece, Yugoslavia, Romania, Hungary, Soviet Union, Iran, India and various regions of America) investigated by Veillon (1964), Blondeau et al. (1968), Plaziat and Renzi (1968), Bignot et al. (1968), Cavelier (1968), Castellarin and Cita (1969), Cita (1969), Dudich et al. (1968), Bombita and Moisescu (1968), Ionesi (1971), Nemkov (1964, 1968), Hottinger et al. (1964), Schaub (1981), Akers and Drooger (1957), Mohan (1958), Rahaghi (1974), Raju (1974) and Mulder (1975).

PALEONTOLOGY

Large foraminifera such as Nummulitidae, Discocyclinidae, Lepidocyclinidae, Miogypsinidae families and species of these families are described in this section.

The stratigraphic distributions of the collected micro and macrofossils are shown in a table (Fig. 12) via realization of the paleontologic systematic.

Description of species

Ordo : Foraminiferida Eichwald, 1830

Family : Nummulitidae De Blainville, 1825

Genus : Nummulites Lamarck, 1801

Nummulites pinfoldi Davies, 1940
(Plate I, fig. 1-2)

1940 *Nummulites pinfoldi* Davies, Davies, p. 209

1976 *Nummulites pinfoldi* Davies, Sirel and Gündüz, p. 31-44

Description: Macrospheric figure : The shell is 2 mm in diameter and is 1.1 - 1.2 mm thick. Form of the shell: Lenticular, the central part is bulbed with a white patch; the division lines are thick and form a radiating pattern of divisions. The planspiral has four tours with wide coiling; is 50-70 microns thick. The divisions are slightly inclined to straight and height of the chambers slightly exceeds the width. The first chambre is isolepidine and is 70 microns in diameter.

Microspheric figure: The measured diameter and thickness of the shell are respectively 1.7-2.15 mm and 0.85-1.35 mm. The outer features are the same as described for the macrospheric figure. The planspiral has five tours with wide coiling and is 50-70 microns thick. The first chamber is small.

Stratigraphic distribution: Middle Lutetian.

Occurrence: Northwestern Malatya, vicinity of Medik-Ebreme.

Nummulites beamonti D'Archiac and Haime, 1853
(Plate I, fig. 7-10)

1853 *Nummulites beamonti* D'Archiac and Haime, Archiac and Haime, p. 133

1951 *Nummulites sub-beamonti* De La Harpe, Dacı, p. 215

YAŞ Age	e									
	e1						epb	ea	eb	
	e1 ₁		e1 ₂		e1 ₃					
BIYOZONLAR Biozones	VELATES SCHIEDALI	NUMMULITES LAEVICATUS	NUMMULITES PINFOLDI	NUMMULITES MILLICAPUT	NUMMULITES AFRICUS	NUMMULITES FABIANII	MIOCYPSINOIDES COMPLANATUS	MIOCYPSINA IRREGULARIS	MIOCYPSINA INTERMEDIA	
CALİŞMALAR Studies										
TÜRKİYE - Turkey	ÖRÇEN, S. (1984)	x		x		x	x	x	x	
	DACI, A. (1951)		x			x	x			
	DACI-DİZER, A. (1953)					x				
	DİZER, A. (1962a)					x	x			
	DİZER, A. (1962b)							x	x	
	SİRİL, S. ve GÜNDOĞDU, N. (1976)		x	x						
	SİRİL, S. (1976)					x	x			
	SAHİNC, M. (1982)							x	x	
	DİZER, A. (1982)		x		x	x	x	x	x	
	DİZER, A. (1982)		x		x	x	x	x	x	
DÜNYA - The World	ANKERS, A.H. ve DHOOGBER, C.A. (1957)						?	x	x	
	MEJHAN, K. (1958)							x		
	VEILLON, K. (1964)		x			x	x			
	HOTTINGER, L. ve diğ. (1964)		x		x	x	x			
	DEMKOV, G.-I. (1964)		x			x	x			
	BLODINSKY, A. ve diğ. (1968)					x	x			
	MAKGEREL, J. (1968)					x				
	FLAZIAT, J.C. ve BENZI, M. (1968)	x								
	FIGROT, G. ve diğ. (1968)					x				
	CAVELIER, C. (1968)					x	x			
	PAPA, A. (1968)		x			x	x			
	DUDICH, E. ve diğ. (1968)				x	x	x			
	MORITA, O. ve diğ. (1968)	x				x	x			
	DEMKOV, G. (1968)		x			x	x			
	CASTELLEJAN, A. ve CITA, M.-B. (1969)					x	x			
	CITA, M.-B. (1969)		x			x	x			
	IONESI, L. (1971)					x	x			
	RAHAGHI, A. (1974)							x	x	
	RAJU, D.S.N. (1974)							x	x	
	DEMULDER, K. (1975)							x	x	
SCHAUB, F. (1981)		x		?	x	x				

Fig. 11 - Correlation of the defined biozones with that of Turkey and of localities in other parts of the world.

Description: Macrospheric figure: The measured diameter and thickness of the shell are respectively 2-6.1 mm and 0.8-3 mm. Lenticular, the margins are sharp and the central part is bulbed with a white patch. The division lines are turbinate in the centre and is arched towards the edges. There is a transversal trabecule in the margin of the shell. The planspiral has 4 to 8 tours with wide coiling with a thickness of 60-150 microns. The divisions are thin, slightly inclined and straight. The height of the chamber is greater than the width. The first chamber is isolepidine with a diameter of 0.15-0.30 mm.

Microspheric figure: The diameter of the test varies between 5.9-9.75 mm, the thickness of the test ranging from 2.8 mm to 4.2 mm. External characters of the shell are the same as in the macrospheric form. It is counted 11-16 whorl within the shell. The thickness of the spire is 75-200 μ . The septa are thin, slightly inclined and straight. The height of the chambers are greater than the width of the chambers. The proluculus is very small.

Stratigraphic distribution: Upper Lutetian.

Occurrence: Northwest of Malatya, vicinity of Medik-Ebreme.

Nummulites puschi D'Archiac, 1850
(Plate II, fig. 4-6)

1850 *Nummulina puschi* D'Archiac, Archiac, p. 241

Description: Macrospheric figure: The measured diameter and thickness of the shell are respectively 7-7.4 mm and 2.2-2.4 mm. The shape of the shell is lenticular, flattened, the margins are sharp and the central part is slightly bulbed. The division lines are thick and distinct in the margins of the shell and are reticuled. There is a granule coating on the surface of the shell. The planspiral has 8 tours, the coiling is wide initially with transitional lightning and has a thickness of 100 microns. The divisions are thin and short, slightly inclined and arched. The width of the chamber is greater than the height. The first chamber is subspherical with a diameter of approximately 1.4 mm.

Microspheric figure: The measured thickness and diameter of the shell are 5-5.2 mm and 29.5-30 mm respectively. The outer features are as described in the macrospheric figure. The planspiral has 28 tours with wide coiling and has a thickness of 150-250 microns. The divisions are thin, short, and slightly arched and inclined. The width of the chamber is greater than the height. The first chamber is very small.

Stratigraphic distribution: Upper Lutetian.

Occurrence: Northwest of Malatya, vicinity of Medik-Ebreme.

Nummulites aturicus Joly and Leymerie, 1848
(Plate I, fig. 14-17)

1848 *Nummulites aturica* Joly and Leymerie, Joly and Leymerie, p. 171, 218

1953 *Nummulites aturicus* Joly and Leymerie, Dacı and Dizer, p. 270-299, Plate 8, fig. 9

1963 *Nummulites aturicus* Joly and Leymerie, Schaub, p. 285

Description: Macrospheric figure: The measured diameter and thickness of the shell are 4.6-7 mm and 2.4-3.75 mm respectively. The shape of the shell is lenticular with fairly sharp edges. The division lines are radiating, thin and slightly undulatory. The granules are large in the centre fining towards the margins with a nonuniform distribution. The planspiral has 6-7 tours with wide coiling. The thickness is approximately 120-200 microns. The divisions are thin to medium, short, inclined, arched and occasionally unquulatory. The width of the chambers is greater than the height. The first chamber is subspherical and has a diameter of 0.5-1 mm.

Microspheric figure: The measured diameter and thickness of the shell are 10.1-12.9 mm and 2.85-5.8 mm respectively. The division system are meandering with meandering, undulatory and thin division lines. The granules, fairly large in the centre and fine in the margins, are on and between the division lines. The planspiral has 12-19 tours with wide coiling and a thickness of 100-200 microns. The divisions are inclined, arched, occasionally subhorizontal and undulatory. The width of the chambers is greater than the height. The first chamber is very small.

Stratigraphic distribution: Upper Lutetian.

Occurrence: Northwest of Malatya, vicinity of Medik-Ebreme.

Nummulites perforatus (De Montfort), 1808
(Plate II, fig. 1-3)

1911 *Nummulites perforatus* Denys De Montfort, Boussac, p. 15-16, 29-30, plate VI, fig. 1,8; plate XXII, fig. 1; plate VI, fig. 5

1972 *Nummulites perforatus* Montfort, Blondeau, p. 161, Plate XXXIV, fig. 6-11

Description: Macrospheric figure: The measured diameter and thickness of the shell are 5.3-7.75 mm and 2.35-4.15 mm respectively. The shape of the shell is lenticular, bulbed with fairly sharp edges. The division system is radiating with thin and slightly undulating division lines. The granules, fairly large in the centre and fine grained in the margins, occur on and between the division lines. The planspiral has 5-6 tours with wide coiling and a thickness of 100-180 microns. The divisions are thin to thick, short, inclined, arched, occasionally subhorizontal and undulatory. The first chamber is nonuniform, elyptoidal with a diameter varying between 0.85-1.5 mm.

Microspheric figure: The measured diameter and thickness of the shells are 18.2-29 mm and 8.4-15.2 mm respectively. The shape of the shell is lenticular, extremely bulbed with rounded edges. The division system is meandering. There are fine meanders on the division lines. There are fine to medium grained granules of a nonuniform distribution on and between the division lines. The planspiral has 25-45 tours. The system of coiling has a three stage development in the well-evolved individuals. Coiling is tight for the initial 6-7 tours slackening for the eight-nineteenth and becoming extremely tight for the twentieth-forty-fifth. The gap between tours is extremely small for the latest stage of coiling, with rare twinning. The thickness of the planspiral is about 150-250 microns. The divisions are slanted, arched, extremely slanted and undulatory. The width of the chambers exceeds the height. The first chamber is very small.

Stratigraphic distribution: Upper Lutetian.

Occurrence: Northwest of Malatya, vicinity of Medik-Ebreme.

Nummulites praefabianii Varentsof and Menner, 1933
(Plate I, fig. 18-20)

1933 *Nummulites praefabianii* Varentsof and Menner, Varentsof-Menner, p. 104

Description: Macrospheric figure: The measured diameter and thickness of the shells are 1.8-2.5 mm and 0.8-1.3 mm respectively. The shape of the shell is lenticular and flattened with fairly sharp edges. The division system is reticuled. The division lines are thick and are distinct at the margins. There is a large granule in the centre circled by a set of uniform and fine grained granules. The planspiral has 4-6 tours with slack coiling and a thickness of 50-100 microns. The divisions are thick, slanted, arched and the edges are thick. The first chamber is isolepidine and has a diameter of 0.1-0.15 mm.

Microspheric figure: The measured diameter and thickness of the shells are 2.8-4.6 mm and 1.3-1.65 mm respectively. The outer features are as described in the macrospheric figure. The planspiral has 8 tours with slack coiling and a thickness of about 160-200 microns. The divisions are thick, slanted and slightly arched. The width of the chambers exceeds the height. The first chamber is very small.

Stratigraphic distribution: Upper Lutetian.

Occurrence: Northwest of Malatya, vicinity of Medik - Ebreme.

Nummulites fabianii (Prever), 1905

(Plate I, fig. 21)

1911 *Nummulites fabianii* Prever, Boussac, p. 79-84, plate I, fig. 6,13; plate IV, fig. 9,10

1938 *Nummulites fabianii* Prever in Fabianii, Flandrin, p.48-51, plate III, fig. 71-76

1951 *Nummulites fabianii* Prever, Dacı, p. 206

1972 *Nummulites fabianii* (Prever), Blondeau, p. 156, plate III, fig. 1-5

Description: Macrospheric figure: The measured diameter and thickness of the shells are 1.8-2.5 mm and 0.8-1 mm respectively. The shape of the shell is lenticular and flattened with sharp edges. The divisional system is reticulated with thick division lines intersecting on the spirs. There is a large granule in the centre encircled by circles made up by fine grained granules. The planspiral has 5-6 tours with slack coiling and a thickness of 80-100 microns. The divisions are thin, slightly slanted and arched, and the edges are thick. The width of the chamber is greater than the height. The first chamber is isolepidine with a diameter varying between 0.1-0.12 mm.

Microspheric figure: The measured thickness and diameter of the shell are 1.2-1.5 mm and 4.2-4.5 mm respectively. The shape of the shell is flattened with sharp edges. The divisional system and the granulation are the same as that described for the macrospheric figure. The planspiral has 7-8 tours with slack coiling and a thickness of 60-65 microns. The divisions are thin, arched, occasionally extremely slanted and the edges are thick. The width of the chambers is greater than the height. The first chamber is very small.

Stratigraphic distribution: Lower Priabonian.

Occurrence: Northwest of Malatya, vicinity of Medik-Ebreme.

Nummulites chavannesi De La Harpe, 1878

(Plate I, fig. 11-13)

1911 *Nummulites chavannesi* De La Harpe, Boussac, p.69, plate XVII, fig. 10

1938 *Nummulites chavannesi* De La Harpe, Flandrin, p.254-255, plate XIV, fig. 15

1951 *Nummulites chavannesi* De La Harpe, Dacı, p.210, plate II, fig. 9

1972 *Nummulites chavannesi* De La Harpe, Blondeau, p. 146, plate XXII, fig. 1-3

Description: Macrospheric figure: The measured diameter and thickness of the shell are 2.5-4.5 mm and 0.85-2.1 mm respectively. The shape of the shell is lenticular with a bulbed centre and sharp edges. The divisional system is radiating; the lines of divisions are thin, close to one another and are slightly curved towards the edges of the shell. There is inconspicuous patch in the central part. The planspiral has 4-6 tours with tight coiling and a thickness averaging 60 microns. The divisions are thin, long, slightly slanted, initially straight getting arched later on. The height of the chambers are greater than the width. The first chamber is unisolepidine with a diameter varying between 0.11-0.15 mm.

Microspheric figure: The measured diameter and the thickness of the shells are 4.0-5.5 mm and 0.85-2 mm respectively. The outer features are the same as the macrospheric figure. The planspiral has 6-7 tours with tight coiling and a thickness of 60 microns. The divisions are thin, close and slightly arched. The height of the chambers are greater than the width. The first chamber is very small.

Stratigraphic distribution: Lower Priabonian.

Occurrence: Northwest of Malatya, vicinity of Medik-Ebreme.

Nummulites incrassatus De La Harpe, 1883

(Plate I, fig. 3-6)

1883 *Nummulites vasca* var. *incrassata* et var. *tenuispira* De La Harpe, De La Harpe, plate VII, fig. 27, 28, 29, 32

1911 *Nummulites incrassatus* De La Harpe, Boussac, p. 32-34

1938 *Nummulites incrassatus* De La Harpe, Flandrin, p. 40-42, plate III, fig. 24, 50

1951 *Nummulites incrassatus* De La Harpe, Daçı, p. 207-209, plate II, fig. 5, 6

Description: Macrospheric figure: The measured diameter and thickness of the shell are 1.9-3.3 mm and 0.85-1.9 mm respectively. The shape of the shell is lenticular, bulbed in the centre and has sharp edges. The divisional system is radiating. The division lines are thick, starts as straight lines from the centre slightly curving towards the exterior. There is a white button in the centre of the shell. The planspiral has 4-5 tours with slack coiling and a thickness of 50-100 microns. The height of the chamber is greater than the width. The first chamber is isolepidine and unisolepidine and has a diameter of 0.15-0.20 mm.

Microspheric figure: The measured thickness and diameter of the shells are 1.8 mm (average) and 3.2-2.75 mm respectively. The outer features are the same as that of the macrospheric figure. The planspiral has 6-7 tours with slack coiling and has an average thickness of 120 microns. The divisions are thin, slanted, slightly arched and closely spaced. The height of the chambers exceeds the width. The first chamber is very small.

Stratigraphic distribution: Lower Priabonian.

Occurrence: Northwest of Malatya, vicinity of Medik-Ebreme.

Genus: *Assilina* D'Orbigny, 1839

Assilina exponens (Sowerby)

(Plate II, fig. 7-8)

1840 *Nummulites exponens* Sowerby, Sowerby, p. 719, plate XII, fig. 14

1911 *Assilina exponens* (Sowerby), Boussac, p. 100

1938 *Assilina mamillata* (D'Archiac), Flandrin, p. 79-80, plate VIII, fig. 6-16

1953 *Assilina mamillata* (D'Archiac), Daçı-Dizer, p.267-268, plate IX, fig. 5-6

1976 *Assilina exponens* (Sowerby), Sirel ve Gündüz, p. 39-40, plate X, fig. 9; plate XI, fig. 1-9

Description: Macrospheric figure: The measured diameter and thickness of the shells are 9.1 mm and 1.7-1.85 mm respectively. The shape of the shell is a lentiform of extremely flattened habit with rounded edges. Spirs and divisions are distinct on the surface of the shell. There are a few granules in the central part of the shell. The planspiral has six tours with slack coiling and has an approximate thickness of 200-300 microns. The divisions are thin, slightly slanted and aligned perpen-

dicular to the tours. The chambers are roughly quadrangular whose height is greater than its width. The first chamber is unisolepidine and oval shaped with a diameter of about 0.38 X 0.70 mm.

Stratigraphic distribution: Upper Lutetian.

Occurrence: Northwest of Malatya, vicinity of Medik-Ebreme.

Family: Discocyclinidae Galloway, 1928

Genus : Discocyclina Gümbel, 1870

Discocyclina sella (D'Archiac), 1850

(Plate II, fig. 9-11)

1850 *Orbitolites sella* D'Archiac, Archiac, p. 405, plate VIII, fig. 10-12

1903 *Orthophragmina sella* D'Archiac, Schlumberger, p. 278, plate IX, fig. 14-16, 25

1951 *Discocyclina sella* D'Archiac, Dacı, p. 228-229

1958 *Discocyclina sella* (D'Archiac), Neumann, p.106-109, plate XXII, fig. 1; plate XXVI, fig. 2-4

Description: Macrospheric figure: The measured diameter and thickness of the shell are 2.5-5.5 mm and 1.1-1.8 mm respectively. The shape of the shell is lenticular with a bulbed centre and thin-sharp edges. The granules have a diameter averaging 120-130 microns in the central part. They are smaller in the exterior parts and are encircled by rosettes with 7-8 petals. The embryonic organism is of the eudoscoidine type. The protoconch is spherical with a diameter of approximately 125 microns. The deuteroconch has not fully encircled the protoconch. It has a diameter of 290 X 330 microns and has flattened edges. The periembryonic chambers are in two lines. The first line contains 26 chambers. The equatorial chambers are initially close to a square (40 X 45 microns) and become quadrangular in shape (35 X 60, 55 X 85 microns). The wall of the chambers has a thickness of about 17-20 microns.

Stratigraphic distribution: Lower Priabonian.

Occurrence: Northwest of Malatya, vicinity of Medik-Ebreme.

Genus: Actinocyclina Gümbel, 1870

Actinocyclina radians (D'Archiac), 1850

(Plate III, fig. 1-3)

1850 *Actinocyclina radians* (D'Archiac), Archiac, p. 397-456, plate VIII, fig. 15, 16

1951 *Actinocyclina radians* D'Archiac, Dacı, p. 232-233, plate IV, fig. 17,21

1958 *Actinocyclina radians* (D'Archiac), Neumann, p. 106-109, plate XXII, fig. 1-8; plate XXVI, fig. 5-7; plate XXXVI, fig. 2-4, 33

Description: Macrospheric figure: The measured diameter of the shell averages 8.4 mm. The shape of the shell is extremely flattened and the central part is bulbed. The granules on the central bulb and radial cords are relatively larger. The embryonic organism is of the nephrodiscoidine type. The protoconch is spherical with a diameter of approximately 145 x160 microns. Deuteroconch has not entirely encircled the protoconch and has a diameter of 340x480 microns. The equatorial chambers are initially close to a square (30 X 40 microns) and become quadrangular in shape (60 x140 microns).

Stratigraphic distribution: Lower Pnabonian.

Occurrence: Northwest of Malatya, vicinity of Medik-Ebreme.

Family : Lepidocyclinidae Scheffen, 1932

Genus : Lepidocyclina Gumbel, 1870

Subgenus : Nephrolepidina H.Douville, 1911

Lepidocyclina (Nephrolepidina) tournoueri Lemoine and Douville), 1904
(Plate III, fig. 4)

1904 *Lepidocyclina tournoueri* Lemoine and Douville, Lemoine and Douville, p.19, plate 1, fig. 5, plate II, fig. 2,14; plate III, fig. 7

1962 *Lepidocyclina (Nephrolepidina) tournoueri* (Lemoine and Douville, Dizer, p.73-74, plate VIII, fig. 4-6

1975 *Lepidocyclina (Nephrolepidina) tournoueri* Lemoine and Douville, Mulder, p.64-66, plate 3, fig. 10; plate 4, fig. 1-3

1982 *Lepidocyclina (Nephrolepidina) tournoueri* (Lemoine and Douville), Sakinç, p. 257-258

Description: Macrospheric figure: The measured diameter and thickness of the shells are 1.7 mm and 0.85-1.15 mm respectively. The shape of the shell is lenticular with the central part bulbed and thin edges. There are 3-5 granules in the central part of the shell. The nucleocon is of the nephrolepidine type. The protoconch has an elyptoidal shape with a diameter of approximately 290-420 microns. Deuteroconch has a diameter varying between 420-530 microns partially encircling the protoconch. The nepionic chambers are aligned around the nucleoconch. The neanic chambers have an hexagonal shape.

Stratigraphic distribution: Aquitanian, Burdigalian.

Occurrence: Northwest of Malatya, vicinity of Medik-Ebreme.

Family : Miogypsinidae Vaughan, 1928

Genus : Miogypsinoides Yabe and Hanzawa, 1928

Miogypsinoides complanatus (Schlumberger), 1900
(Plate III, fig. 5-6)

1900 *Miogypsina complanata* Schlumberger, Schlumberger, p. 330, plate 2, fig. 13-16; plate 3, fig. 18-21

1957 *Miogypsinoides complanatus* (Schlumberger), Hanzawa, p. 92

1959 *Miogypsina (Miogypsinoides) complanata* (Schlumberger), Drooger and Magne, p.273, fig. 6-9, plate 3, fig. 3-7

1962 *Miogypsina (Miogypsinoides) complanata* (Schlumberger), Dizer, p.76, plate 6, fig. 4

1974 *Miogypsinoides (Miogypsinoides) complanata* Schlumberger, Raju, p.78, plate 1, plate 2, fig.1-3

1982 *Miogypsinoides complanatus* (Schlumberger), Sakinç, p. 259-260

Description: Macrospheric figure: The measured thickness and diameter of the shell are 0.5 mm (mean value) and 1.5 mm respectively. The shape of the shell is fanlike, the apex is bulbed and the surface is covered by large granules. The embryo-nepionic section lies in the apex of the shell. The protoconch is spherical with a diameter of 155 microns. Deuteroconch is nonuniform and elyptoidal and its diameter was measured as 140x180 microns. The embryo-nepionic section consists of a 1.5 tour spiral having 10-14 nepionic chambers. The angle between the apical frontal and medio-embryonic lines is negative and obtuse. The neanic chambers have thick walls and are of a rhombic shape that are initially short lengthening later. Lateral chambers are incipient.

Stratigraphic distribution: Aquitanian.

Occurrence: Northwest of Malatya, Medik-Ebreme region.

Genus: *Miogypsina* Sacco, 1893

Miogypsina irregularis (Michelotti), 1841

(Plate III, fig. 7-8)

1900 *Miogypsina irregularis* (Michelotti), Schlumberger, p. 328, plate II, fig. 1-7,9,10; plate III

1940 *Miogypsina irregularis* (Michelotti), Bronnimann, p. 88-94, plate 8, fig. 1-11; plate 10, fig. 6-11; plate II, fig. 4

1952 *Miogypsina (Miogypsina) irregularis* (Michelotti), Drooger, p.54, plate II, fig. 25,29

1958 *Miogypsina (Miogypsina) irregularis* (Michelotti), Mohan, p. 378-380, plate 1, fig. 1-18

1959 *Miogypsina (Miogypsina) irregularis* (Michelotti), Drooger and Magne, p. 277

1962 *Miogypsina (Miogypsina) irregularis* (Michelotti), Dizer, plate IV, fig. 4; plate VI, fig 7

1982 *Miogypsina irregularis* (Michelotti), Sakınç, plate VII, fig. 3-7

Description: Macrospheric figure: The measured diameter and thickness of the shell are 1.5-2.4 mm and 0.5-0.75 mm respectively. The shape of the shell is biconvex, flattened and the apex is conspicuous. There are granules large in the apex and small in the margins. The spherical protoconch with a diameter of 110-235 microns is partially encircled by the subspherical deuteroconch with a diameter of 155-340 microns in the embryo-nepionic section. The nepionic spiral has 1/2 tour with 5-6 chambers. The angle γ is acute and positive. The neanic chambers have thin walls, ogeval shaped after the nepionic spiral and ogeval-rhombic shaped towards the margin of the shell.

Stratigraphic distribution: Burdigalian.

Occurrence: Northwest of Malatya, Medik-Ebreme region.

Miogypsina intermedia Drooger, 1952

(Plate III, fig. 9-10)

1952 *Miogypsina intermedia* Drooger, Drooger, p. 54-55

Description: Macrospheric figure: The measured diameter and thickness of the shell are 1.4-2 mm and 0.45-0.6 mm respectively. The shape of the shell is fanlike, planoconvex and the surface is covered by fine granules. The embryo-nepionic section lies in the apex. The spherical protoconch has a diameter of 145-175 microns. The nepionic spiral has 1/2 tours with 4-5 chambers. The angle γ is positive and acute. The neanic chambers are ogeval in the first phase and become rhombic towards the margins. There are three sets of lateral chambers in the axial section.

Stratigraphic distribution: Burdigalian.

Occurrence: Northwest of Malatya, Medik-Ebreme region.

PALEOECOLOGY

The organisms collected from various units defined in this investigation constitute faunal associations dwelling in various environments for the periods of Jurassic-Cretaceous and specially Tertiary. These associations and environments of dwelling are shown in a table (Fig. 13).

	LAGÜN Lagoon	KUMSAL Beach	SIĞ ŞELF Shallow shelf	AÇIK ŞELF Open shelf
mb		10	10 12:Reef/Reef	11
ma			9	
epb ₁			8	7
el ₃			5,6	4
el ₂			3	
el ₁	1	2		
ep				
J-K				V. jurassica C. jurassica

Fig. 13 - The environments of dwelling of the fossil associations defined for the investigated area (numbers indicate the association numbers given in the text).

The association (1) *Valvulinella Jurassica* and *Clypeina Jurassica* dwelled in the open shelf environment during the time interval of Upper Jurassic-Lower Cretaceous.

The benthonic association (2) of *Quinqueloculina*, ostracods, pelycypods and gastropods dwelled in lagoonal and the benthonic association of *Velates schmiedelli*, *Lucina corbaricus*, *Cerithium*, *Conus*, *Ostrea*, *Quinqueloculina* and *Triloculina* dwelled in beach environments during the time interval of Lower Lutetian.

The benthonic association (3) of *Nummulites pinfoldi*, *Orbitolites complanatus*, *Fabiania cassis*, *Sphaerogypsina globulus*, *Alveolina*, *Quinqueloculina* lived in a shallow shelf in depths not exceeding 20-30 m during the time interval of Middle Lutetian.

The benthonic association of (4) *Nummulites aturicus*, *Nummulites perforatus*, *Nummulites beaumonti*, *Nummulites puschi*, *Nummulites praefabianii*, *Fabiania cassis*, *Linderina brugesi*, *Discocyclusina*, *Operculina* and echinids lived in the open shelf environment of depth 30-50 m; the association (5) *Discorbis*, ostracoda and thin shelled pelycypods lived in shallow marine; and the benthonic association of (6) *Quinqueloculina*, *Textularia*, *Rhapydionina*, *Peneroplis*, *Orbitolites* dwelled in the shallow shelf environment of depth 10-20 m for the time interval of Upper Lutetian.

The benthonic association (7) of *Nummulites fabianii*, *Nummulites chavannesi*, *Nummulites incrassatus*, *Fabiania cassis*, *Linderina brugesi*, *Chapmanina gassinensis*, *Halkyardia minima*, *Baculogypsinoides tetraedra*, *Discocyclusina sella*, *Actinocyclusina radians*, *Operculina* lived in the open shelf with depths of approximately 30-40 m and the benthonic association of (8) *Quinqueloculina* (ample) *Chapmanina gassinensis*, *Fabiania cassis*, *Gypsina marianensis*, *Eorupertia magna*, *Lituonella*, *Peneroplis* dwelled in shallow shelf environment in depths of 20-30 m. for the time interval of Lower Priabonian.

The benthonic association of (9) *Miogypsinoides complanatus*, *Archaias kirkukensis*, *Operculina complanata*, *Spiroclypeus margaritatus*, *Lepidocyclusina (Nephr.) tournoueri*, *Amphistegina lessonii*, bryozoa and algae dwelled in shallow shelf environment in depths of 20-35 m for the time interval of Aquitanian.

The association of (10) comprising the foraminifera *Miogypsina irregularis*, *Amphistegina lessonii*, *Quinqueloculina*, *Textularia* and the macrofossils *Flabellipecten burdigalensis*, *Flabellipecten cf. solarium*, *Chlamys cf. scabrella*, *Scutella cf. paulensis* lived in the beach or shallow shelf; the benthonic association of foraminifera (11) *Miogypsina irregularis*, *Lepidocyclusina (Nephr.) tournoueri*, *Lenticulina vortex*, *Amphistegina lessonii*, *Sphaeroidina bulloides*, *Pullonia bulloides*, *Uvigerina*, *Heterostegina* and the planctonic foraminifera of *Globigerinoides*, *Globoquadrina* and *Globigerina* dwelled in the open shelf of depths 50-80 m; the association (12) formed by the macrofossils of corals, algae, pelycypoda, and gastropoda and the benthonic foraminifera *Miogypsina intermedia*, *Borelis melo*, *Quinqueloculina*, *Textularia* and *Aceryulina* lived in reefal environments for the time interval of Burdigalian.

The fact that the texts by Henson (1950), Blondeau (1972) and Dizer (1982) were most useful in interpretations of the environments of dwelling, must gratefully be acknowledged.

PALEOGEOGRAPHIC EVOLUTION

Upper Jurassic-Lower Cretaceous period, during which the Horasan9al formation was deposited, the area of investigation was represented by an open shelf. Sedimentation might have continued until Paleocene; however, this section was most probably eroded away.

The deposits of these aluvial fans were tilted by tectonic movements during Late Paleocene (?) and Lower Eocene resulting in a new depositional environment during Lower Lutetian. Alluvial fans and braided streams continued their deposition contemporaneous to the transgression during Lutetian resulting in formation of lagoonal environments on these continental sediments. The sediments laid down in braided streams and alluvial fans was followed by sediments (Zeynepoğlu member) deposited along¹ the shore of and in a lagoonal environment prior to deposition of beach sands and shallow marine carbonates (Yoğunsakız member) with progression of the transgression. Along with this first transgression in the region, shallow, marine organisms (mainly Miliolidae) were abundant, although they were soon replaced by organisms of the open shelf such as *Nummulites*, and *Operculina* as there were no obstacles (such as reefs) on the off-shore area. A temporary period of regression, implied by the Çorak member (Upper Lutetian) was preceded by a lagoonal environment, that

previously represented a marine environment, covering a large area, also resulting in formation of a positive area further north. Çorak member was not deposited on this positive area, thus Çivril member was deposited unconformably on the Yoğunsakız member via the transgression following a temporary period of regression. Çivril member, on the other hand, was deposited on the lagoonal Çorak member. This section is followed by a continuous transgressive section during Eocene. The İriağaç member overlying Çivril member consists of shelf carbonates in contrast to the shallow marine environment prevailing in the north. This picture is compatible with the topographic inclination expected for the period of regression, Thus it seems very likely, that the northern parts of the area of investigation was relatively higher and deepening of the environment was increasing towards south, southeast and east. The Tohma formation, of Middle-Upper Eocene age, emerged during Oligocene, was tilted and partly eroded.

The region was a positive area during Oligocene. This nondepositional period is implied by the absence of any sedimentation during this epoch. However, continental Oligocene was reported (Yoldaş, 1972) in the N, outside the investigated area, in the vicinity of the villages of Dostal and Katilköy.

During the period of Miocene, the first transgression occurred during Aquitanian. This transgression, responsible for the deposition of the shallow marine Çavuş formation, was extremely rapid implied by formation of a thin horizon of basal conglomerates sharply transitional to shallow marine carbonates. The Çavuş formation emerged, tilted was partly eroded during late Aquitanian indicated by the angular unconformity basing the Burdigalian sediments. Bortliyenli member is the first product of the last Tertiary transgression. A wide beach full of elastics of carbonates was formed at the beginning of this process. The same area was converted to a shelf on which deposition of marls was realised. This shelf, on which benthonic foraminifera were dwelling with the planctonic, gradually emerged resulting in formation of set reefs (İkiztepe member). These reefs contain abundant algae and corals; in fact, some are made up of these organisms. The evolution of post-Burdigalian is not known as there is no overlying unit in the area of investigation.

The last depositional period in the area is Plio-Quaternary. The alluvial fans and braided streams of this period laid down the sediments of the Mısırdere formation. The Plio-Quaternary basin of Malatya is bounded by faults, resulting in generation of alluvial fans towards the interior parts and a braided stream, most probably having the same course with the current Tohma stream, has left its sediments in the stream bed excavated in these alluvial fans.

CONCLUSIONS

The area of investigation was mapped lithostratigraphically at the scale of 1:25 000 and six formations and seven members were differentiated. The Horasançal formation of Upper Jurassic-Lower Cretaceous age is unconformably overlain by the Medik formation of Paleocene age. There is an angular unconformity at the base of the overlying Tohma formation whose İriağaç member comprises the conformable transition of Upper Lutetian and Lower Priabonian. There are angular unconformities at the bases of Çavuş and Ansurçay formations, respectively of Aquitanian and Burdigalian age. Mısırdere formation, Plio-Quaternary in age, overlies all the units exposed in the area with an angular unconformity.

The range biozones of *Nummulites aturicus* and *Nummulites fabianii* the abundance biozones of *Velates schmiedeli*, *Nummulites pinfoldi*, *Miogypsinoides complanatus*, *Miogypsina irregularis*, *Miogypsina intermedia* and the abundance subbiozones of *Nummulites perforatus* and *Chapmanina gassinensis*

were distinguished in the area for the first time. 552 thin sections and 311 wash samples were examined in detail. The samples were collected from three type sections and nine complementary measured stratigraphic sections. A biozone map showing the distribution of the biozones and locations of the measured stratigraphic sections was prepared. These biozones were matched, biostratigraphically and chronostratigraphically with their equivalents in Turkey and in other parts of the world.

16 species of the families Nummulitidae, Discocyclinidae, Lepidocyclinidae, Miogypsinidae were systematically described in the paleontology section.

12 faunal associations of Middle-Upper Eocene and Miocene series deposited in lagoonal, beach, reefal, shallow and open shelf environments are described with their paleoecologic settings.

The paleogeographic evolution of the region was interpreted through a thorough evaluation of the lithostratigraphic, biostratigraphic and paleontological characteristics of the sediments examined by field and laboratory methods.

ACKNOWLEDGEMENTS

I am thankful to my supervisor, Prof. Dr. A. Dizer, for her kind encouragement, assistance and critical review of the theses. I also thank Y. Hakyemez for his kind negotiation and suggestions on sedimentologic problems. I must acknowledge the contributions of B. Akyürek, M. Y. Barkurt, E. Bilginer, B. Akbaş, H. Mengi and Ş. Pehlivan in preparation of this work.

Manuscript received December 4, 1984

REFERENCES

- Akers, W.H. and Drooger, C.W., 1957, Miogypsinids, planktonic Foraminifera, and Gulf Coast Oligocene-Miocene correlation: Bull. Am. Ass. Petrol. Geol., 41, 656-678.
- Akkuş, M.F., 1971, Stratigraphic and geologic investigation of Darende-Balaban basin (ESE Anatolia): MTA Bull., 76, 1-60, Ankara (in Turkish).
- Archiac, A.D., 1850, Histoire de progres de la geologie de 1834 a 1849, Paris, France: Soc. Geol. France., 3, 241.
- and Haime, J., 1853, Description des animaux fossiles du groupe Nummulitique de l'Inde precedee d'une resume geologique et d'une monographie les Nummulites: 133 p., Gide and J. Baudry, Paris.
- Ayan, T., 1961, Detailed geology and petroleum potential of the Hekimhan-Ebreme region (north of Malatya): MTA Rep., 4186 (unpublished), Ankara (in Turkish).
- Bignot, G.; Hommeril, P. and Larssonneur, C., 1968, Le Lutetian au Large Cotentin: Colloque Eocene, Mem. Bul. Rech. Geol. Min., Fr., 58, 405-416.
- Blondeau, A., 1972, Les Nummulites: 72 p. Paris Lib. Vulbert, Paris.
- ; Bodelle, J.; Campredon, R.; Lanteaume, M. and Neumann, M., 1968, Repartition stratigraphique des grands foraminifères de l'Eocene dans les Alpes-Maritimes (franco-italiennes) et les Basses-Alpes: Colloque Eocene, Mem. Bull. Rech. Geol. Min., Fr., 58, 13-26.
- Bombita, G. and Moisescu, V., 1968, Donnees actuelles sur le Nummulitique de Transylvanie: Colloque Eocene, Mem. Bul. Rech. Geol. Min. Fr., 58, 693-729.

- Boussac, J., 1911, Etudes stratigraphique et paleontologique sur le Nummulitique de Biarritz: Ann. Hebert, 5, 96.
- Bronnimann, P., 1940, Über die tertiären Orbitoididen und die Mrogypsiniden von Nordwest Marokko: Schweiz., Pal. Abh., 63, 1-113.
- Castellarin, A. and Cita, M.B., 1969, Etude de quelques de coupes priaboniennes dans le Monte Baldo (Prov. Verona et Trento, Italie) et discussion des limites de l'etage: Colloque Eocene, Mem. Bul. Rech. Geol. Min., Fr., 69, 119-143.
- Cavelier, C., 1968, Le Paleogene des forages de Marcoussis (Essonne): Colloque Eocene, Mem. Bul. Rech. Geol. Min., Fr., 58, 389-400.
- Cita, M.-B., 1969, Le Paleocene et l'Eocene de l'Italie du Nord: Colloque Eocene, Mem. Bul. Rech. Geol. Min., Fr., 69, 417-428.
- Dacı, A., 1951, Etude paleontologique entre Küçükçekmece et Çatalca: Publication of University of Istanbul, Faculty of Sciences, B, XVI, 3, I, 89-112; II, 207-246.
- Dacı-Dizer, A., 1953, Contribution a l'etude paleontologique du Nummulitique de Kastamonu: Pub. of Univ. of İstanbul, B, XVIII, 34, 207-299.
- Davies, L.M., 1940, The Upper Kharthar beds of north-west India: Geol. Soc. London, Quart., Journ., London, 96, 209.
- Dizer, A., 1962 a, Les foraminiferes de l'Eocene et l'Oligocene de Denizli: Pub. of Univ. of İstanbul, Fac. of Sciences, B, XXVII, 1-2, 39-47.
- , 1962 b, Foraminifera of the Miocene of the Sivas basin (Turkey): Publications of University of İstanbul, Faculty of Sciences, B, XXVII, 1-2, 49-83.
- , 1982, Paleogeography and some foraminifera of the Tertiary period: To the memory of Prof. Dr. Ümit Yaşar Doğanay, 251-291, Pub. of Univ. of İstanbul, Faculty of Political Sciences, İstanbul (in Turkish).
- Drooger, C.W., 1951, Study of American Miogypsinidae: Univ. Utrecht Thesis, 90 p., Zeist., Netherlands.
- and Magne, J., 1959, Miogypsinids and planctonic foraminifera of the Algerian Oligocene and Miocene: Micropaleontology, 5, 273-284.
- Dudich, E.; Gidai, L.; Kecskemeti, T. and Kopek, G., 1968, Quelques problemes actuels de l'Eocene dans la montagne centrale transdanubienne (Hongrie): Colloque Eocene, Mem. Bul. Rech. Geol. Min., Fr., 58, 675-682.
- Flandrin, J., 1938, Contribution a l'etude paleontologique du Nummulitique Algerien: Mat. pour la Carte Geol. Algerie, 1. serie Pal., 8,7, 7-155.
- Hanzawa, S., 1957, Cenozoic Foraminifera of Micronesia: Geol. Soc. Amer. Mem., 66, 1-163.
- Harpe, P.D.L., 1883, Nummulites de la Suisse: Mem. Soc. Pal. Suisse, X, VII, 27-32.
- Hedberg, D.H., 1975, International Stratigraphic Guides: Translation of İ.E. Altınlı, 116 p. TPAO Earth Sciences Publication, Ankara (in Turkish).
- Henson, I.R.S., 1950, Cretaceous and Tertiary deef formation and associated sediments in the Middle East: Bull. Am. Ass. Petrol. Geol., 34, 215-238.
- Hottinger, L.; Lehmann, R. and Schaub, H., 1964, Donnees actuelles sur la biostratigraphie du Nummulitique Mediterranee: Mem. Bul. Rech. Geol. Min., Fr., 28, 611-652.
- Ionesi, L., 1971, Flişul Paleogen dm bazinul vail Moldovei: 238 p. Edit. Acad. Soc. Romania, Bucureşti.
- Joly, N. and Leymerie, A., 1848, Memoire sur les Nummulites considerees zoologiquement et geologiquement: Acad. Roy. Sci. Inscr. Belles-Lettres Toulouse, Mem., 3, 4, 171-218.
- Kurtman, F., 1978, Geology and tectonic aspects of the Gürün region: MTA Bull., 91, 1-12 (in Turkish).
- Lemoine, P. and Douville, R., 1904, Sur le genre *Lepidocyclus* Gümbel: Soc. Geol. France, Mem. Pal. Paris, 12, 2, 32, 1-141.
- Margaret, J.-P., 1968, Les petites foraminiferes de l'Eocene de l'Quest de la France et leur interes stratigraphique: Colloque Eocene, Mem. Bul. Rech. Geol. Min., F., 58, 93-99.
- Mohan, K., 1958, Miogypsinidae from Western India: Micropaleontology, 4,373-390.

PLATES

PLATE - I

Nummulites pinfoldi Davies

- Fig. 1 - Outer appearance, macrospheric figure, (437), X 10
Fig. 2 - Equatorial section, macrospheric figure, (1-624), X 17

Nummulites incrassatus De La Harpe

- Fig. 3 - Outer appearance, microspheric figure, (1-684/I), X 5
Fig. 4 - Outer appearance, macrospheric figure, (1-684/I), X 5
Fig. 5 - Equatorial section, microspheric figure, (1-674), X 6
Fig. 6 - Equatorial section, macrospheric figure, (1-684/G), X 7

Nummulites beaumonti D'Archiac and Haime

- Fig. 7 - Outer appearance, microspheric figure, (508), X 5
Fig. 8 - Equatorial section, microspheric figure, (508), X 5
Fig. 9 - Outer appearance, macrospheric figure, (1-662/B), X 6
Fig. 10 - Equatorial section, macrospheric figure, (1-664/A), X 5

Nummulites chavannesi De La Harpe

- Fig. 11 - Outer appearance, microspheric figure, (1-684/P), X 7
Fig. 12 - Outer appearance, macrospheric figure, (1-684/A), X 6
Fig. 13 - Equatorial section, macrospheric figure, (1-684/P), X 6

Nummulites aturicus Joly and Leymerie

- Fig. 14 - Outer appearance, microspheric figure, (1-670), X 4
Fig. 15 - Equatorial section, microspheric figure, (1-670), X 4
Fig. 16 - Outer appearance, macrospheric figure, (1-660/B), X 5
Fig. 17 - Equatorial section, macrospheric figure, (1-660/A), X 5

Nummulites praefabianii Varentsof and Mener

- Fig. 18 - Outer appearance, microspheric figure, (109/S), X 6
Fig. 19 - Equatorial section, microspheric figure, (1-670), X 4
Fig. 20 - Equatorial section, macrospheric figure, (1-669), X 8

Nummulites fabianii (Prever)

- Fig. 21 - Equatorial section, microspheric figure, (1-682/C), X 5

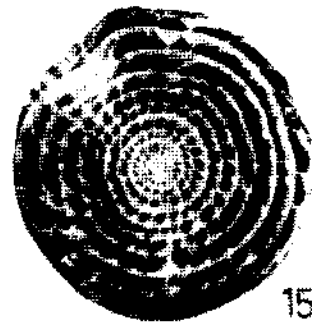
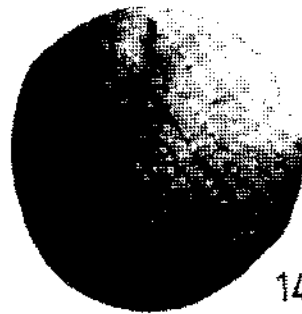
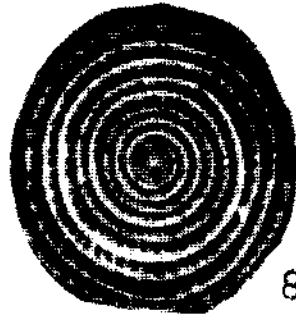
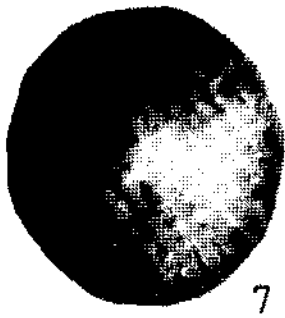
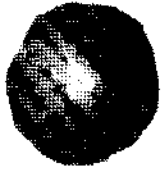
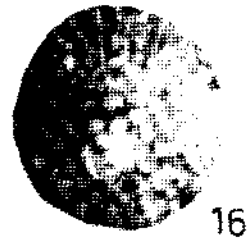
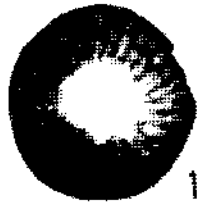


PLATE - II

Nummulites perforatus (De Montfort)

Fig. 1 - Equatorial section, microspheric figure, (I-684/A), X 4

Fig. 2 - Outer appearance, macrospheric figure, (I-676), X 5

Fig. 3 - Equatorial section, macrospheric figure, (114/A), X 6

Nummulites puschi D'Archiac and Haime

Fig. 4 - Equatorial section, microspheric figure, (453), X 3

Fig. 5 - Outer appearance, macrospheric figure, (453), X 5

Fig. 6 - Equatorial section, macrospheric figure, (453), X 5

Assilina exponens (Sowerby)

Fig. 7 - Outer appearance, macrospheric figure, (507), X 4

Fig. 8 - Equatorial section, macrospheric figure, (507), X 4

Qiscocyclina sella (D'Archiac)

Fig. 9 - Outer appearance, macrospheric figure, (I-684/J), X 22

Fig. 10 - Equatorial section, macrospheric figure, (I-684/J), X 25

Fig. 11 - Embryonic section, equatorial section, macrospheric figure, (I-684/J), X 100

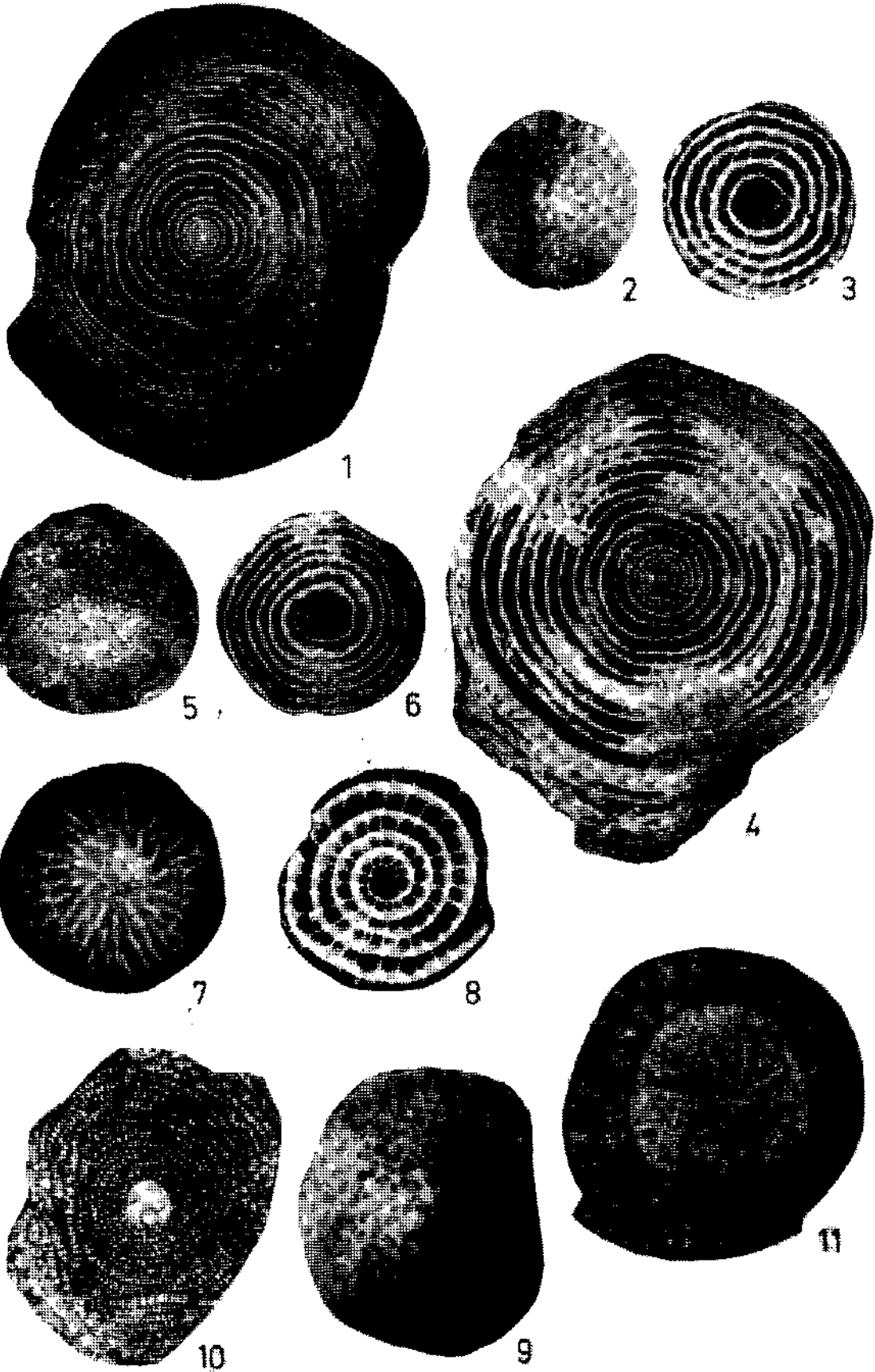


PLATE - III

Actinocyclus radians (D'Archiac)

- Fig. 1 - Outer appearance, macrospheric figure, (I-684/Ī), X 8
Fig. 2 - Equatorial section, macrospheric figure, (I-684/Ī), X 12
Fig. 3 - Embryonic section, equatorial section, macrospheric figure, (I-684/Ī), X 29

Lepidocyclus tournoueri (Lemoine and Douville)

- Fig. 4 - Equatorial section, macrospheric figure, (I-690/D), X 25

Miogypsinoides complanatus (Schlumberger)

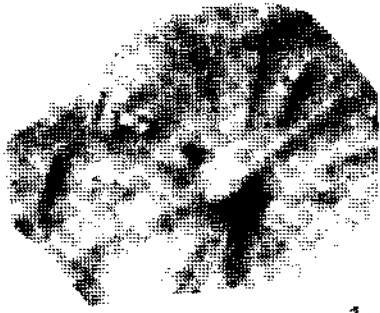
- Fig. 5 - Equatorial section, macrospheric figure, (156/1), X 28
Fig. 6 - Equatorial section, macrospheric figure, (I-688/D), X 40

Miogypsina irregularis (Michelotti)

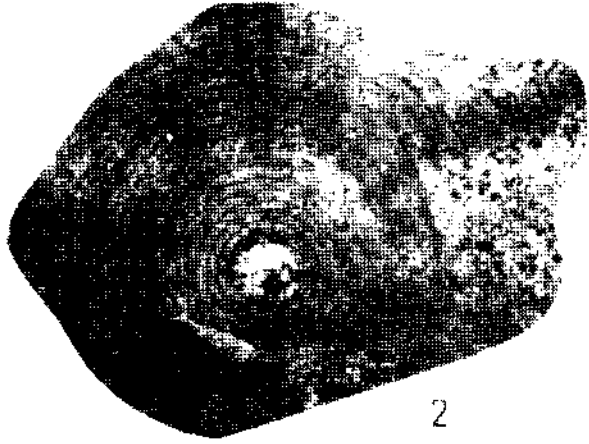
- Fig. 7 - Outer appearance, macrospheric figure, (201), X 20
Fig. 8 - Equatorial section, macrospheric figure, (201), X 21

Miogypsina intermedia Drooger

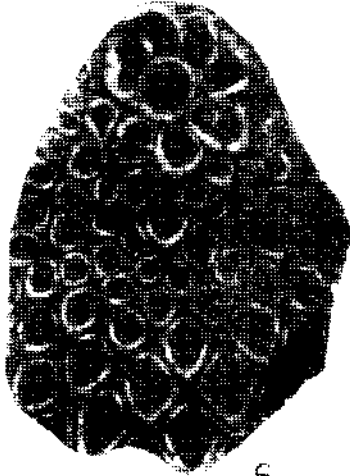
- Fig. 9 - Outer appearance, macrospheric figure, (Ī-203), X 23
Fig. 10 - Equatorial section, macrospheric figure, (Ī-203), X 27



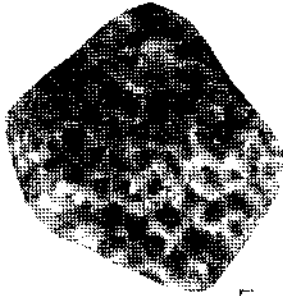
1



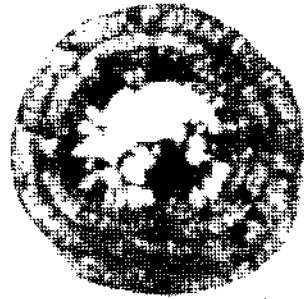
2



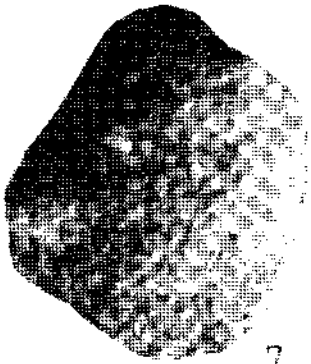
3



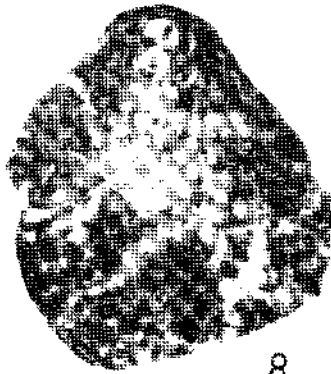
4



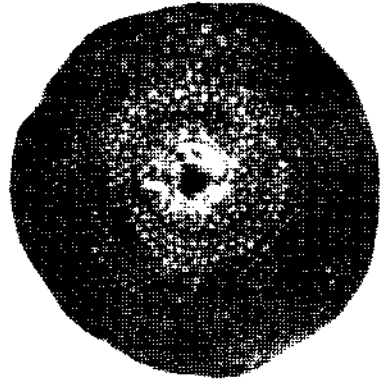
5



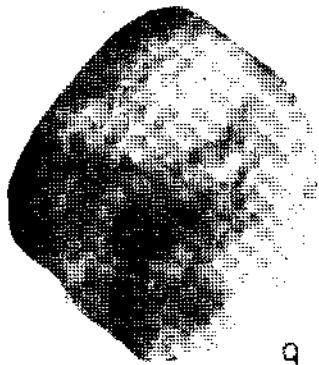
6



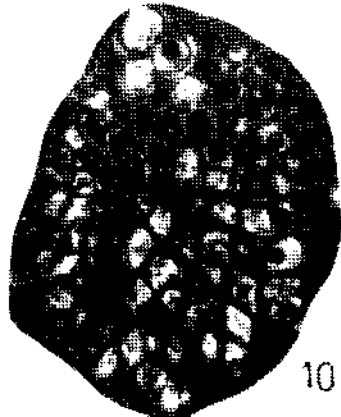
7



8



9



10

- Mulder, E.F.J., 1975, Microfauna and sedimentary-tectonic history of the Oligo-Miocene of the Ionian Islands and western Epirus (Greece): Utrecht Micropal. Bull., 13, 5-129.
- Nemkov, G.I., 1964, Distribution zonale des assises Eocenes de l'U.R.R.S. d'après les Nummulitides: Mem. Bul. Rech. Geol. Min., Fr., 28, 761-765.
- , 1968, Les Nummulites de l'U.R.R.S., leur evolution, systematique et distribution stratigraphique: Colloque Eocene, Mem. Bul. Rech. Geol. Min., Fr., 58, 71-78.
- Neumann, M., 1958, Revision des Orbitoides du Cretace et de l'Eocene en Aquitaine occidentale: Mem. Soc. Geol. Fr., 83, 174 p.
- Papa, A., 1968, Les molasses Eocenes de l'Albanie sud-orientale: Colloque Eocene, Mem. Bul. Rech. Geol. Min., Fr., 58, 663-673.
- Plaziat, J.-C. and Renzi, M., 1968, Correlation a l'aide de macrofaunes marines entre l'Ilerdien du Bassin de Tremp (Lerida-Espagne) et la serie cuiso-lutetienne des Corbieres (Aude-France): Colloque Eocene, Mem. Bul. Rech. Geol. Min., Fr., 58, 575-581.
- Rahaghi, A., 1974, Etude de quelques grands Foraminiferes de la formation de Qum (Iran Central): Revue de Micro-paleontologie, 16, 1, 23-38.
- Raju, A., 1974, Study of Indian Miogypsinidae: Utrecht Micropal. Bull., 9, 1-128.
- Sakıncı, M., 1982, Geology, biostratigraphy and paleontology of the Mollababa-Uruman (Muş province): Bull. of the Earthsciences, Istanbul, 3, 1-2, 235-275 (in Turkish).
- Schaub, H., 1963, Ueber einige Entwicklungsreihen von Nummulites und Assilina: Evolutionary trends in foraminifera, The Van Der Vlerk Annivers'de, 282-297, Elsevier, Amsterdam.
- , 1981, Nummulites et Assilines de la Tethys Paleogene; Taxinomie, phylogenese et biostratigraphie: Schweizerische Paleontologische Abhandlungen, Memoires Suisses de Paleontologie, 105.
- Schlumberger, C., 1900, Note sur le genre Miogypsina: Bul. Soc. Geol. France, 28, 3, 327-333.
- , 1903, Troisieme note sur les Orbitoides: Bul. Soc. Geol. France, 273-290.
- Sirel, E., 1976 *a*, Description of the species of Rhapydionina liburnica (Stache) and Rhapydionina malatyaensis and a new approach to the genus Rhapydionina stache: MTA Bull., 86, 99-104 (in Turkish).
- , 1976 *b*, Description of the Eoannularia conica sp. and a new approach to the limestones in the vicinity of Darende-Gürün (W of Malatya), of Upper Lutetian-Lower Priabonian: Bull. of Geol. Soc. of Turkey, 19, 2, 79-82 (in Turkish).
- and Gündüz, H., 1976, Stratigraphic distribution and description of the Some of the species of the genus Nummulites, Alveolina and Assilina of Ilerdian, Cuisian and Lutetian: Bull. of Geol. Soc. of Turkey, 19, 1, 31-44 (in Turkish).
- Sowerby, C.J. DE., 1840, In: Sykes, W.H., A notice respecting some fossils collected in Cutch, by Capt. Walter Smee, of Bombay Army: Geol. Soc. Trans., London, 2,5, 715-719.
- Varentsov, M.I. and Menner, V.V., 1933, On the age of some horizons of the Paleogene of the Gorsky region of Georgia (Russian): Neftianyi geologo-racvedochnyi institut, Informatsionnyi Sbornik (Information Bull. of the Oil Geol. Inst.), 2-3, 104, Moscow.
- Veillon, M., 1964, Les zones de Foraminiferes du Ealeogene Nord-Aquitain et leur valeur stratigraphique: Mem. Bul. Rech. Geol. Min., Fr., 28, 227-242.
- Yoldaş, R., 1972, Geology and petroleum potential of the region north of Malatya: MTA Rep. 4936 (unpublished), Ankara (in Turkish).

EXISTANCE OF UPPER LUTETIAN IN THE MUŞ TERTIARY BASIN

Şükrü UYSAL*

ABSTRACT.— The studied area lies in the north of Azakpur town in the east of Muş Tertiary basin. In this study, the age of the towermost levels of the basin, which was unknown, has been determined as the Upper Lutetian. These Upper Lutetian rocks consist of claystone-sandstone-conglomerate alternation. Lower levels gradually pass marine sequence. Lower-Middle Oligosen rocks, consisting of a limy claystone-sandstone alternation, overlie unconformably Upper Lutetian rocks with a conglomeratic level. Upper Oligocene-Lower Miocene rocks overlie the Lower-Middle Oligocene sequence conformably. They are made up of limy claystone-sandstone alternation with rare limestone interbeds and they reflect deep marine conditions. Lower Miocene rocks comprise limy claystone, conglomerate, sandy limestone and reefal limestone, and indicate shallow marine conditions. Pliocene terrigenous formations unconformably overlie the Lower Miocene rocks and composed of conglomerate, sandstone and claystone. They also include some lacustrine limestone and volcanic levels.

GEOCHEMICAL PROSPECTING FOR CARBONATE-BEARING LEAD-ZINC DEPOSITS IN THE WESTERN ZAMANTI (ALADAĞLAR-YAHYALI) REGION

Ahmet AYHAN* and Mehmet ERBAYAR**

ABSTRACT. — Characteristic sampling methods and dispersion types formed by secondary processes (karstification) have been determined for the exploration of burried carbonate-bearing lead-zinc deposits in the Aladağ Region by studying such minor elements as Cu, Pb and Zn. The most favorable geochemical prospecting method in this area is determined to be soil surveying of the overburden, tectonically crushed zones and rock talus fans. The widespread secondary dispersions are created by chemical and mechanical accumulations. The dispersions cover rather wide areas, due to the soil formation, effects of surface-and undergroundwaters and glacial movements. A study of anomalies of Pb and Zn elements deposited by chemical means is the best way for the prospecting of burried ore deposits.

INTRODUCTION

The lead-zinc belt of Zamanti region is the most important mining district from the view of tonnage and distribution among the similar ore deposits of Taurus Mountains. Aladağ region is located in the western part of this belt in the vicinity of Yahyalı (Kayseri) and Çamardı (Niğde) (Fig- 1).

There are a lot of carbonate-bearing lead-zinc deposits and occurrences in the Aladağ region. Some of these occurrences and ore deposits, which were formed by karstification processes, are not exposed. Any effective geochemical prospecting method to find out either burried ore deposits showing no outcrops, or probable ore bodies between operating mines has not yet been developed for this area.

Kaleköy lead-zinc deposit situated in the central part of Zamanti in the eastern part of the studied area, was investigated by Köksoy (1964), who carried out his geochemical studies both directly upon the deposit and its surroundings. Because of the development of a residual soil cover on the Devonien limestones, suitable for a detailed geochemical prospecting, he collected systematical soil samples and correlated SP anomalies. Number of occurrences and ore deposits in the lead-zinc belt of Zamanti are found mainly in the sequences of carbonates of the different tectonic units deposited in different environments during the time between Devonien and Cretaceous. Because of absence of a proper soil cover on the rocks, systematical soil sampling was not possible. For this reason, the study carried out in Aladağ region, is considered to be the most convenient geochemical prospecting method applicable to the Zamanti belt. In the present study a suitable general geochemical prospecting method is proposed. In addition, definite sorts of secondary dispersion are also ascertained.

GEOLOGY

In the Aladağ region the following tectonic units are determined from north to south (Fig. 1):

- Yahyalı nappe (Devonian-Triassic)
- Siyah Aladağ nappe (Upper Devonian-Jurassic)
- Çataloturan nappe (Lower Carboniferous-Permian)
- Minaretepelер nappe (Upper Triassic)
- Beyaz Aladağ nappe (Upper Triassic-Jurassic)
- Aladağ ophiolitic melange (Upper Cretaceous)

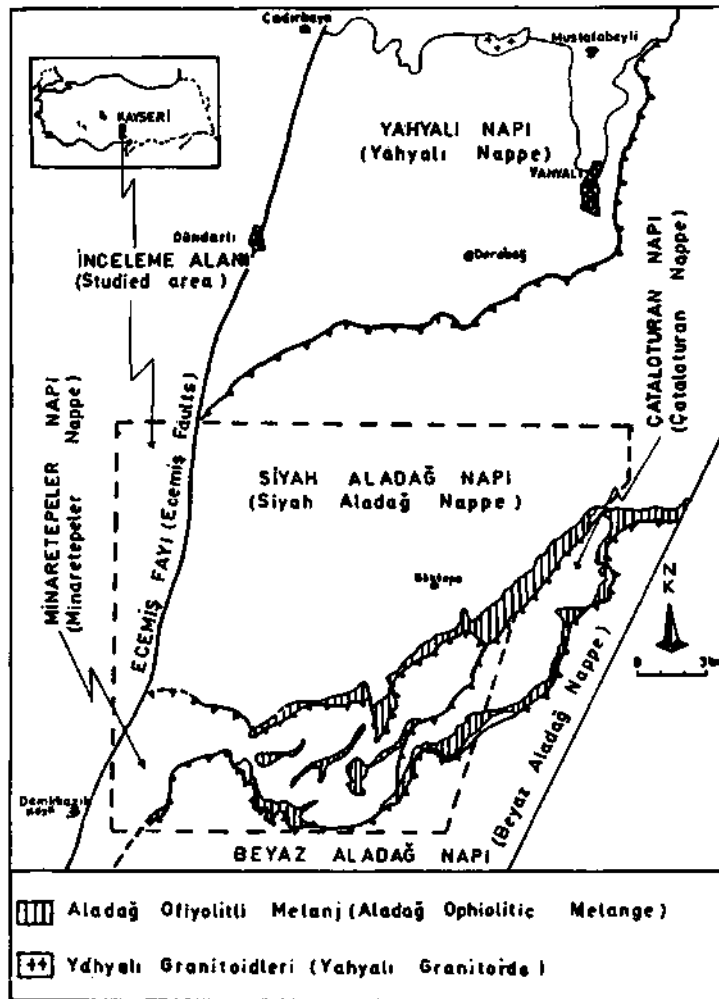


Fig. 1 - Location map and geological setting of studied area in the Aladağ Region.

Yahyalı Granitoids which exposed only along the northern border of Yahyalı nappe to the north of the studied area, intruded into these rocks. They lie under a thick sequence of nappes, placed one on top of the other.

Tertiary sediments are deposited only in a small area between Maden Boğazı and Minaretepelер section. Tectonic units, which have thrust over each other, contain mainly platform carbonates. This region was overthrust in Maestrichtian time (Tekeli, 1980). Apart from Beyaz Aladağ and Çataloturan nappes, all other nappes carry some traces of mineralization.

Primary carbonate-bearing lead-zinc in western Zamantı are deposits believed to be hydrothermal in origin and probably related to Yahyalı granitoids. This phase is represented mainly by sulphide ore minerals such as galenite and sphalerite. After the ore deposits were formed, they were redeposited again by multikarstification processes and meanwhile they were altered into secondary minerals such as smithsonite, serusite and limonite (Ayhan, 1983a, 1983b). Occurrences, which are completely tectonically controlled, replaced the fractures of carbonate rocks, belonging to the above-mentioned three tectonic units. The largest unit of the studied area is the Siyah (Black) Aladağ nappe, which includes the biggest ore deposit.

GEOCHEMICAL PROSPECTION

Methods of sampling and analyses

In the studied area, because of intensive karstification, unsuitable climate conditions and topographic position, a convenient soil cover has not been developed. Very steep parts of the field are covered with the host rocks and talus fans at the both sides of valleys. A very thin overburden originated from its surrounding limestones has been developed only in more or less flat areas. In all other areas there aren't any sort of trees or other wide-spread plantation. Furthermore, the Aladağ Region is topographically in the highest position in the vicinity of Yahyalı and Çamardı, where extremely fractured carbonate rocks exposed. For this reason, no water springs exist in any other formations apart from ophiolitic melange belts and marl-bearing sequences. There is only a seasonal water activity at the beginning of spring time.

Considering the mining activities in the Zamantı District from the Hitite times to present (exploitation and smelting (Metag and Stolberg, 1971), the roads and paths connected the deposits or near settlements, following gentle morphological grounds, valley floors and streams. Under these factors, in the studied area, it's concluded that a suitable geochemical prospection can not be carried out by getting systematical water and stream sediment samples.

In as much as mineralization controlled by tectonic activities, a geological map should include all detailed tectonic structures, before the geochemical prospection starts. The relation between mineralization and tectonic features was investigated during the field work and, hence what sorts of samples from where needed to be collected was established. It's suggested that, the sampling be carried out on profiles perpendicular to the tectonic lines having ore potentials or along certain fault zones and rock talus fans. Soil samples were taken with convenient intervals and enough numbers depending upon the topographic position of the area, the lengths of fracture zones, and the distribution of soil and talus fans. Sampling depth was selected due to thickness of soil and talus fans. Trenches were dug down to host rock where thin soil covers the surface. As the samples were taken from fine fractions of components of covers next to host rocks, sampling in thick covers was proceeded from relatively deeper zones (up to 1-2 m), where finest components of soil were present.

Soils on the ore-bearing fractures are red-brown in colour, because of Pb and Zn oxides. This situation can be easily distinguished in the field from typical mylonites of fault zones and guide probable mineralization part. Fractured zones show similar cases or same colors. 1159 soil samples (200-500 gr) were collected from 300km², dried, sieved to minus 80 meshes fraction and packed.

Development of the cheapest prospecting method to find out carbonate-bearing Pb-Zn deposits was the aim of this work; so base elements such as Cu, Pb and Zn were analysed. These elements have also successfully been used in exploration of many lead-zinc deposits. The elements in soil samples

were analysed in the laboratories of MTA by Atomic Absorption Spectrometre. The results of analyses were carried into the computer and interpreted at the MTA computers center through the programming language of FORTRAN-4 with programmes of Listat and Poponal I and II.

Anomalies and their evaluation:

The Cu, Pb, Zn contents of soil samples, collected from Yahyalı granitoids, Aladağ ophiolitic melange belt, Tertiary sediments and other geological formations, except, the marl-mudstone sequences, were evaluated. Only four groups of these rock units; Siyah Aladağ-Permian limestones, Siyah Aladağ-Jurassic limestones, Minaretepelers limestones and Beyaz Aladağ-Limestones showed typical and certain anomaly populations (Fig. 2 and 3) and cumulative frequency curves of the Pb and Zn values measured from these limestones and plotted in the figure 4 and 5. As it's known from many geochemical studies, elements have log-normal distributions (Ahrens, 1954 and 1957). From this point of view, it's supposed that the Pb and Zn values dispersed in four different limestone groups show log-normal distribution. The values of both elements display narrow distributions around the mean values and their log intervals were calculated as 0.20 (Table 1 and 2). In respect to this log interval, minimum 10 and maximum 16 classes were obtained in each group.

The cumulative frequency points plotted in the probability graphs indicate more than one straight line. The positive skewness point of these lines is known as threshold (t) value. As a background value (b) on the regular cumulative frequencies a point where the frequency line and the line drawn parallel to the abscissa from the 50 % point on the ordinate axis intersect, is taken as a background value. This value gives geometric average of results. Values lying over threshold, represent anomalies. Values of points obtained by intersecting of straight lines and probability lines at 97.5 % and 2.5 % on log probability plot, give ± 2 standard deviation.

All the cumulative frequency curves, which reflect the distribution of Pb element in four different carbonate units, show positive skewness (Fig. 4) The positive skewness of cumulative frequency curves for Minaretepelers and Beyaz Aladağ limestones are found between 25 % and 35 % levels. This situation points out, that the populations in both limestones reveal high values (Lepeltier, 1969). Threshold values calculated for each unit are given in figure 4. Here, the part lying above the threshold line represents the main and normal population and the part below it anomalous populations. The distribution and threshold values of zinc element for the same rock groups, demonstrate same differences with respect to the Pb element (Fig. 5). For example, while on the straight lines indicate low values on the probability graphs for zinc, some breaks were observed, but no breaks on the lines of lead values. Low sensitivity of the analyses is responsible for such sort of breaks like at the curve of Pb. 100 of the 463 samples taken from Siyah Aladağ-Permian limestones have low values under 40 ppm. Although these measurements were repeated by AAS three times, where the values over the error limits (± 20 %). This case caused some breaks and deviations in the low valued parts of the cumulative frequency curves.

The curves belonging to Siyah Aladağ-Permian limestones and Jurassic limestones give clearly positive skewnesses (Fig. 5). On the other hand, as it was illustrated on the curve of Siyah Aladağ-Permian limestones, the positive skewness is found sometimes just below 2.5 % probability line. Such a situation indicates little amounts of high values. If the breakings related to the low values for Minaretepelers and Beyaz Aladağ limestones are not taken into consideration. Although they don't show any important skewnesses (positive and negative) in these limits, they give a single distribution staying in the error limits (Lepeltier, 1969).

Table 1 - Distribution tables of Zn values for soil formation on the rocks (n= number of samples):

- a - Siyah Aladağ-Permian limestones (n=463).
 b - Siyah Aladağ-Jurassic limestones (n=445).
 c - Minaretepelir limestones (n=179).
 d - Beyaz Aladağ limestones (n=67).

Sınıf aralığı (Log. Int.)	a			
	ppm	f	cf	% cf
1.07	11.75	3	463	100.00
1.27	18.60	5	460	99.30
1.47	29.50	12	455	98.20
1.67	46.80	74	443	95.70
1.87	74.10	103	369	79.70
2.07	117.50	113	266	57.50
2.27	186.00	84	153	33.00
2.47	295.00	38	69	14.90
2.67	468.00	17	31	6.70
2.87	741.00	8	14	3.00
3.07	1175.00	1	6	1.30
3.27	1860.00	1	5	1.07
3.47	2950.00	1	4	0.86
3.67	4680.00	2	3	0.64
3.87	7410.00	1	1	0.21
4.07	11750.00	1	1	0.21
b				
1.47	29.5	2	445	100.00
1.67	46.8	16	443	99.70
1.87	74.1	71	427	96.00
2.07	117.5	131	356	80.00
2.27	186.0	105	225	50.50
2.47	295.0	84	120	27.00
2.67	468.0	17	36	8.00
2.87	741.0	9	19	4.20
3.07	1175.0	—	—	—
3.27	1860.0	5	10	2.20
3.47	2950.0	3	5	1.00
3.67	4680.0	2	2	0.45
3.87	7410.0	2	2	0.45
c				
1.47	29.8	4	179	100.00
1.67	46.8	2	175	97.70
1.87	74.1	14	173	93.60
2.07	117.5	32	159	88.80
2.27	186.0	43	127	70.90
2.47	295.0	41	84	46.90
2.67	468.0	24	43	24.00
2.87	741.0	12	19	10.60
3.07	1175.0	6	7	3.90
3.27	1860.0	1	1	0.56
3.47	2950.0	1	1	0.56
d				
1.47	29.5	—	—	—
1.67	46.8	3	67	100.00
1.87	74.1	1	64	95.50
2.07	117.5	18	63	94.00
2.27	186.0	19	45	67.00
2.47	295.0	7	26	38.80
2.67	468.0	12	19	28.35
2.87	741.0	6	7	10.44
3.07	1175.0	1	1	1.49
3.27	1860.0	1	1	1.49

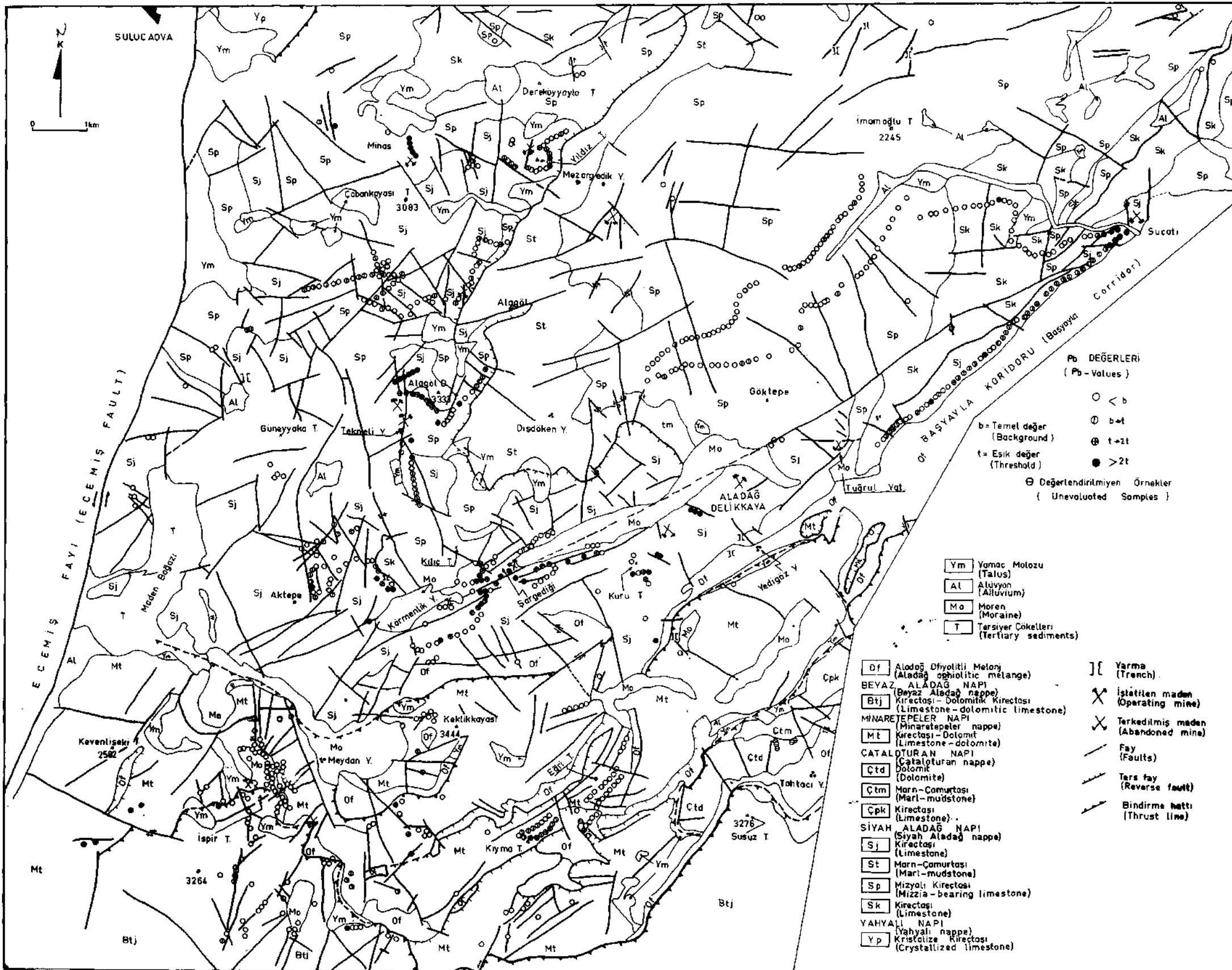


Fig. 2 - Geochemical anomaly map of the Western Zamanlı for lead.

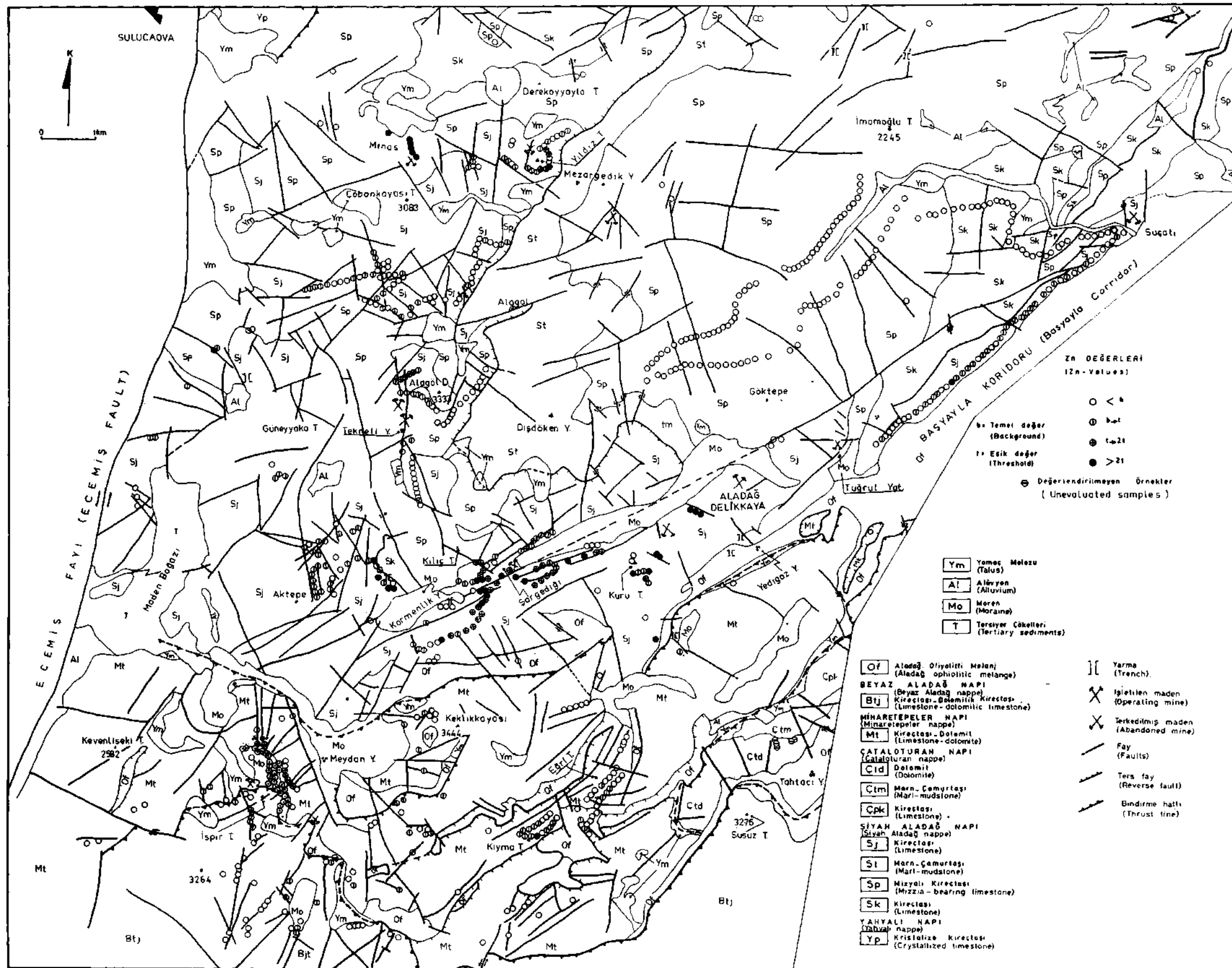


Fig. 3 - Geochemical anomaly map of the Western Zamanlı for zinc.

Table 2 - Distribution tables of Pb values for soil formation on the rocks (n= number of samples):

- a - Siyah Aladağ-Permian limestones (n=463).
 b - Siyah Aladağ-Jurassic limestones (n=445).
 c - Minaretepeler limestones (n=183).
 d - Beyaz Aladağ limestones (n=68).

Sınıf aralığı (Log. Int.)	ppm	a		
		f	cf	% cf
1.27	18.6	4	463	100.00
1.47	29.5	114	459	99.00
1.67	46.8	138	345	74.50
1.87	74.1	113	207	44.70
2.07	117.5	54	94	20.30
2.27	186.0	19	40	8.60
2.47	295.0	9	21	4.50
2.67	468.0	5	12	2.60
2.87	741.0	—	—	—
3.07	1175.0	3	7	1.50
3.27	1860.0	3	4	0.86
3.47	2950.0	1	1	0.21
3.67	4680.0	—	—	—
b				
1.67	46.8	75	445	100.00
1.87	74.1	85	370	83.00
2.07	117.5	130	285	64.00
2.27	186.0	93	155	35.00
2.47	295.0	49	62	14.00
2.67	468.0	—	—	—
2.87	741.0	5	13	2.92
3.07	1175.0	—	—	—
3.27	1860.0	3	8	1.79
3.47	2950.0	1	5	1.00
3.67	4680.0	1	4	0.89
3.87	7410.0	1	3	0.67
4.07	11750.0	3	—	—
c				
1.27	18.6	—	—	—
1.47	29.5	5	180	100.00
1.67	46.8	42	175	97.20
1.87	74.1	63	133	73.80
2.07	117.5	30	73	40.50
2.27	186.0	16	43	23.80
2.47	295.0	11	27	15.00
2.67	468.0	10	16	8.80
2.87	741.0	5	6	3.30
3.07	1175.0	1	1	0.56
3.27	1860.0	—	—	—
d				
1.27	18.6	—	—	—
1.47	29.5	4	68	100.00
1.67	46.8	24	64	94.00
1.87	74.1	16	40	58.00
2.07	117.5	7	24	35.30
2.27	186.0	8	17	25.00
2.47	295.0	4	9	13.30
2.67	468.0	4	5	7.34
2.87	741.0	—	—	—
3.07	1175.0	1	1	1.49
3.27	1860.0	—	—	—

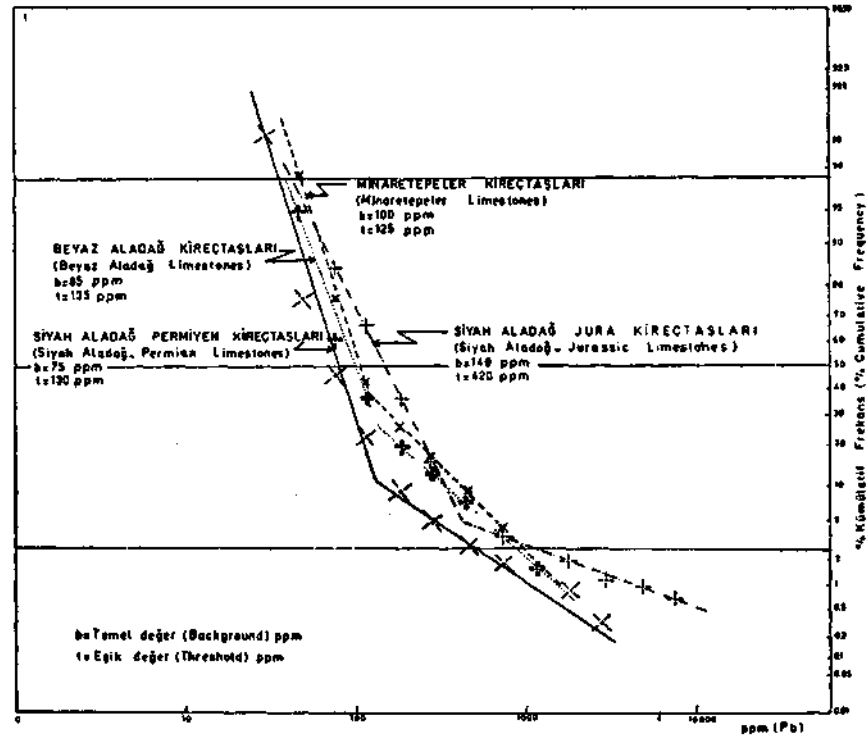


Fig. 4 - Cumulative frequency distribution of lead concentrations.

Although the inflection points of Frequency curves don't coincide with the line of + 2 standard deviation. In this method, the values correspond to the inflection points can be accepted as threshold values. This is simply because the samples collected from the known mineralized areas yielded high values of Pb and Zn and therefore cause the mean of the population to be high. In the north of İspir Tepe there is a moraine cover with a maximum thickness of 15 m., from where the soil samples were collected and Pb and Zn elements were determined. Their element contents reach up to 10.000 ppm. The main reason for high values is the İspir Tepe ore deposits, which occurred next to the southwest of moraine covers. Ore minerals were transported from ore deposits which mentioned above by the effects of mechanical processes such as glacier. After that, they were dispersed into fine grained components of moraines by partly chemical alteration. Chemical dispersion has a wide dimension, especially where the Pb and Zn sulfides can be solved, chemically transported and deposited under oxidation conditions at pH=6-8.5 and Eh (+) (Garrels, 1951).

The probable sources of anomaly values determined from soil samples, which lie on the Jurassic limestones of Siyah Aladağ Nappe extending along western slope of Başyayla Corridor, can be interpreted as in the following ways: a) The anomalies indicate a buried occurrence situated under a ridge chain extending toward Göktepe region, b) They can be originated from solutions of the Aladağ-Delikkaya mine, occurrences in the vicinity of Göktepe and Tuğrul mine, c) Mechanical transportation by glacial movements. Considering the second probability, the anomaly is concerned within non-significant anomalies. Because the topographic position inconvenient for the solution to move, possibilities are weak to cause such anomalies. The same situation was observed along western slope of Zindandere in the east of Mezargedik occurrences. On the other hand, it must be considered, that the distribution and the movements of acidic waters derived from a mining waste, might cause of such non-significant anomalies.

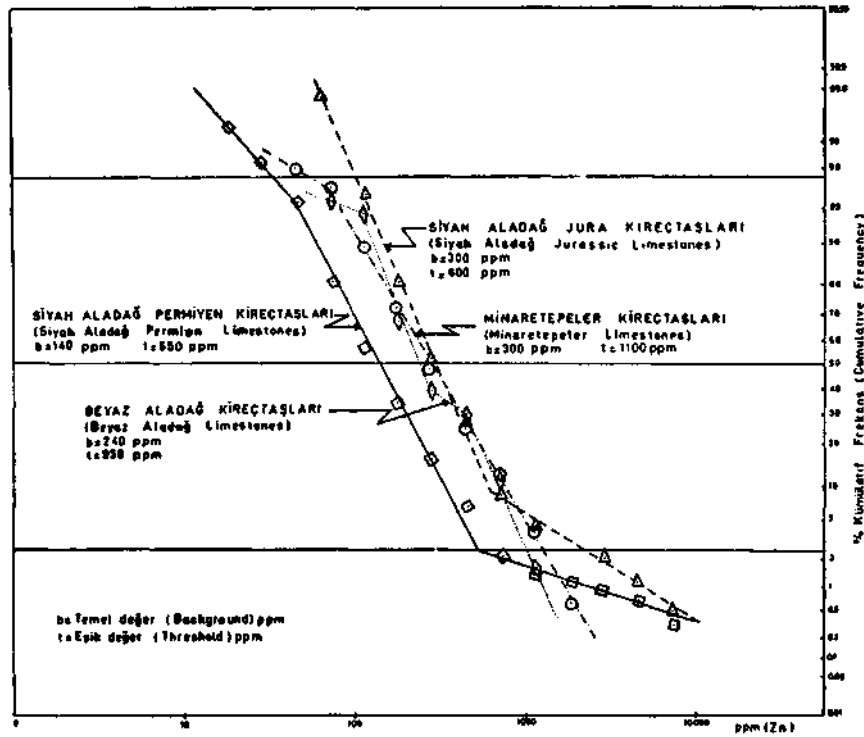


Fig. 5 - Cumulative frequency distribution of zinc concentrations.

Samples taken from the soil formation on the Upper Permian and Jurassic limestones of the Siyah Aladağ Nappe, contain high values of Pb and Zn. These values are higher than the values obtained in other countries. Zn contents of soil samples collected from different countries and determined by Swaine (1955) vary between 10 and 300 ppm with an average of 70 ppm. According to this researcher, the average value of soil is 15 ppm. The higher Pb and Zn anomaly values of samples taken from our area is related first of all to the widespread occurrences exposed in the region. Moreover, the elements bound in clays, iron oxides and organic materials would be transported to certain distances, is another fundamental reason for the high values. This concept was confirmed by the following factors: Carbonate sequences of Siyah Aladağ Nappe contain high bituminous material, and pyrite minerals were weathered into iron oxides during the karstification stages and therefore, clay minerals occurred in karstification environment (Ayhan, 1983a).

Table 3 - Cu values of soil formations on the rocks.

Birim (Unit)	Örnek Sayısı (Number of samples)	Min. değer (Min. value)	Mak. değer (Max. value)
Siyah Aladağ - Permian	238	5 ppm	264 ppm
Siyah Aladağ - Jura	384	6 ppm	66 ppm
Minaretepe	157	12 ppm	89 ppm
Beyaz Aladağ	56	20 ppm	72 ppm

The Zn contents of analysed samples are generally higher than Pb contents. Because, the metal ions such as Zn^{+2} , Cu^{+2} , Pb^{+2} , Hg^{+2} and Fe^{+3} possess a low geochemical mobility under supergen conditions and the mobility decreases from zinc to iron (Dall'Aglia and Tonani, 1972). Beside the mobilities of both elements, their solubility differences rule the dimensions of secondary dispersions. Minerals such as cerussite and anglesite generated from galenite under oxidation conditions can not be desolved easily. On the other hand, zinc and copper sulphates formed under similar conditions can be easily soluble and they create widespread characteristic secondary dispersions (Levinson, 1974). The Pb values are relatively higher than the Zn values in İspir Tepe and Kargediği. Main reason for this situation is, both chemical dispersion occurred during multikarstification processes and mechanical dispersions appeared during glacial movements, which formed U-shaped valleys in this parts of the Aladağ Region.

Cu contents of soil samples collected from all carbonate sequences didn't give any anomalous populations. As it is observed in table 3, they showed copper content in the range of 5 to 264 ppm. However, most of the samples contain under 50 ppm Cu, copper values of samples taken from various parts of Tekneli Pb-Zn deposit vary between 20 and 100 ppm (Metag and Stolberg, 1971). On the other hand this element, which was measured in carbonate rocks of the same deposit, shows the varying values between 4 and 10 ppm (Ayhan, 1985). Copper minerals in Pb-Zn deposits of the region can be recognized only in microscopic scale. Therefore, soil formations found around this deposit include more Cu element than the soil formations of other sterile parts of the region. These indicate, that the higher Cu values could have been originated from lead-zinc occurrences.

CONCLUSIONS

Soil samples taken from talus fans, fractured zones and soil formations developed on five nappes lying one upon another in the Aladağ region were geochemically determined. Pb and Zn contents of soil formations on a few carbonate rocks belonging to Siyah Aladağ, Minaretepel and Beyaz Aladağ gave typical and certain anomalous populations. The following threshold values were found on the cumulative frequency curves for Pb and Zn: Siyah Aladağ-Permian limestones: 130 ppm and 530 ppm, Siyah Aladağ-Jurassic limestones: 420 ppm and 600 ppm, Minaretepel limestones: 125 ppm and 1100 ppm, Beyaz Aladağ limestones: 135 ppm and 240 ppm. Most of the cumulative lines show generally a positive skewness (and stay in the confidence limits, i.e. in general 5 %).

The results of analyses of the geochemical soil samples taken from the studied area having an irregular thin soil cover were interpreted together with field observations and three sorts of secondary dispersions obtained from lead-zinc prospection were distinguished:

- 1 — Dispersion through directly mixing of ore minerals with the soils during the formation of soil and rock talus fans,
- 2 — Dispersion through mechanical and chemical transportation of ore-forming constituents by underground waters into fractured tectonic lines and previously formed soil covers,
- 3 — Dispersions created both by the breaking out of the ore-bearing occurrences and by transportation of soil formations rich in Pb and Zn found in the vicinity of occurrences during glacial movements.

The chemical kind of dispersions especially posses a key character for the prospection of burried occurences. For this reason, the probably located occurences effected by these processes can be detected by sampling and interval of 20-50 m.

As primary mineralization originated from hydrothermal solutions which migrated and dispersed in short distances, except along some fractures and furthermore the anomalies derived from them have been fully overprinted by the widespread secondary dispersions, it's impossible for favorable geochemical prospection to be carried out by the primary dispersions.

Soil samples collected from the studied area show high values of Pb and Zn. These values are directly related to the presence of many occurrences in the region to effectiveness of glacial movements and to dispersions bounded with the clayey and bituminous materials. Some Pb anomalies are higher than the Zn anomalies. This confirms, that the mechanical transportation and dispersion were effective than the chemical one in some places.

The anomalies obtained from the north of Kıyma Tepe, in the eastern part of Minaretepelers nappe, were created either by a probable mineralization situated at depth or by leakages originated from Aladağ-Delikkaya mine.

In the light of field observation and geochemical data, anomalies obtained from some parts of Kargediği, western slope of Zindandere and Başyayla Corridor, from the south and north part of Çobankaya Tepe indicate the necessity of a more close geochemical sampling (Detailed prospecting) and of excavation of shallow trenches and short galleries, where the high values of both minor elements were measured.

ACKNOWLEDGEMENTS

Grateful acknowledgement is made at General Directorate of MTA for the facilities of this work. We wish to express our thanks to Turhan İnam, Yunus Lengeranlı and Necmettin Çeltak from Mineral Exploration Department of MTA, who collected samples.

Manuscript received, October 18, 1985

REFERENCE

- Ahrens, L.H., 1954, Lognormal distribution of the elements: *Geochim. Cosmochim. Acta*, 5,49-73.
- , 1957, Lognormal-type distributions: *Geochim. Cosmochim Acta*, 11, 205-212.
- Ayhan, A., 1983a. Aladağ yöresi karbonatlı kurşun-çinko-yataklarının kökeni: *Türkiye Jeol.Kur. Bült.*, 26,2,105-116.
- , 1983b, Genetic comparision of Pb-Zn deposits of Ceatral Taurus: 1. International Symposium on Taurus Belt, Abstracts, 100-101, Ankara.
- , 1985, Tekneli (Çamardı-Niğde) Pb-Zn yatağında jeokimyasal incelemeler ve Bleischweif oluşumu (hazırlanmakta).
- and Lengeranlı, Y., 1985, Yahyalı-Demirkazık arasının (Aladağlar) jeolojisi (hazırlanmakta).
- Dall'Aglio, M. and Tonani, F., 1972, Hydrogeochemical exploration for sulfide deposits: Jones, M.J., ed., *Geochemical exploration da.*, 305-314 London.

- Garrels, R.M., 1953, Mineral species as functions of pH and oxidation-reduction potentials, with special reference to the zone of and secondary enrichment of sulfide ore deposits: *Geochim. Cosmochim Acta*, 4, 5, 153-158.
- Köksoy, M., 1964, Kaleköy Madeninin (Develi)'de jeokimyasal prospeksiyon çalışmaları: *Symposium on Mining Geology and the Base Metals*, 249-258, Ankara.
- Lepeltier, C., 1969, A simplified treatment of geochemical data by graphical representation: *Econ. Geol.*, 54, 5, 538-550.
- Levinson, A.A., 1974, *Introduction to exploration geochemistry*-.Applied Publishing, Calgary, 612 s.
- Metag and Stolberg, 1971, Zamantı kurşun-çinko projesi nihai raporu, Maden sahalarının jeolojisi ve paleontolojisi: DPT Müsteşarlığı Rap., c.IV, 191 s. (unpublished) Ankara.
- Swaine, D.J., 1955, The trace element contents of soils: *Commonwealt Bureau Soil Sci. Techn., Comm.*, 48, England.
- Tekeli, O., 1980, Toroslarda Aladağların yapısal evrimi: *Türkiye Jeol. Kur. Bült.*, 23, 1, 11-14.

REMARKS ON DIFFERENT METHODS FOR ANALYZING TRONA AND SODA SAMPLES

Gülay ATAMAN*; Süheyla TUNCER* and Nurgün GÜNGÖR*

ABSTRACT. — Trona is one of the natural forms of sodium carbonate minerals. It is well known as «sesque carbonate», «urao» or «trona» in the chemical literature, and the chemical formula of the compound is $[\text{Na}_2\text{CO}_3, \text{NaHCO}_3, 2\text{H}_2\text{O}]$. The aim of this work is to adapt the standard methods for the analysis of trona samples, considering the interferences arising from silicates and other minerals found together with trona samples. In order to reduce the experimental errors, the analyses used for the determination of trona samples have been revised. The experimental results using potentiometric titration, AgNO_3 external indicator and BaCl_2 titration methods have been compared to theoretical results using statistical evaluations. 95 % confidence level, which is commonly used by analytical chemists, was employed as the basis of evaluation, R values, Student's t calculated at 95 % confidence level of 7 trona samples from Beypazarı, Student's t tabulated for the percentages of Na_2CO_3 , were found to be 0.008 in BaCl_2 method, 3.25 for AgNO_3 external indicator method and 3.26 for potentiometric method; for the percentages of NaHCO_3 the same values are 0.59 for BaCl_2 method, 2.83 for AgNO_3 external indicator method and 3.59 for potentiometric method. Systematic error is indicated when $R > 1$. In addition to quantitative analysis of trona samples, qualitative XRD analyses have been routinely performed for each sample and the results were found to be in good agreement.

INTRODUCTION

Trona is a naturally occurring form of sodium carbonate minerals. It may be named as «sesque carbonate», «urao» or «trona» the general formula for the compound is $[\text{Na}_2\text{CO}_3, \text{NaHCO}_3, 2\text{H}_2\text{O}]$. A double salt of sodium carbonate-sodium bicarbonate, trona is soluble in water. Crystals of this mineral is transparent or white, the color darkens with increased impurities. Its density is 2.1 g/cm^3 and hardness is 2.5-3 on Mohs scale.

Production of soda ash from trona is somewhat simpler than Solvay or Leblanc processes and can be accomplished at a lower cost. Solvay or Leblanc processes are well described in literature (1). Two variations of production of soda ash from trona are in use. One starts by dissolving trona ore (trona process); the other first calcines trona and then dissolves the crude soda ash thus produced (monohydrate process) (2). In both processes production of soda is particularly simple.

Sodium carbonate is one of the basic chemicals, and increase in its usage generally is parallel to the economical growth. Sodium carbonate is commonly employed in glass and ceramic, petroleum, aluminium, paper industries, manufacture of soap and detergents, in the production of caustic soda and sodium nitrate, ferrous and non-ferrous metallurgical processes.

The first natural resources of trona were discovered in the United States; initially in the west later in Green River, Wyoming (2). The other important resources are Mogadi Lake in Kenya and Texaco underground brines in Mexico. Ninety percent of world's production comes from the United States of America. In 1939, seventeen Solvay factories were actively operating in the U.S.A. Today only one of these is in operation, the rest have been replaced by natural soda. In Europe, however, the dependency on solvay process is still valid as no significant resources have been discovered.

TRONA RESOURCES IN TURKEY

Natural soda in Turkey, is present in lake Van and lake Arm which is nearby the former. The concentration of soda in lake water, however, is low and the time available for the use of solar energy is only 2-3 months per year; therefore soda production is not economical at the present time.

The first trona deposit in Turkey was found by Mineral Research and Exploration Institute (MTA) around Beypazarı, during coal exploration studies. The studies showed that trona is present 130-140 m deep, in layers which are thicker and richer in quality compared to the ones in the U.S.A. The results obtained from only such a limited area indicated the presence of nearly 200 million tons of trona. This reserve may be small in comparison to 50 billion tons reserve in Wyoming (U.S.A.). However, exploration activities in the same area show that discovery of new orebodies is possible. Such a resource will allow the production of chemicals such as "soda, sodium hydroxide and other sodium derivatives for about a hundred years. The resource which was found by MTA has been transferred to Etibank.

Scope of the work

The main purpose in trona analysis is the quantitative determination of water soluble carbonates. In most cases, however, trona is also present in clays and other minerals. Despite this fact, analytical methods were not developed considering these matrix conditions. The kind and quantity of clays and other carbonate compounds not separated from aqueous phase, require different kind of analytical methods. The purpose of this study has been the application of several analytical methods on core samples obtained from Beypazarı trona field. Investigations have been carried out in order to eliminate several analytical interferences affecting the accuracy of the results.

General information on analytical methods

X-ray diffraction spectrometry (XRDS) was used for qualitative analysis of samples, where other analytical methods were employed for quantification.

X-ray diffraction spectrometry: XRDS is a common method to determine the kind of minerals. The principle is the determination of the distances between crystal layers, employing the diffraction of X-rays of known wavelength, a diffractometer is used for analysis.

Other Analytical Methods: Two basic aims of the study were to find out the percentage of trona and determination of impurities. The analytical methods applied for these purpose are listed below.

Determination of trona percentage

- a. Total alkalinity-potentiometry
- b. Na_2CO_3 percentage-calculation by (a) and (c)
- c. NaHCO_3 percentage-potentiometry, volumetry (AgNO_3 and BaCl_2 methods)

Determination of impurities

- a. Water insoluble content (ASTM, 1980)
- b. SO_4 determination-Gravimetry (ASTM, 1980)

- c. Cl determination-Mohr method (ASTM, 1980)
- d. Ca⁺⁺ and Mg⁺⁺ determination-EDTA complexometry (ASTM, 1980)

Basic features of analytical methods used are given in «Experimental section».

EXPERIMENTAL

Reagents and solutions

All analytical reagents were of analytical purity. Deionized water used, contained all the species determined below their detection limits. All the solutions were prepared according to the directions in the references given below.

Instrumentation

A Jeol JDX-8P spectrometer with a Cu source operated at 40 kV and 20 mA, Ni filter were used for instrumentation.

For potentiometric measurements, initially a system consisting of a Corning Model pH-meter with a peristaltic pump, magnetic stirrer and a strip chart recorder was used. In later stages of the study, a TOA HSM 10A fully automatic titrator and finally Fisher model CAT automatic titrator with a microprocessor control were employed to further verify the results.

Conventional burettes and other glassware were used for AgNO₃-external indicator, BaCl₂, Mohr's and EDTA complexometric methods. Gravimetric determinations were realized by necessary conventional apparatus.

Preparation of samples

Solid samples were dried at 30°C and powdered prior to XRD analysis. For other analytical methods, samples were powdered and dried at 30°C and was dissolved in deionized water to yield a 20 g/l solution; after standing overnight, aliquots were drawn from this solution for analyses.

Analytical methods

For determination of trona percentage, the methods applied and their fundamental principles are given below and the, necessary adaptations have been made.

1. Potentiometry (Skoog, 1969)
2. BaCl₂ volumetric titration (Monographs, 1981)
3. AgNO₃ titration with external indicator (ASTM, 1980)
4. X-ray diffraction spectrometry

1. Potentiometric method. — Trona samples were titrated with 0.1 N HCl; and total alkalinity was calculated from second endpoint where carbonate and bicarbonate contents were calculated by using first endpoint. A titration curve and endpoints of a trona solution is given in Figure 1. In addition, the studies were carried out on pure Na₂CO₃ and synthetic Na₂CO₃-NaHCO₃ mixtures, clay+trona and finally dolomite (CaCO₃+MgCO₃) +clay+trona mixtures, in order to investigate on possible interferences in this method.

2. *BaCl₂ volumetric titration method.* — The principle in this method is transformation of bicarbonate ions into carbonate by NaOH, precipitation as BaCO₃ by BaCl₂, and back titration of excess NaOH by acid. Concentration of bicarbonate is thus determined. Carbonate content is found by calculation using also total alkalinity values.

3. *AgNO₃ titration with external indicator.* — The principle in this method is the determination of bicarbonate ions using NaOH as a titrant and AgNO₃ as an external indicator. Carbonate content is found by calculation using also total alkalinity values.

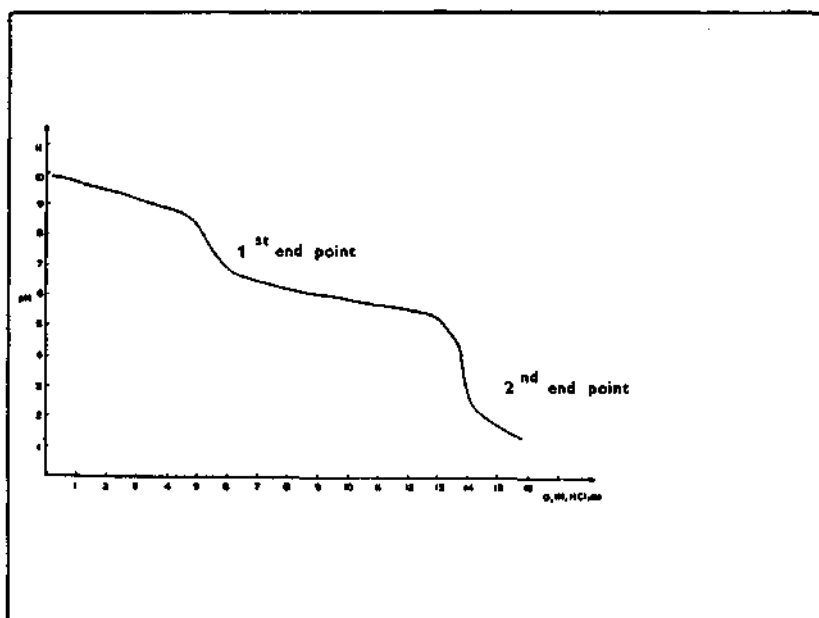


Fig. 1 - The endpoints in potentiometric titration of a trona sample with hydrochloric acid.

Appendix 1 — Some definitions for trona analysis

Total alkalinity : This represents the total of CO₃²⁻ and HCO₃⁻ ions contained by water soluble part of the sample, in terms of Na₂O and Na₂CO₃. This corresponds to total of Na₂CO₃ and NaHCO₃.

Example :

A sample which consists of 100 % trona, has a total alkalinity of

41.13 as Na₂O %, or

70.34 as Na₂CO₃ %

Na₂CO₃ % value : This corresponds to the real Na₂CO₃ as weight percentage in the sample.

Example :

A sample which consists of 100 % trona; has a Na₂CO₃ % value of 46.89.

NaHCO₃ % value : This value corresponds to the real NaHCO₃ as weight percentage in sample.

Example :

A sample which consists of 100 % trona has a NaHCO₃ % value of 37.16.

Trona % value : When the sample is known to be trona, this is a value as calculated from «total alkalinity».

Example :

For a sample which contains trona and possibly clay and other compounds, if total alkalinity is 41.13 % as Na₂O, trona % value should be 100.

Appendix 2 — Other minerals coexist with trona in Ankara-Bey pazari samples

<i>Mineral</i>	<i>Formula</i>
Trona	$\text{Na}_2\text{CO}_3 \cdot \text{NaHCO}_3 \cdot 2\text{H}_2\text{O}$
Pirssonite	$\text{Na}_2\text{CO}_3 \cdot \text{CaCO}_3 \cdot 2\text{H}_2\text{O}$
Gaylussite	$\text{Na}_2\text{CO}_3 \cdot \text{CaCO}_3 \cdot 5\text{H}_2\text{O}$
Nahcolite	NaHCO_3
Thermonatrite	$\text{Na}_2\text{CO}_3 \cdot \text{H}_2\text{O}$
Brugnatellite	$\text{Mg}_6\text{FeCO}_3(\text{OH})_{13} \cdot 4\text{H}_2\text{O}$
Natron	$\text{Na}_2\text{CO}_3 \cdot 10\text{H}_2\text{O}$
Mirabilite	$\text{Na}_2\text{SO}_4 \cdot 10\text{H}_2\text{O}$
Thenardite	Na_2SO_4
Glauberite	$\text{Na}_2\text{SO}_4 \cdot \text{CaSO}_4$
Dolomite	$\text{CaCO}_3 \cdot \text{MgCO}_3$
Analcite	$\text{Na}_2\text{O} \cdot \text{Al}_2\text{O}_3 \cdot 4\text{SiO}_2 \cdot 2\text{H}_2\text{O}$

Appendix 3 — Some conversion factors employed in evaluation of trona analysis results

<i>Result given</i>	\times	<i>Factor</i>	=	<i>Result sought</i>
Na_2CO_3		.58483		Na_2O
Na_2CO_3		2.1324		Trona
Trona		.41139		Na_2O
Trona		.46894		Na_2CO_3
Trona		.37167		NaHCO_3
Trona		.15939		H_2O
Trona		.2965		Ignition Loss
Trona		.7034		Na_2CO_3 Equivalent
Trona		.1991		H_2O
Trona		.0974		CO_2
NaHCO_3		.36895		Na_2O
NaHCO_3		2.6905		Trona
NaHCO_3		.3691		$\text{H}_2\text{O} + \text{CO}_2$
NaHCO_3		.6309		Na_2CO_3 Equivalent

Appendix 4 — Some definitions for statistical evaluations

Standard deviation, s ; individual result, x ; ; mean value, \bar{x} ; number of results, n ; true value, μ and student's t value have their common meanings. Student's t can be calculated as follows, where t_{table} is a table value at a given confidence level.

$$t_{\text{calculated}} = \frac{|\mu - \bar{x}| \sqrt{n}}{s}$$

$$R = \frac{\text{calculated}}{t_{\text{table}}}$$

A value of R which is larger than 1.0 indicates systematic error for a set of results. A confidence level of 95 % has been employed in this study.

4. *X-ray diffraction spectrometry.* — Finely powdered sample is rotated in front of X-ray beam to allow the formation of Bragg angles critical for all the crystal layers. The layers corresponding to these angles cause constructive interference of source radiation; and high intensity of source beam thus formed is detected by diffractometer to form convenient spectra. These spectra are further evaluated and by d values of (hkl) surfaces, mineral composition of sample is determined by the aid of ASTM data cards.

RESULTS

The studies were carried out to adopt standard methods for the analysis of trona samples, considering the interferences arising from silicates and other minerals present in trona samples. Among the methods in literature for the speciation of NaHCO_3 - Na_2CO_3 in trona samples, the most applicable ones are BaCl_2 titration, AgNO_3 external indicator, and potentiometric titration. These three methods were tried on synthetic Na_2CO_3 - NaHCO_3 mixtures for comparisons of analytical performances. Typical results are given in Table 1 for a synthetic sample. Total alkalinity values given in Table 1 and in other results were determined by potentiometric titration method. The errors found in Na_2CO_3 - NaHCO_3 speciation by potentiometric method were higher than other methods. In order to further investigate this, a synthetic solution containing Na_2CO_3 only was analyzed by potentiometric titration method and Na_2CO_3 percentage was found as 106 ± 1 from the first end point and 100 ± 1 from the second end point. These predeterminations demonstrated that total alkalinity determined by potentiometric titration were correct but speciations were not correct. Seven trona samples obtained from Beypazarı were analyzed using AgNO_3 external indicator, BaCl_2 titration and potentiometric titration for the comparison of Na_2CO_3 - NaHCO_3 speciation and the selection of a simple routine method for this analytical problem (Table 2). In these samples, the values of total alkalinity by potentiometric titration, trona percentages, XRDS results and results by other methods were also given (Table 3). The results of analyses were compared with theoretical trona values by student's t test; where the total alkalinity results are taken as basis for the theoretical values. 95 % confidence level, which is commonly used by analytical chemists, was employed as the basis of evaluation. The results of analytical determinations of seven trona samples were compared to theoretical results. At 95 % confidence level, R values of trona samples from Beypazarı for the percentages of Na_2CO_3 are 0.008 in BaCl_2 method, 3.25 for AgNO_3 external indicator method and 3.26 for potentiometric method; for the percentages of NaHCO_3 the same values are 0.59 for BaCl_2 method, 2.83 for AgNO_3 external indicator method and 3.59 for potentiometric method, systematic error is indicated when $R > 1$. The results of BaCl_2 method show that this method gives the results which are closest to the theoretical values; compared to the other methods.

Table 1 - Representative results for synthetic trona sample
True values; 33.3 % NaHCO_3 , 66.6 % Na_2CO_3

Method	% Value found, ($\bar{X} \pm S$)	
	NaHCO_3	Na_2CO_3
Potentiometry	29.0 \pm 1.0	71.0 \pm 1.0
AgNO_3	33.0 \pm 0.5	67.1 \pm 0.5
BaCl_2	34.0 \pm 0.5	66.0 \pm 0.5

Table 2 - Detailed analytical results for Beypazarı trona samples

Sample no.	Total alkalinity (%)	Trona (%)	Water insoluble part (%)	SO ₄ (µg/g)	Cl (µg/g)	Ca + Mg (µg/g)	Diagnastic result by XRD
06.16A.1A	69.17	98.33	0.44	<100	<100	<100	Trona, brugnatellite
06.16A.2A	55.28	78.59	20.44	<100	<100	<100	Trona, dolomite
06.23.1A	68.77	97.77	1.06	<100	<100	<100	Trona
06.21.1	68.77	97.77	1.37	<100	<100	<100	Trona
06.21.2	67.30	95.68	2.75	<100	<100	<100	Trona
06.23.2A	13.35		80.67	<100	<100	<100	Dolomite, quvars, analcite, feldspar, natron
06.21.3	68.77	97.77	1:11	<100	<100	<100	Trona, brugnatellite

Table 3 - Comparison of the results for Na₂CO₃ and NaHCO₃ content in Beypazarı trona samples by different methods

Sample no.	Na ₂ CO ₃ % by the method indicated				NaHCO ₃ % by the method indicated			
	BaCl ₂	AgNO ₃	Potentiometric	Theoretical ^a	BaCl ₂	AgNO ₃	Potentiometric	Theoretical
06.16A.1A	45.76	46.90	50.79	46.04	37.10	35.30	31.00	36.47
06.16A.2A	37.08	37.28	40.74	36.80	28.84	28.53	24.10	29.15
06.23.1A	45.73	46.63	51.32	45.78	36.54	35.12	30.60	36.26
06.21.1	45.68	46.24	48.68	45.78	36.61	35.72	32.30	36.26
06.21.2	44.82	45.50	50.26	44.80	35.63	34.56	28.07	35.49
06.21.3	45.90	46.84	48.15	45.78	32.26	34.77	33.11	36.26

^a Theoretical values as calculated from total alkalinity results (Appendix 1).

As it was mentioned in «Introduction», some studies were done to investigate the possible interferences in analysis by clays and other chemicals present in trona mineral.

The impurities were predetermined by XRD spectrometry, and analyses were modified according to the interferences thus known. In order to decide on modifications, following studies were done on potentiometric titration method which is capable of giving results rapidly.

Interference of clays: In order to verify the interferences of clay minerals on carbonate-bicarbonate end points, separate titration curves were drawn for the mixtures of i) Na₂CO₃, clay and water and, ii) Na₂CO₃ and water. As it is shown in Figure 2, the presence of clays has no effect on carbonate-bicarbonate end point. The mixtures were prepared as described in «experimental». This procedure involves leaving the solution overnight, thus allowing effective sedimentation of clay. When the solutions were titrated without waiting overnight, titration curves ambiguous and irreproducible end points.

Interference of dolomite: Possible interference of dolomite was also investigated, titration curves were drawn for the cases of i) Na₂CO₃, dolomite and water; ii) dolomite and water unfiltered mixture; iii) dolomite and water, filtered mixture. The results are shown in Figure 3. It has been observed that carbonate-bicarbonate end point was affected when dolomite containing sample was not filtered. In this case, during the course of titration, as pH is lowered after the first end point probably a part of dolomite gradually is dissolved causing a higher content of bicarbonate ion. Consequently, second end point is delayed.

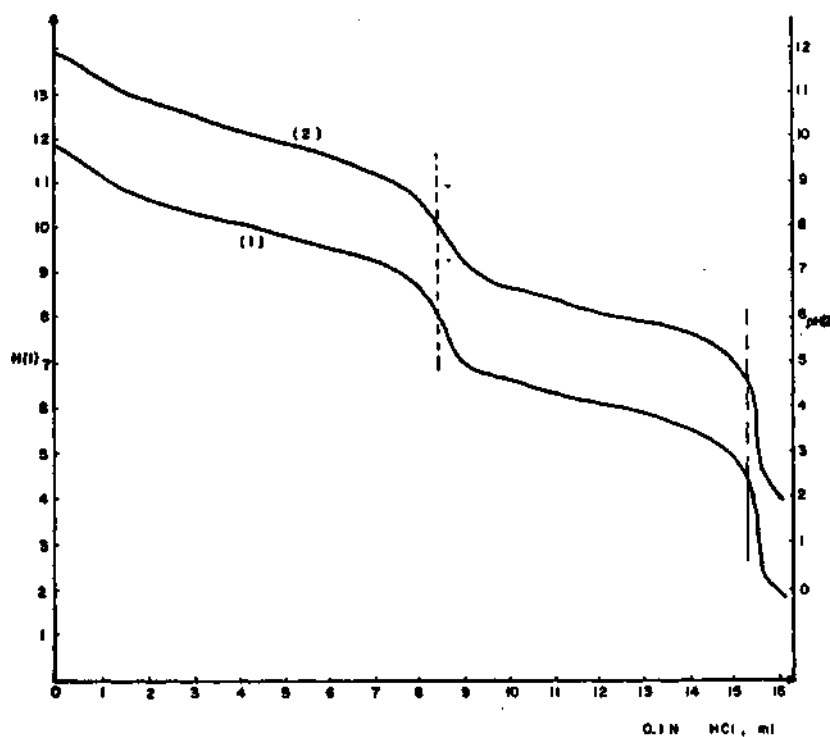


Fig. 2 - The effect of clay minerals on potentiometric titration of Na_2CO_3 .
 (1) 1.0 g Na_2CO_3 + 0.5 g clay + 100 ml distilled water (pH (1) scale);
 (2) 1.0 g Na_2CO_3 + 100 ml distilled water (pH (2) scale).

In Figure 4, titration curves for a natural trona solution containing dolomite are shown. When solution was left for 3 hours, titration of aliquot taken from the clear part of the mixture gave end points corresponding to Na_2CO_3 content only. On the other hand a stirred mixture gave erroneous end points because of interference effects by dolomite which is gradually dissolved by addition of titrant, HCl.

According to the statistical evaluation, BaCl_2 titration method is the best approach for carbonate-bicarbonate speciation. This method was applied on 5 duplicates of a trona sample. Results and statistical evaluation are given in Table 4. Compared to the theoretical values, results involve errors of 0.4 % and 0.6 % for Na_2CO_3 and NaHCO_3 , respectively. The same trona sample's XRD spectrum is given in Figure 5. This sample contains 95 % trona where XRD and other analytical results are consistent.

Although BaCl_2 method provides the best analytical results, potentiometric titration method is faster and more widely used. In the latter method, predetermined pH values of 8.30 and 4.5 are used for end points. However, in the working conditions, 8.30 for the first end point does not give accurate results as mentioned before. In order to find an empirical value for the first end point, 20 trona samples were analyzed by using total alkalinity and BaCl_2 titration results as well. First end point pH values to give accurate results, varied between 8.60 to 8.85 with an average value of 8.70 and a standard deviation of 0.07. Therefore, 8.70 ± 0.07 and 4.5 have been suggested as empirical pH values for predetermined end points.

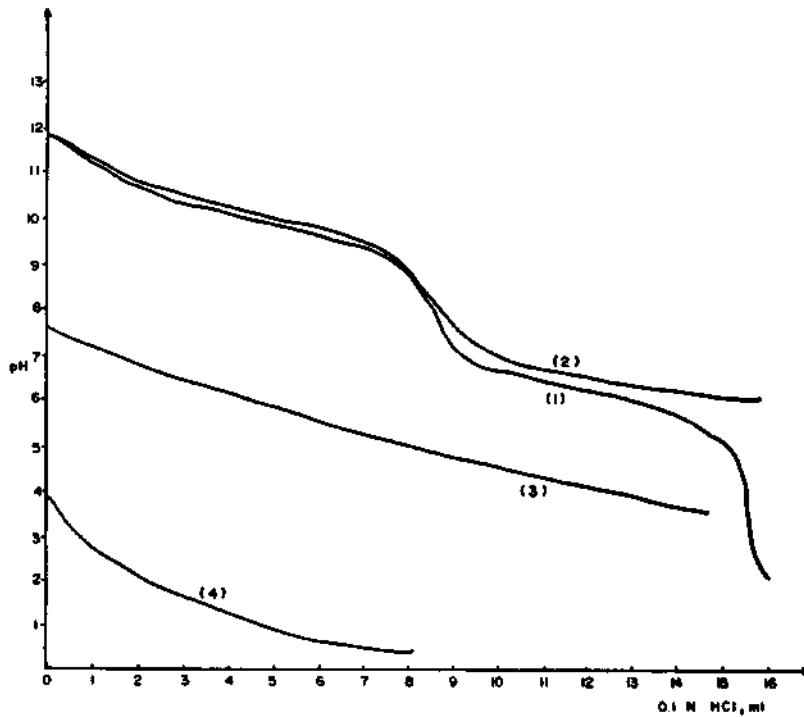


Fig. 3 - The effect of dolomite on potentiometric titration of Na_2CO_3 .
 (1) 1.0 g. Na_2CO_3 + 100 ml distilled water; (2) 1.0 g. Na_2CO_3 + 0.5 g dolomite + 100 ml distilled water. The mixture was not filtered or left to stand for sedimentation; (3) 0.5 g dolomite + 100 ml distilled water, unfiltered; (4) 0.5 g dolomite + 100 ml distilled water, filtered.

Table 4 - Results obtained by BaCl_2 titration and theoretical methods for a trona sample

	Total alkalinity $\text{Na}_2\text{O}\%$	BaCl_2 titration		Theoretical	
		$\text{Na}_2\text{CO}_3\%$	$\text{NaHCO}_3\%$	$\text{Na}_2\text{CO}_3\%$	$\text{NaHCO}_3\%$
1	39.14	44.36	35.81	44.61	35.36
2	39.14	44.43	35.70	44.61	35.36
3	39.22	44.42	35.91	44.70	35.43
4	39.45	44.42	35.91	44.97	35.64
5	39.30	45.08	35.07	44.79	35.50
\bar{x}	39.25	44.54	35.68	44.74	35.46
s	0.13	0.30	0.35	0.15	0.12

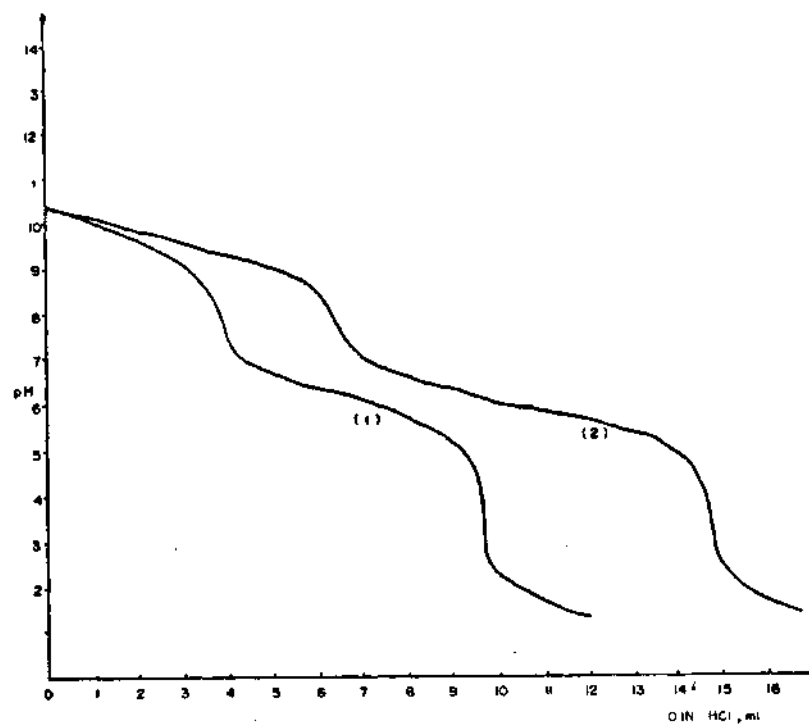


Fig. 4 - The interference of dolomite on potentiometric titration of trona samples.
 Sample : 10.0 g / 500 ml dolomite
 (1) Titration of clear solution after waiting for 3 hours for sedimentation;
 (2) The titration of the mixture as in (1) after being stirred.

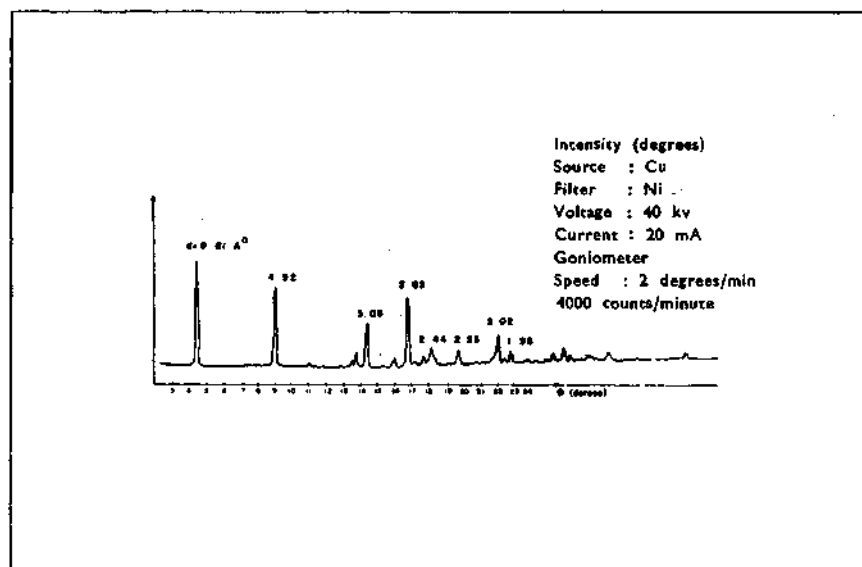


Fig. 5 - X-ray diffraction spectrum of a trona sample.

DISCUSSION

It can be concluded that for rapid trona analyses, potentiometric titrations using corrected pH values as predetermined end points, can both provide accurate results and give total alkalinity and Na_2CO_3 percentages in one step process. On the other hand, BaCl_2 titration method can provide results more accurate than those by potentiometry; but for total alkalinity values still another method is required. Therefore BaCl_2 method is a longer method with consequently higher expenses. In this study, the quality of the analytical performance by potentiometry has been improved. The difference between the theoretical and empirical end point values, however, could not be explained at this stage.

In addition, the results of this study suggest that major impurities in a trona sample should be qualitatively predetermined by XRD Spectrometry and necessary precautions for possible interferences thus can be taken.

ACKNOWLEDGEMENTS

Authors thank Mr. Esen Orhon for his helps and contributions related to instruments used in this study; and MTA Research, Planning and Coordination Department, Computer Service for performing the statistical calculations.

Manuscript received November 8, 1985

REFERENCES

- Frint, W.R., 1971, Processing of Wyoming trona: Contributions to Geology, 10, 43.
- Stanley J. Lefond (ed.), 1980, 4th Edition, Industrial Minerals and Rocks, Port City Baltimore, 1061-1080.
- Sungun, K.D., 1983, Dünyada ve Türkiye'de soda problemleri: Kimya Sanayii, Haziran-Eylül, 99-123.
- Skoog, D.A. and West, D.M., 1969, Fundamentals of Analytical Chemistry: 2nd Edition. Holt Rinehart Winston Inc.
- Food Chemical Codex III, Monographs, 299, 3rd Edition, 1981.
- Annual Book of ASTM Standards, Part 30, 1980 Easton, Md Inc., USA.
- Laitinen, H.A., 1960; Chemical Analysis: Mc Graw Hill Book Co., Toronto, 611.

DISTRIBUTION OF THE MAJOR AND TRACE ELEMENTS IN THE VOLCANIC ROCKS OF YOZGAT AREA, TURKEY

Gönül BÜYÜKONAL*

ABSTRACT. — The investigation has been carried out the petrographical and geochemical properties of the volcanic rocks in Yozgat area. These volcanic rocks are compared with some other volcanic formations and their origins are examined. The volcanic rock units of investigated area are pre-Lutetian diabases, amygdaloidal basalt intercalated with Lutetian sediments, tuff, agglomerates and post-Lutetian andesite-basalts. These volcanic rocks of the region present an affinity to the calc-alkaline suites of the island-arcs.

INTRODUCTION

Purpose of this investigation is to determine the petrological and geochemical characteristics and to establish the conditinal origin of the rocks in Yozgat area. By using the analysis of major and trace elements of lavas in this research region, were explained about the plate tectonics attitude of this area and this result will be provided to the future studies. The age of the layers have been determined by the work on lithology and stratigraphy of the area (Büyükonal, 1979). The oldest unit of the lavas, namely diabases, which is overlain by Lutetian sandstones around the Kösekközü region. The amygdaloidal basalt crop out around Yozgat city and generally west and south-west of the investigated area. Basalt-andesite which is the youngest unit is existed the northwest of Yozgat city (Fig. 1).

Some geological studies were made for different purposes by the researchers in Yozgat area. Between 1867 and 1950 the researchers agreed that the area was interior region of Kırşehir massif which is Paleozoic age (Chaput, 1947; Lahn, 1949 and Bailey-McCallien, 1950). Most of acidic and basic igneous rocks in the region are influenced by Hersinien and Alpine orogeny.

New studies and age determination carried out after 1950 were under the hypothesis that plutonites are Tertiary in age and these acidic and basic rocks combinational settled at the same or within a very close time interval (Ketin, 1954, 1955, 1961, 1966; Ataman, 1972, 1974). Tümer-Remzi (1975), found hematite, magnesite and wolframite ores in vicinity of Yozgat. The contact of the acidic intrusion and sedimentary units bearing-flourite have been explained.

GEOLOGY

Magmatism is dominant in the studied area. In the vicinity of Yozgat was cropped out by pre-Lutetian diabases, the submarine volcanic units, of Lutetian age, tuff, sandstones in rich fossils and consisting fine holocrystalline texture of basalt-andesite of post-Lutetian age with basic and acidic plutonites. The acidic plutonites are essentially granites, but the basic plutonites are gabbros. The age of these plutonites are the Upper Cretaceous-Eocene and they have been overlaid by the Eocene flysh. The region studied were under the effect of Alpin orogeny and exhibits a faulty structural generally, in the direction of southeast and northwest (Büyükonal, 1973).

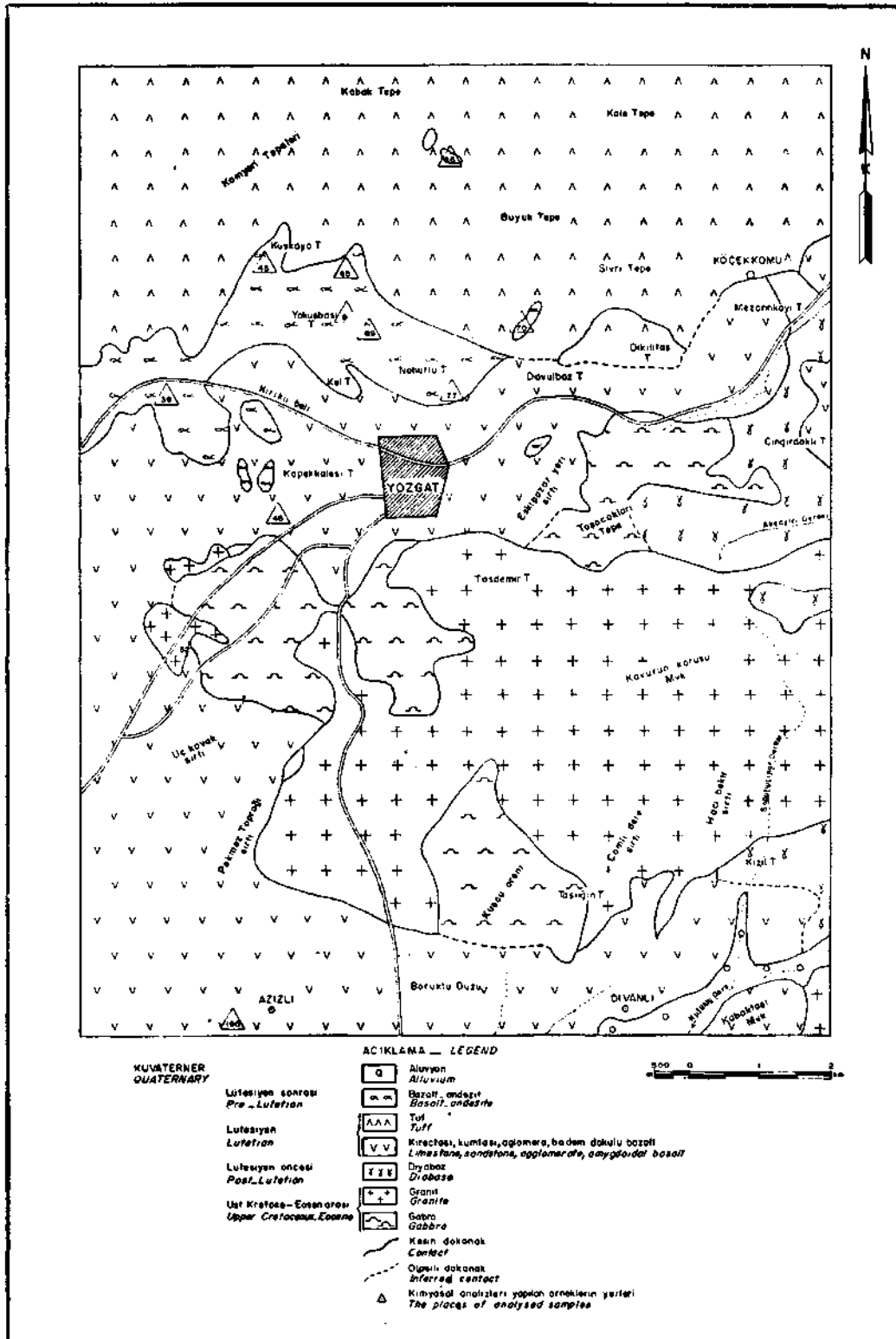


Fig. 1 - Geological map of Yozgat region.

The volcanic units as amygdaloidal basalt and diabases in Yozgat region are altered. Also, the amygdaloidal basalt are intercalated with agglomerates and Lutetian sandstones. On the other side, the basalt-andesite are very dark colour and show column structure.

PETROLOGY OF THE LAVAS OF YOZGAT

Thin-sectional lavas examination shows, diabasic, porphyric and holocrystalline textures. The chloritisation at all of the crystals in the matrix were observed and most of the feldspars in the lavas show the albitisation.

The most of lavas consist of diabase, amygdaloidal basalt and andesite-basalt units. The term andesite-basalt were used based on its mineralogical and-petrographical characteristics (Moorhouse, 1972) and (Coat, in Hess and Poldervaart, 1968). The two investigators used the terms andesite-basalt or basaltic-andesite interchangeably. The amygdules of the amygdaloidal basalts filled with chalsedony, zeolite (natrolite) and quartz. The magma samples to which lavas belong were examined and interpretation of the field completed under the light cast by the principles of plate tectonics. The major and trace elements analysis carried out at Oxford University and at the University of Vienn, by utilization of the XRF melting method, on 10 lava samples taken from the area for the purpose of solving problems of origin were utilized and the results produced were evaluated. Places where the samples were taken are shown in Figure 1 and the chemical results of the major and trace elements are shown at Table 1 and 4.

Rittmann parameters, CIPW norms and SI index were computed.

Since the classification of volcanic rocks of Yozgat were completed according to alkali ($\text{Na}_2\text{O}+\text{K}_2\text{O}$) and SiO_2 contents Irvine and Baragar (1971), MacDonald and Katsura (1964) and Kuno (1960), it can be observed by using the concept of segmantation most lavas are at the subalkalin region, but majority between the lines dividing MacDonald and Katsura with Kuno (Fig. 2).

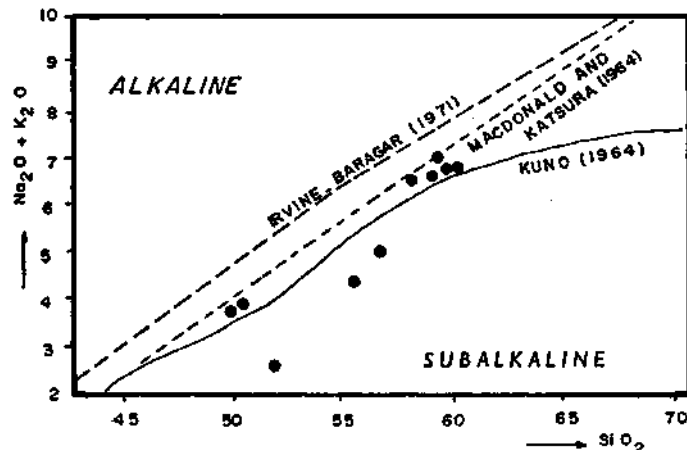


Fig. 2 - Classification of the volcanic rocks of Yozgat region according to alkaline versus silica content.

On the other hand, the samples taken from the Yozgat area were shown in the Rittmann (1953) diagram (Fig. 3) and they formed a calc-alkaline region according to these diagram arrangements which was made according to the An-SiO₂ contents.

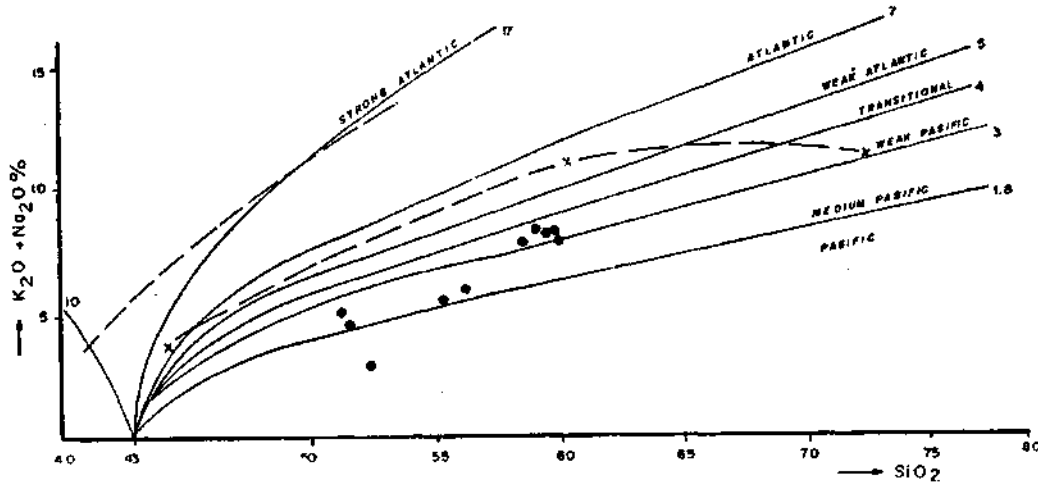


Fig. 3 - Rittmann (1962; in Wright, 1969) diagram of the volcanics of Yozgat region.

The using serial index contemplated by Rittmann (1962) and Wright (1969), to determine the origin of the volcanic rocks of the region, were computed for the lavas. It came to a conclusion that the values all the samples except one, ranges between 1.84 to 3.05. This indicates that a less the four Rittmann index is enough to classify calc-alkaline P values of the area lavas were computed by use of Rittmann parameters and are changing between 59 and 62. This is an occurrence supporting the conclusion that the volcanic rocks are of calc-alkaline type (Fig. 4).

Other parameters were used to classify Rittmann (1953) volcanics and it was seen that samples on the hand could be classified under such names as pigeonite, andesite, olivine andesite-basalt, dacite and trachy andesite (Table 2). However, it must be expressed here that the quartz, olivine and pigeonite formations theoretically extracted during the norm analysis were not observed during the microscopic studies. This condition is used to explain that there could not always be a complete match in classification of volcanics solely by basing them on mineralogical compound norm analysis (Büyükonul, 1979).

The samples from the studied area were classified according to the Rittmann (1952) normative names in addition to Taylor (1973) who based his classification on K₂O contents of the SiO₂ function. The normative plagioclase and normative color index of Irvine-Baragar (1971) together with diagrams drawn by Cox and others (1979) according to the Na₂O+K₂O and SiO₂ contents appear along with the diagrams of Di Paola (1974), in Ercan and others (1983) where K₂O/Na₂O and SiO₂ functions are given. Table 3 classifies units by using of the principle of comparing them with each other. In addition to this classifications by Taylor, Irvine-Baragar, Di Paola, Cox and et al. are given by the following diagrams in Figure 5, 6, 7, 8, 9.

The samples of the region are evaluated-in diagrams of Rittmann (1952), Taylor (1973), Cox, et al. (1979), Irvine and Baragar (1971) and Di Paola (1974 in Ercan et al., 1983). However the character of calc-alkaline, have been taken in different names when evaluated in these diagrams mentioned above (Table 3). Having K₂O/Na₂O > 1 also indicate that these are the calc-alkaline origin.

Table 1 - Chemical analysis and CIPW norms of volcanic rocks of Yozgat region

Samples no.	BCR-39	BCR-48	BCR-45	BCR-43	BCR-70	BCR-77	BCR-90	BCR-66	BCR-89	BCR-190	W-380-
SiO ₂	59.90	51.50	56.35	59.71	55.30	59.70	60.30	59.00	51.50	52.90	52.38
TiO ₂	0.67	1.24	0.69	0.35	0.69	0.67	0.72	0.66	1.24	0.71	1.14
Al ₂ O ₃	16.80	15.60	17.06	17.87	15.07	16.80	17.18	16.80	14.60	13.24	15.50
Fe ₂ O ₃	1.25	3.76	2.19	1.29	3.96	1.81	1.25	1.16	1.80	2.33	3.25
FeO	4.20	4.32	3.78	3.44	4.08	3.70	4.20	3.92	6.08	5.46	6.41
MnO	0.14	0.14	0.13	0.08	0.15	0.14	0.15	0.13	0.14	0.13	0.20
MgO	1.56	9.76	4.03	3.25	0.56	1.56	1.42	1.82	9.76	11.60	4.64
CaO	5.24	6.22	6.66	5.03	11.11	5.24	5.18	4.96	6.22	7.48	5.31
Na ₂ O	5.20	3.04	3.95	5.16	3.04	5.20	5.14	5.37	3.04	1.97	5.30
K ₂ O	1.60	1.34	1.27	1.92	1.72	1.60	1.82	1.30	1.34	0.66	0.05
H ₂ O +	—	—	—	—	—	—	—	—	—	—	—
H ₂ O -	—	—	2.00	2.18	2.13	—	—	2.18	1.68	1.93	2.73
P ₂ O ₅	2.99	2.50	1.27	0.17	0.25	2.99	3.01	2.02	2.50	1.99	0.10
CO ₂	—	—	1.14	—	2.43	—	—	0.75	—	—	2.96
Total	99.55	99.42	100.52	100.45	100.49	99.61	100.37	100.07	99.90	100.40	99.97
CIPW norms											
Or	9.46	7.92	7.51	8.69	10.17	9.46	10.76	7.68	7.92	3.90	0.30
Ab	44.00	25.72	33.42	43.15	25.72	44.00	43.49	45.43	25.72	16.67	44.84
An	6.46	14.53	17.54	20.66	22.40	6.46	6.03	11.41	14.53	24.11	18.36
Qz	15.76	6.48	13.00	9.59	15.60	16.39	16.09	12.69	4.27	7.95	1.48
Hy	9.72	27.35	14.27	9.58	—	8.34	9.31	9.92	32.20	36.06	16.21
D ₁	—	—	—	1.52	9.33	—	—	—	—	—	5.98
Ap(OH)	7.05	5.90	—	0.40	0.59	7.05	7.10	4.77	5.90	4.69	0.24
Il	1.27	2.35	1.31	1.10	1.31	1.27	1.37	1.25	2.35	1.35	2.16
C	4.15	3.83	2.76	—	—	4.15	4.55	2.38	2.83	0.45	—
Mt	1.81	5.45	3.17	1.51	5.74	2.62	2.26	1.68	2.61	3.38	4.71

Table 2 - Rittmann parameters of the volcanic rocks of Yozgat region (Rittmann, 1953)

Sample no.	SiO ₂	Al	Alk	An	CaO	Fm	k	Ca	P values
BCR 39	59.90	15.12	9.40	0.2357	5.24	9.144	0.1702	1.772	56
BCR 48	51.50	14.04	5.90	0.4082	6.22	28.186	0.2270	1.336	57
BCR 45	56.35	15.35	7.20	0.3617	6.66	14.551	0.1765	1.765	60
BCR 43	59.71	16.08	9.66	0.2494	5.03	11.662	0.1987	1.177	57
BCR 70	55.33	13.56	6.28	0.3669	11.11	9.773	0.2738	6.741	59
BCR 77	59.70	15.12	9.40	0.2357	5.24	12.134	0.1702	1.818	56
BCR 90	60.30	15.46	9.53	0.2364	5.18	8.875	0.1908	1.627	57
BCR 66	59.00	15.12	9.36	0.2984	4.98	9.255	0.1591	0.786	55
BCR 89	51.50	13.14	5.90	0.3803	6.22	28.162	0.2271	1.876	56
BCR 190	52.90	11.92	3.62	0.5344	7.48	31.719	0.1825	2.4994	65

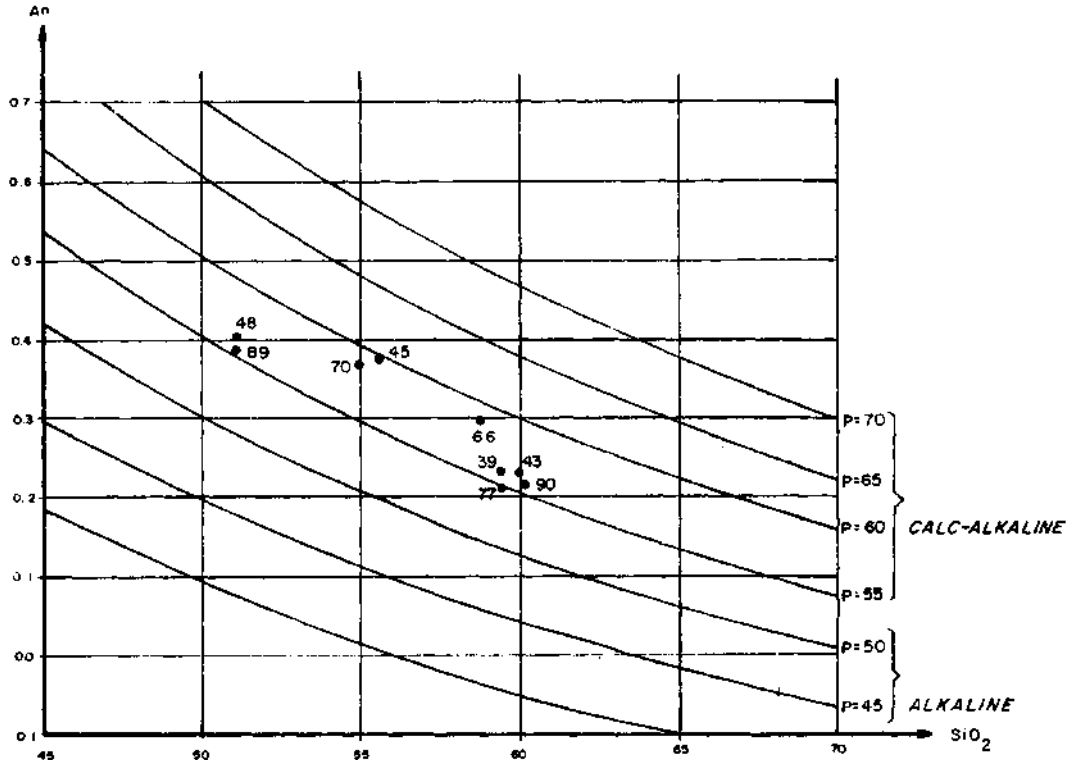


Fig. 4 - The places of the volcanic rocks of Yozgat region according to P values in the diagram of an versus SiO_2 of Rittmann (1953).

Table 3 - Classification of the volcanic rocks in Yozgat region according to another investigators.

Sample no.	Rittmann (1952)	Taylor (1973)	Irvine-Baragar (1971)	Di Paola (1974)	Cox, and et al. (1979)
BCR 39	Dacite	Andesite	Andesite	Andesite	Trachy-andesite
BCR 48	Olivine andezine basalt	Al. rich basalt	Basalt	High Al. basalt	Basalt
BCR 45	Pigeonite, andesite	Andesite	Andesite	Andesite	Basaltic-andesite
BCR 43	Pigeonite, andesite	Andesite	Andesite	Andesite	Trachy-andesite
BCR 70	Trachy-andesite	Poor Si. andesite	Andesite	Poor Si. andesite	Basaltic-andesite
BCR 77	Pigeonite, andesite	Andesite	Dacite	Andesite	Trachy-andesite
BCR 90	Dacite	Andesite	Dacite	Andesite	Trachy-andesite
BCR 66	Dacite	Andesite	Dacite	Andesite	Trachy-andesite
BCR 89	Olivine, andezine basalt	Al. rich basalt	Basalt	High Al. basalt	Basalt
BCR 190	Pigeonite, basalt	Al. rich basalt	Basalt	High Al. basalt	Basaltic-andesite

Table 4 - The trace elements (Zr, Y, Sr, Rb), Ti (ppm) and K % values and the ratios of K/Rb, Rb/Sr, the volcanic rocks of Yozgat region

Sample no.	Zr ppm	Y ppm	Sr ppm	Rb ppm	Ti ppm	% K	K/Rb	Rb/Sr
BCR 39	193.96	15.75	321.90	47.48	4020	0.66	139	0.147
BCR 48	107.49	17.98	380.38	25.41	7440	0.56	220	0.067
BCR 45	142.45	16.29	308.44	98.80	4140	0.53	54	0.320
BCR 43	134.86	15.54	312.15	46.93	2100	0.80	170	0.150
BCR 70	58.86	17.89	328.59	25.18	4140	0.71	282	0.077
BCR 77	145.55	16.49	327.23	59.98	4020	0.66	110	0.183
BCR 90	146.70	16.80	327.53	51.15	4320	0.76	149	0.156
BCR 66	142.45	16.29	308.44	98.80	3960	0.54	55	0.320
BCR 89	109.49	17.98	380.38	25.41	7440	0.56	220	0.067
BCR 190	61.44	13.81	436.72	46.74	4260	0.27	58	0.107

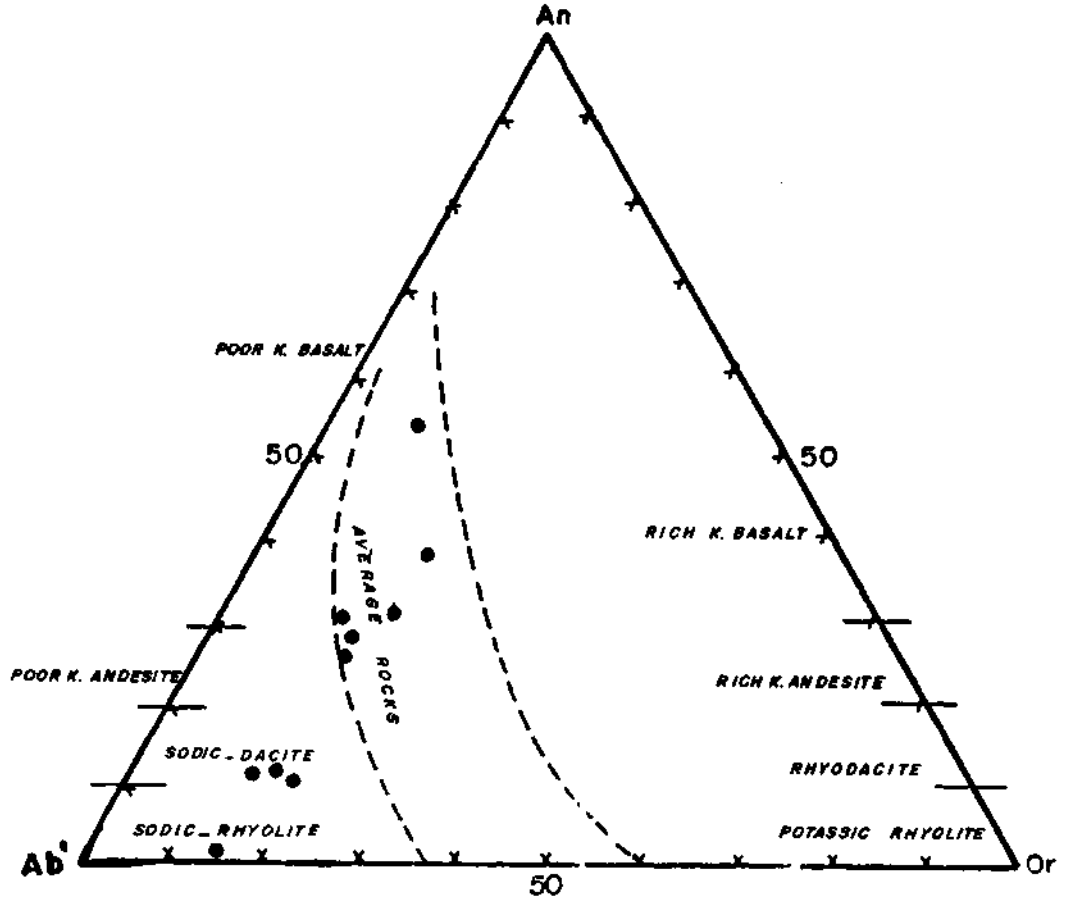


Fig. 5 - Classification of the volcanic rocks of Yozgat region in Irvine-Baragar (1971) diagram.

The SI index of the samples were used in the classification of the volcanic rocks (Hutchison, 1974). According to these, the lavas of the region have been named as basalt, andesite, basaltic-andesite and dacitic-andesite (Büyüköнал, 1979).

Furthermore, according to the diagram of An+Ab'+Or of Irvine and Baragar (1971), the volcanics of the area could be classified as transitional and generally sodic in character (Fig. 5). However, while some of the rocks show sodic dacite character, others take place in the section of andesites poor in K in this diagram.

Trace element contents such as Y, Zr, Rb and Sr of some of the lavas of Yozgat and its close vicinity are given at Table 4 together with Ti, K, K/Rb and Rb/Sr ratios.

The Y distribution of the lavas of this area range between 16 and 18 ppm. Calc-alkaline rocks' Zr values are relatively higher than tholeiites (Jakes-White, 1972). According to the Zr values, the samples of this area can again be classified as calc-alkaline type.

The Rb distribution of volcanic rocks of Yozgat, broadly varies between 0.32 ppm and 98.80 ppm. The highest values may be interpreted as tendency progressing towards the shoshonites (Jakes-White, 1972).

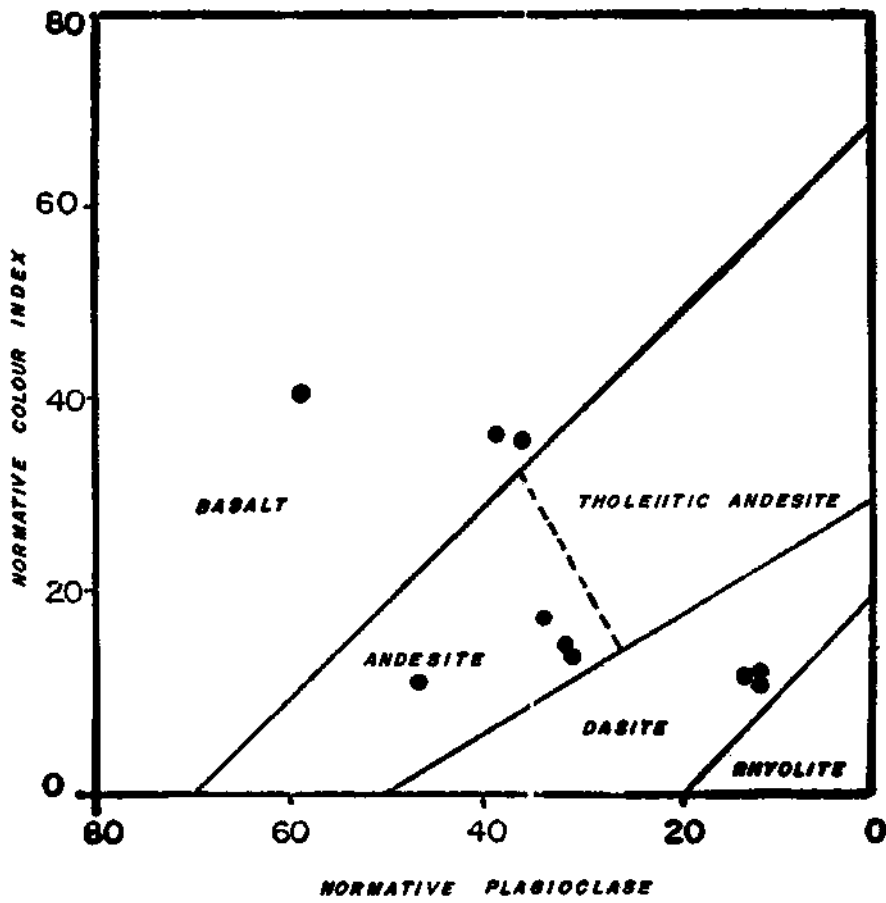


Fig. 6 - Classification of the volcanic rocks according to normative plagioclase versus normative colour index in Yozgat region (Irvine-Baragar, 1971).

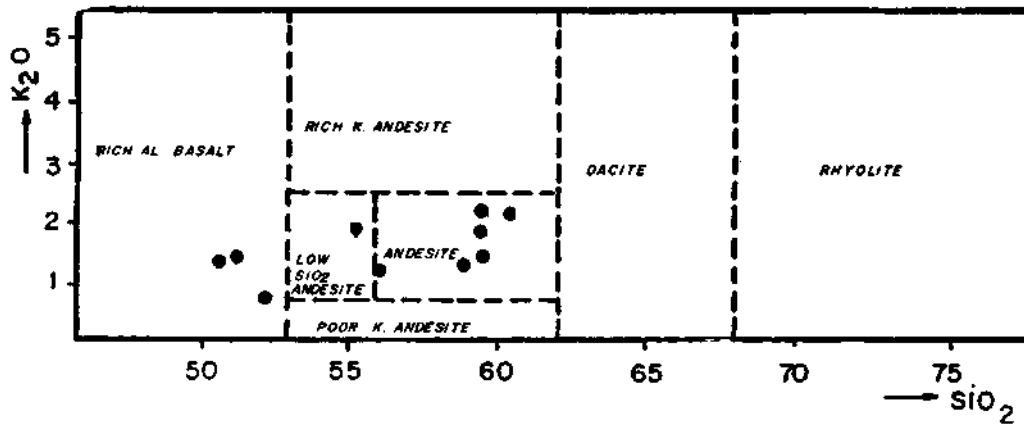


Fig. 7 - Classification of the volcanics of Yozgat region according to K₂O/SiO₂ ratios (Taylor, 1969; from McCurry-Wright, 1977).

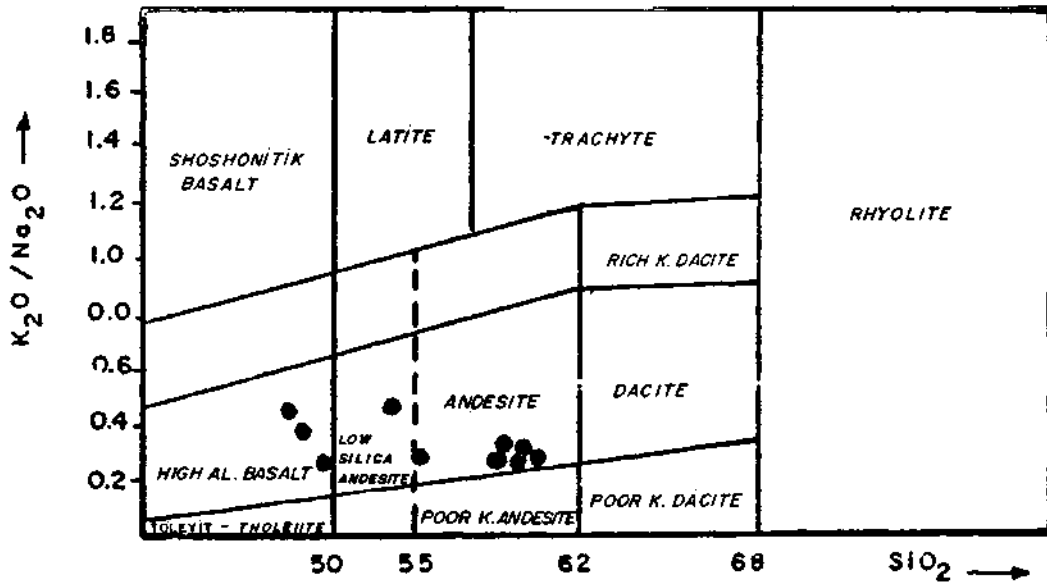


Fig. 8 - Classification of the lavas of Yozgat region according to ratios of K_2O/Na_2O and SiO_2 content (Di Paola, 1974; in Ercan, Günay, Baş, 1983).

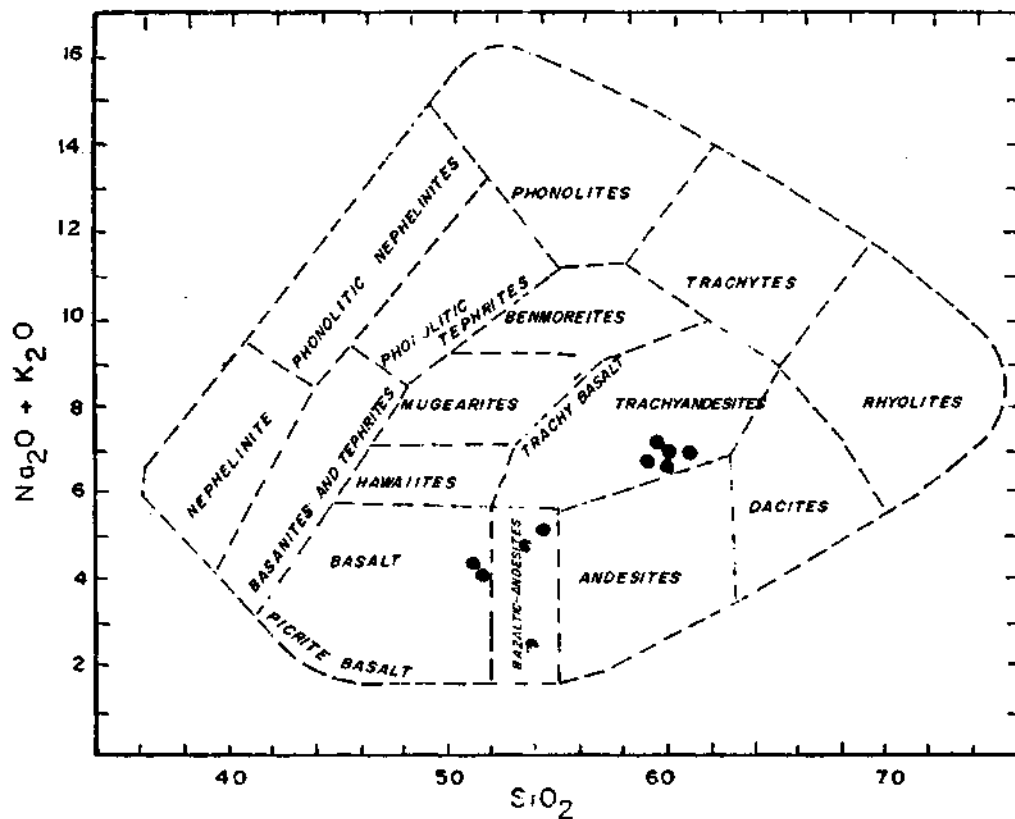


Fig. 9 - Nomenclature of the volcanic rocks of Yozgat region according to Cox et al. (1979).

However, the Sr values are rather stable. Except two samples Sr contents range between 300 and 380 ppm. The concentration of Sr plays an important role for identification of the island arc tholeiites. The geochemical characteristics of the samples of Yozgat region conform to the calc-alkaline suites of the island-arcs. The mobility of the Rb contents of samples caused to raise a family broad range in K/Rb ratios. A decreasing in the K/Rb ratios of the volcanics of the island-arc towards the continent in favor of shoshonites, had been asserted by Jakes and White (1972). Besides these, the lavas of the investigated area display a calc-alkaline trend in the diagram of Pearce (1973), McCurry and Wright (1977) employed Zr versus Sr (Fig. 10).

Pearce and Cann (1973), Bickle and Pearce (1974) in their diagrams showed Ti+Zr+Y (Fig. 11), Ti+Zr+Sr (Fig. 12) and Zr+Ti (Fig. 13) relationships and places of the volcanic rocks of Yozgat region generally with the island-arc calc-alkaline partly of tholeiitic calc-alkaline.

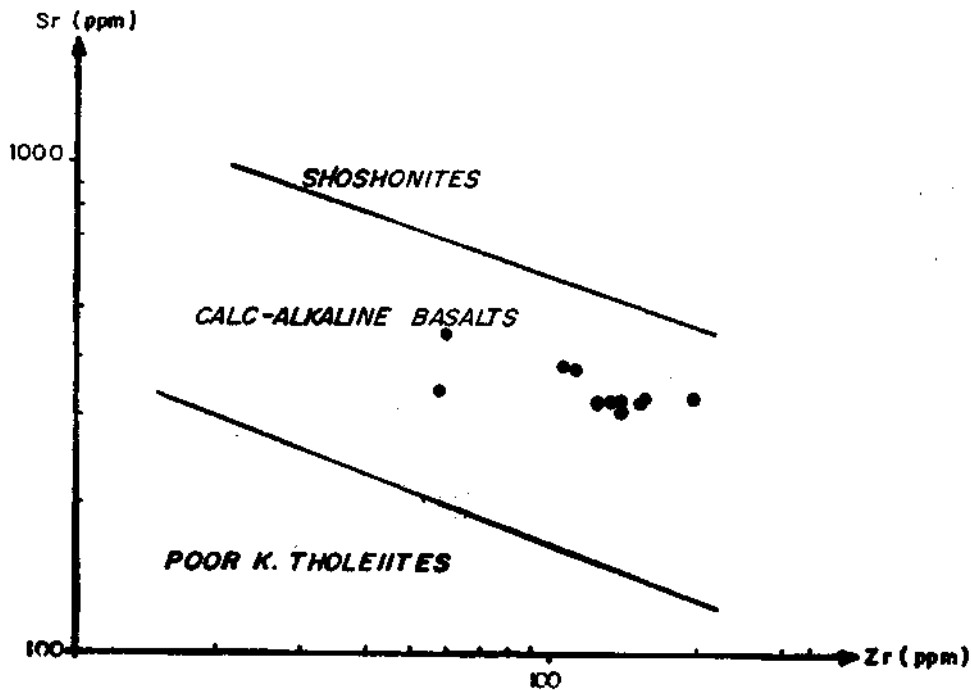


Fig. 10 - Sr/Zr diagram of the lavas in Yozgat region.

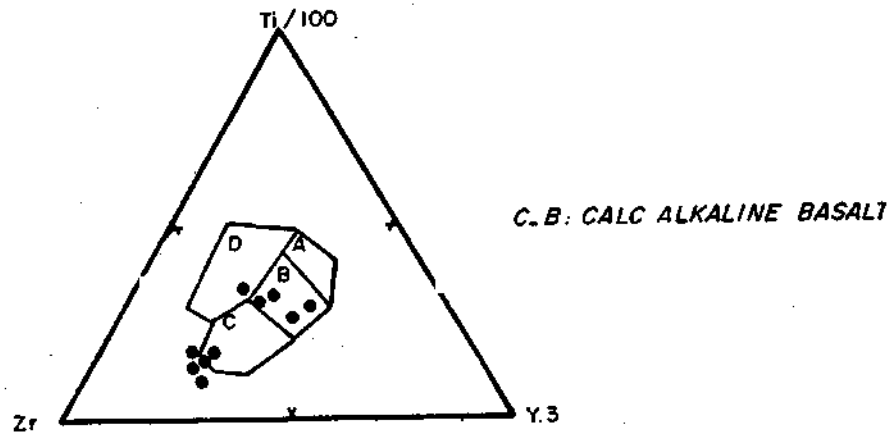


Fig. 11 - Triangle diagram of Ti+Zr+Y of volcanics in Yozgat region.

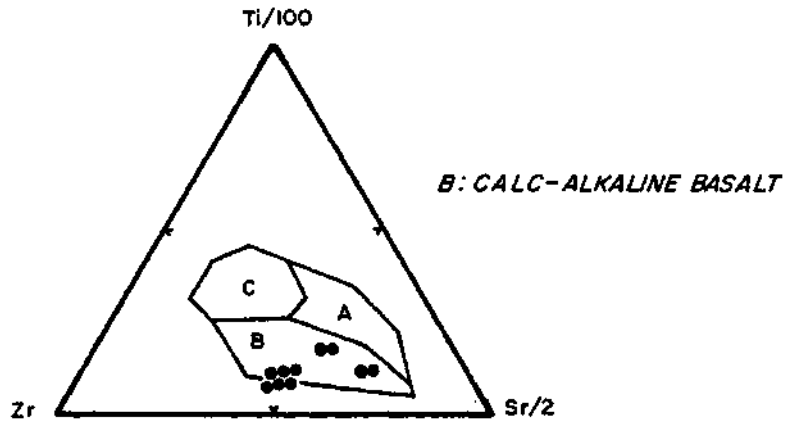


Fig. 12 - Triangle diagram of Ti+Zr+Sr of the lavas in Yozgat region.

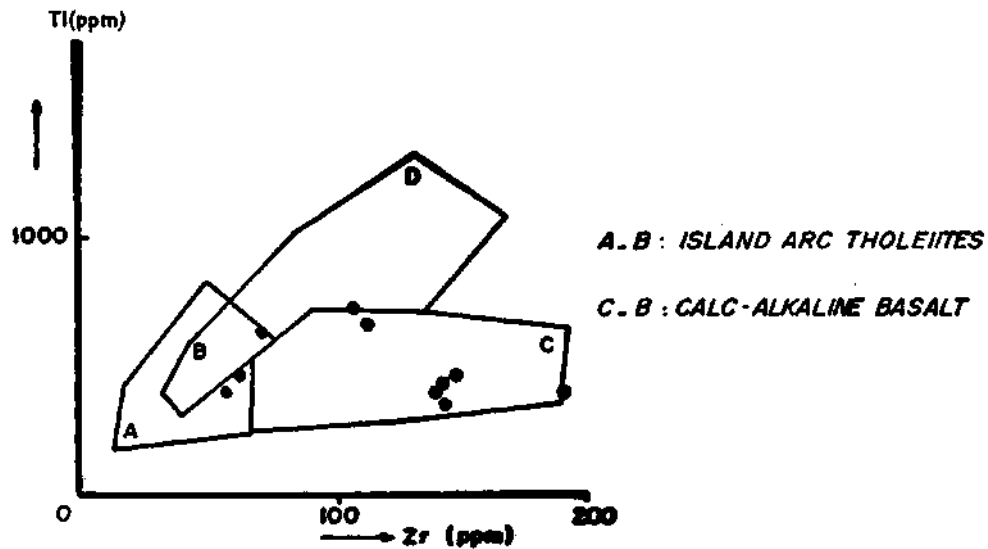


Fig. 13 - Diagram of the Ti versus Zr of the Yozgat region's volcanics.

CONCLUSION

Following interpretations are given for further discussion of the results of studies on the volcanic rocks of Yozgat area composed partly of the Kırşehir massif which is located in the Central Anatolia. The Zr in calc-alkaline rocks is higher than tholeiites and reported to be around of 100 ppm (Jakes-White, 1972). Zr value of volcanic rocks of Yozgat is generally higher than 100 ppm which may show, a calc-alkaline trend.

In general, trace elements such as Rb and Sr exhibit very broad distributions in concentration and increase towards the continental margin commencing from oceanic side, and also increase towards the youngest unite (Jakes-White, 1972). The Rb distribution is observed between 0.32 and 98.80 in the lavas of the area. The highest Rb value is interpreted as a transition towards the shosho-

nite. The Sr varies between 300 and 380 ppm in the rocks which is consistent to the calc-alkaline suites of the islandarcs. The changings in the concentration of the Rb control the K/Rb ratios. It was reported by Jakes and White (1972) that the K/Rb ratio indicates the highest value in the island-arc, tholeiites and decrease towards the shoshonites which are formed in the interior parts of the continent. Therefore, volcanic rocks of Yozgat, extends in character between tholeiites and shoshonites and generally exhibit a calc-alkaline trend. In the diagrams of Pearce, 1973 and McCurry-Wright, 1977 based on the relation of Zr and Sr, the lavas of Yozgat are taken place in the calc-alkaline section. This statement is also consistent to the view of Bickle and Pearce (1975).

In conclusion, it can be asserted that the lavas of the area were generally, in calc-alkaline character, but very few of them display a tholeiitic calc-alkaline trend.

In future studies, making increase the number of samples and examining of the trace and REE would help to clarify the geotectonical settlement problem of the region.

ACKNOWLEDGEMENTS

I would like to express my thanks to Prof. Dr. A.E. Vincet and to Prof. Dr. H. Wieseneder for providing facilities in the Geochemical Laboratories of Oxford and Vienna Universities, Dr. J.W.E. Whittekar, Dr. J.D. Bell and Dr. K.G.Cox for their contributions.

Besides these the financial support of the UNESCO and the Government of Austria arc greatly acknowledged.

Manuscript received January 29, 1985

REFERENCES

- Ataman, G., 1972, Ankara'nın güneydoğusundaki granitik-granodiyoritik kütlelerden Cefalık dağın radyometrik yaşı hakkında ön çalışma: Hacettepe Fen Müh. Bilim. Bull., 2, 1, 44-49.
- , 1974, Revue geochronologique des Massif Plutoniques et Metamorphiques de l'Anatolie: Hacettepe Bull. Natural Sci. Engin., 3, 75-87.
- Bailey, E.B. and McCallien, W.J., 1950, Ankara Melanjı ve Anadolu Şaryajı: MTA Bull., 40, 12-17.
- Bickle, M.J. and Pearce, J. A., 1975, Oceanic mafic rocks in the Eastern Alps: Contrib. Mineral. Petrol. 49, 197-189.
- Büyükonak, G., 1973, Kırşehir Masifinin Yozgat ve yakın çevresinde magmatik kayalarda petrokimyasal-petrografik bir araştırma: A.Ü.F.F.Jeoloji Müh. Böl. (unpublished).
- , 1979, Yozgat yöresi plütönit ve volkanitlerinin petrolojisi: A.Ü.F.F. Jeoloji Müh. Böl. (unpublished).
- Chaput, E., 1947, Türkiye'de jeolojik ve jeomorfolojik teknik seyahatları (Türkçe tercümesi): İst. Üniv. Publ., 324, Ed. Fak. Coğ. Enst. Publ., 11, İstanbul.
- Coat, R.R., 1968, Basaltic andesites: pp. 639-736. In H.H. Hess and A. Poldervaart, ed. Basalts, volume 2. Interscience publishers a division of John Wiley and Sons, London, New York, 862 pp.
- Cox, K.G.; Bell, J.D. and Pankhurst, R.J., 1979, The interpretation of igneous rocks: George Allen and Unwin Ltd. London, 450 pp.
- Di Paolo, G.M., 1974, Volcanology and petrology of Nisyrosisland (Dodecanese, Greece): Bulletin Volcanologique, 38/4, 944-987.

- Ercan, T.; Günay, E. and Baş, H., 1983, Denizli volkanitlerinin petrolojisi ve plaka açısından bölgesel yorumu: TJK Bull., 26, 153-160.
- Hutchison, C.S., 1974, Laboratory handbook of petrographic techniques: John Wiley and Sons, Inc., New York, 525 pp.
- Irvine, T.N. and Baragar, W.P.A., 1971, A guide to the chemical classification of the common volcanic rocks: Canadian Jour. of Earth Scien., 8, 523-548.
- Jakes, P., 1972, Major and trace element abundances in volcanic rocks of orogenic areas: Geological Society of America Bull., 83, 29-40.
- Ketin, İ., 1954, Yozgat bölgesinin jeolojik lövesi hakkında memuar (Yozgat bölgesinin 1:100 000 lik 59/1, 2, 3 paftalar: Jeolojik lövesi ait memuar): MTA Rep., 2141 (unpublished), Ankara.
- , 1955, Yozgat bölgesinin jeolojisi ve Orta Anadolu Masifinin tektonik durumu: TJK Bull., 6/1, 40.
- , 1961, Türkiye'de magmatik faaliyetler: TJK Bull., 2, 16-33.
- , 1966, Tectonic unit of Anatolia (Asia Minor): Bull. Min. Res. Explo. Inst. Turkey (foreign edition), 66, 23-44.
- Kuno, H., 1960, High alumina basalt: Journal of petrology 1, 121-145.
- Lahn, E., 1949, Orta Anadolu'nun jeolojisi hakkında: TJK Bull., 2, 1, 90.
- MacDonald, G.A. and Katsura, J., 1964, Chemical composition of Hawaiian lavas: Journal of Petrology, 5, 82-133.
- McCurry, P. and Wright, J.B., 1977, Geochemistry of calcalkaline volcanic in north-western Nigeria and a possible Pan-Africa suture zone: Earth and Planetary Sci. Letters, 37, 90-96.
- Moorhouse, W.W., 1959, The study of rocks in thin section: Harper and Brother, New York, 514 pp.
- Pearce, J.A., 1973, Some relationships between the geochemistry and tectonic setting of volcanic rocks: Dh. Thesis. Univ., of East Anglia.
- and Cann, J.R., 1973, Tectonic setting of basic volcanic rocks determined using trace element analyses: Earth and Planet. Sci. Lett., 19.
- Rittmann, A., 1952, Nomenclature of volcanic rocks: Bull., Vole., 11, 12, 75-102.
- , 1953, Magmatic character and tectonic position of the Indonesian volcanoes: Bull., Volcan., 11, 45-58.
- , 1962, Volcanoes and their activity: John Wiley and Sons, New York, London, 305 pp.
- Taylor, S.R., 1969, Trace element chemistry of andesites and associated calcalkaline rocks, in: Proc. Andesite Conf. A.R. McBirney, ed., Dep. Geol. Miner. Res. Orogen. 65, 43-63.
- Turner, T. and Renzi, H., 1975, Yozgat-Akdağmadeni ve civarının genel grafit prospeksiyonu ile Hatapalan 1 dere zuhurunun detay ön etüdü raporu: MTA Rep., 5382 (unpublished), Ankara.
- Wright, J.B., 1969, A simple alkalinity ratio and its application to questions of non-orogenic granite genesis: Geol. Mag, 106/4, 370-384.

GEOCHRONOLOGICAL DATA FROM THE SOUTHERN PART (NİĞDE AREA) OF THE CENTRAL ANATOLIAN MASSIF

M. Cemal GÖNCÜOĞLU*

ABSTRACT. — In the Niğde massif, which forms the southern end of the Central Anatolian massif, three formations are exposed. These are, from bottom to top: 1. Gümüşler formation, composed mainly of metaclastics; 2. Kaleboynu formation, which is formed by the alternation of carbonates and elastics, 3. Aşgediği formation, consisting of carbonates. Overlying this sequence, Niğde group, is an ophiolitic melange which has undergone deformation and metamorphism together with the underlain formations. It is assumed that the metamorphism of the sequence has transformed into low P-high T condition from the initial medium P-high T condition. The Niğde group is intruded by posttectonic Üçkapılı granodiorite which is concluded to have crystallized in lower Cenomanian (95 ± 11 m.y.) according to the wholerock Rb/Sr analyses. The initial Sr value ($Sr=0.7104$), which is obtained from the wholerock isochrone, indicates that the granodiorite magma is generated either by the melting of the continental crust itself or by the extensive contamination of the continental crust. The cooling ages of granodiorite and gneisses acquired by Rb/Sr wholerock-mineral method and by K/Ar method are $77.8\pm 1-2$ m.y. and 76.5 ± 1.1 -m.y., respectively. These are the ages for granodiorite and gneisses to cool together down to $300\pm 50^\circ\text{C}$, which is the blocking temperature for micas whose isotope ratios have been measured. These data, obtained by geochronological methods are correlated with the other radiometric ages from the other parts of the Central Anatolian Massif and it is put forward that the main metamorphism and ophiolite emplacement have occurred pre-Cenomanian in the massif.

INTRODUCTION

The Niğde massif is located in the SE of Niğde (Fig. 1) and forms the southern end of the Central Anatolian massif (Ketin, 1956).

The metamorphic rocks in the Niğde massif are all together called Niğde group and according to their lithological characteristics they are differentiated and described as Gümüşler, Kaleboynu, Aşgediği formations and Üçkapılı granodiorite (Göncüoğlu, 1977, 1981 a).

The indirect paleontological data is inadequate to date the deposition and the metamorphism of the Niğde group as well as the intrusion of the granitic rocks in the Niğde massif.

In the north of Çamardı (SE of Niğde massif) in the clayey limestone including granitic and gneissic pebbles and unconformably overlying the Niğde group rocks some Upper Paleocene-Lower Eocene ? microfauna were determined which indicate the metamorphism age as Early-Upper Paleocene-Lower Eocene in the previous studies (Göncüoğlu, 1981 b).

In a recent study in south of study area, west of Kılavuz köy, in an unmetamorphosed turbiditic sequence overlain by Paleocene elastics, are found *Globotruncanita stuarti*, *Rosita contusa* and *Ganserina ganseri* which dates down to Upper Maestrichtian (Sirel, 1985, personal communication). This turbiditic sequence, whose relation is not clear with Niğde group rocks, can be correlated with Haymana formation which is well defined in the north, in many places in Central Anatolian massif while the Paleocene restricted shelf elastics overlying the turbiditic sequence can be correlated with Kartal formation (Sirel, 1985, personal communication). This unit which is defined as Çamardı formation by Yetiş (1978) is intruded by microgranite dykes in south of Çamardı. This new evidence

indicates the presence of a magmatism other than the Üçkapılı granodiorite which crops out widespread. Oktay (1982), verifying the above idea states that, in further south, the basement of the Ulukışla basin comprises the products of an island arc magmatism which starts in Upper Cretaceous or in lowermost Paleocene. He puts forward that a part of the oceanic crust which extends between Tuzgözü-Ulukışla has subducted under Niğde massif (Central Anatolian Continent). Under this circumstances, further research is necessary to reveal the fact if Niğde massif is effected by the subduction, and island arc magmatism.

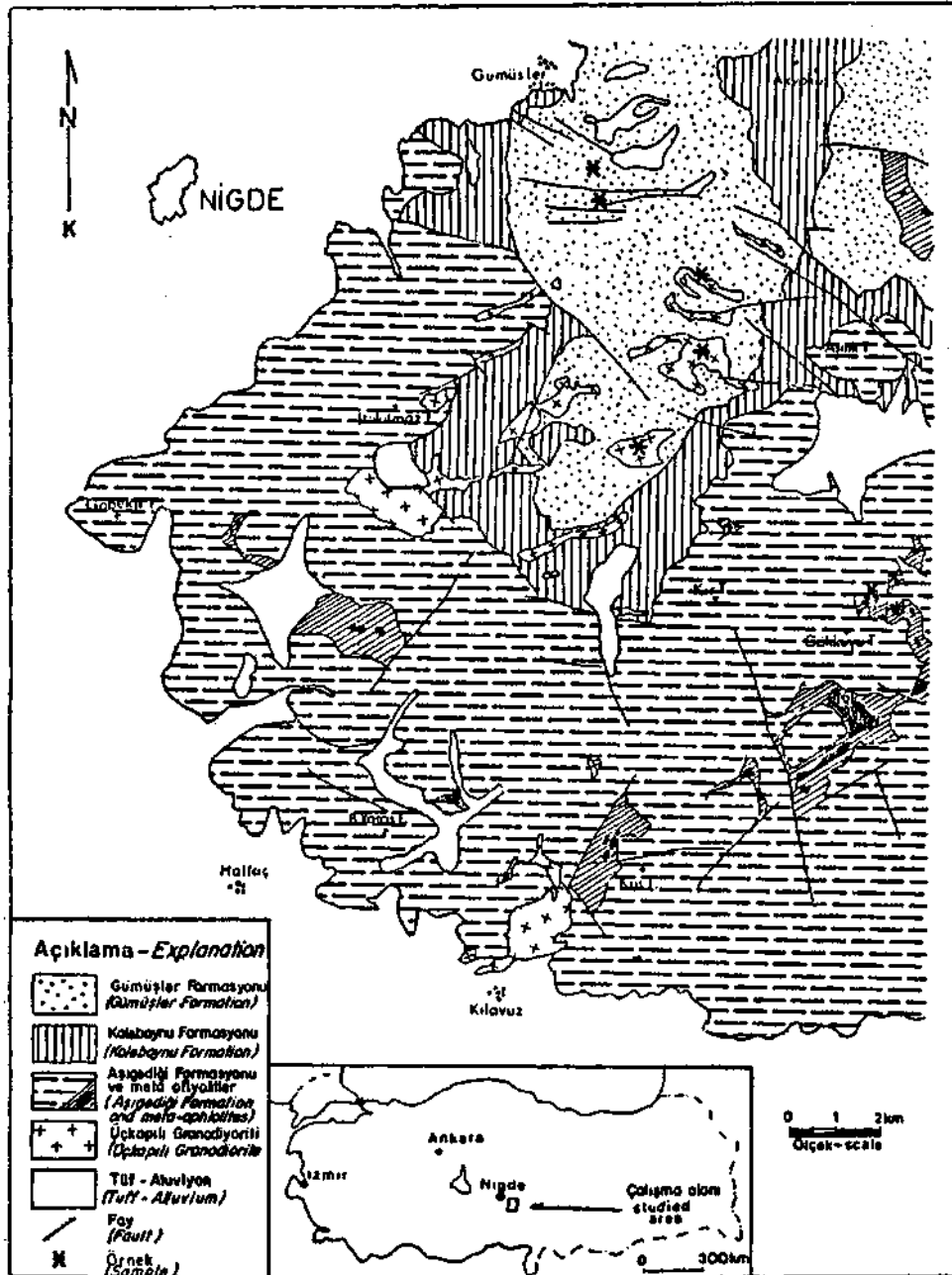


Fig. 1 - A guide map of the studied area and the geological map.

Researches on the age of magmatism and metamorphism in Kırşehir massif which forms the main body the Central Anatolian massif are much more than the ones in Niğde massif. The contradictions in the local and regional studies are still continuing even present day about the age of metamorphic rocks of the region. Some researchers, as discussed in Seymen (1985), suggest that the deposition and the metamorphism ages of the rocks are pre-Mesozoic while Ketin (1956) advocates that the development and the metamorphism of the massif was completed by Laramian phase.

As it is seen by this short discussion, the concrete data that will reveal the geological evolution of the Central Anatolian massif are contradictory and not adequate yet. The inadequacy is very clear if the data is examined which is obtained by the study of the metamorphic and magmatic rocks with various geochronologic methods.

The first geochronologic study in the Central Anatolian massif was carried out by Ayan (1963). He, using the total Pb method, analysed a zircon sample taken from Barana Dag monzonitic granite and proposed the age of intrusion as 54 m.y. in other words, post-Upper Cretaceous. Ataman (1972) pointing out the methodologic disadvantages of Ayan (1963) used Rb/Sr method for two wholerock analyses and a biotite analysis for the samples from Cefalık Dağı granitic mass located in the south of Barana Dag and calculated 71 ± 1 my isochrone age which is equivalent to the age for biotite to cool down for a blocked system for Rb/Sr. The intrusion age for the granite whose origin was interpreted as depending on the palingenesis of juvenile and arkose-graywacke type rock, «regarding the petrological events», is preassumed as 80 m.y. Ataman (1972) reports that this age is consistent with the field observations without mentioning them.

Erkan and Ataman (1981) made some hornblende and biotite K/Ar age determinations from enriched samples of gneisses, mica-schists and amphibolites situated in the NW of Kırşehir. The average age of the three analyzed biotite samples is 69.7 ± 1.7 m.y. while the same value is 74.1 ± 3.2 m.y. for two hornblende samples. Comparing their data with the data of Ataman (1978), the authors suggest that the isotopic system of the metamorphics were wound up by the thermic effect of the intrusion of the granodioritic masses. Also they suggest that the age they calculated as 71 my corresponds to the intrusion/cooling age of the intrusive rocks. The authors, depending on this interpretation, conclude that the effective regional metamorphism has completed its evolution in pre-Cretaceous times. However, since the authors express the age they calculated as «intrusion/cooling age», this data has been used incorrectly by the preceding researchers.

Several samples have been taken from Niğde massif in order to figure out the deposition and the metamorphism of the metamorphic rocks and to date and to study the origin of magmatic rocks. They were analyzed by using Rb/Sr wholerock, Rb/Sr mineral, K/Ar mineral and zircon U/Pb methods. The zircons of biotite-muscovite-sillimanite gneisses taking place in the lowermost part of the Niğde metamorphites have been dated by U/Pb method and it is suggested that the age of the gneiss is 2000 m.y. Also, it is put forward that gneiss has some detritics possibly derived from a magmatic source (Göncüoğlu, 1982). In the same study it was stated that the geological meaning of the second age, 217 ± 3 my, acquired by U/Pb method is not clear since by Rb/Sr, wholerock, Rb/Sr and K/Ar mineral methods, events younger than 217 my were proved. The data obtained by Göncüoğlu (1982) about Alpine events will be given in detail in this study.

For age determination, four samples from Niğde-Üçkapılı granodiorite and two samples from Gümüşler formation, which is represented by gneisses, have been collected. For six of the samples Rb/Sr wholerock, for five of the samples Rb/Sr mineral and for six of the samples K/Ar mineral dating methods have been used for age determinations. Muscovite and biotite grains in different sizes have been used for determinations.

Specimen preparation, chemical analysis and isotope ratio measurements have been made in BGR (Bundesanstalt für Geowissenschaften und Rohstoffe) laboratories in West Germany.

PETROGRAPHICAL FEATURES OF THE MEASURED SAMPLES

Gümüşler formation

The samples numbered NM1 and NM4 used in isotope measurements have been collected from the Gümüşler formation which forms the lowermost unit of Niğde group. This formation consists of gneisses having different mineral compositions and containing lenses and intercalations of marble, amphibolite, quartzitic gneiss and calcilicite marbles (Göncüoğlu, 1977, 1981 *a*). The chemical compositions of the samples are given in Table 1b. The sample NM1 was collected from the lower-

Table 1 - a- Modal combination, b- Chemical combination, of the Gümüşler formation gneisses

	(a)			(b)	
	NM1	NM4a		NM1	NM4a
Quartz	45.4	37.3	SiO ₂	78.90	70.41
K.Feldspar	12.1	16.4	TiO ₂	0.51	0.47
Plagioclase	5.2	7.6	Al ₂ O ₃	9.86	14.85
Biotite	16.1	18.4	Fe ₂ O ₃	2.83	2.73
Muscovite	11.2	9.1	MnO	0.06	0.04
Sillimanite	2.1	3.6	MgO	0.91	1.34
Granat	4.4	1.6	CaO	0.93	2.90
Tourmaline	a	a	Na ₂ O	1.90	4.51
Apatite	a	a	K ₂ O	2.85	1.41
Zircon	a	a	P ₂ O ₅	0.08	0.18
Chlorite	3.5	6.1	Rb(ppm)	111	86
Opaque	a	a	Sr(ppm)	113	175
			Zr(ppm)	191	147
			Y(ppm)	23	34
			Ba(ppm)	591	306
			Cr(ppm)	72	37
			La(ppm)	49	34
			Sc	13	11
			Zn	39	42

most level of the unit in Ören Dere, south of Gümüşler village, on the road to antimony mine. The other one, NM4 was collected 1.5 km. south of this location. The mineralogical composition of the samples are as follows:

NM1: quartz+plagioclase+biotite+muscovite+K-feldspar+sillimanite+tourmaline (+apatite+zircon+rutile);

NM4: quartz+plagioclase+biotite+microcline+garnet (+zircon+apatite+rutile+opaque). In both samples sericitization in plagioclase and chloritization in biotite are seen.

In Gümüşler formation the dominant regional metamorphism conditions are almandine-sillimanite medium grade whereas in the other parts of the Niğde group (with the possible effect of granite) locally, it is thought to have reached cordierite-almandine high degree (Winkler, 1976) and have caused partial melting in gneisses of pelitic origin.

Sillimanite formation in Niğde metamorphics starts with staurolite and in coarse garnet (almandine) blasts, staurolite blasts are observed as inclusions (Fig. 2). In samples having cordierite the presence of relict sillimanite, staurolite and garnet is striking. Petrographic studies show that staurolite disappears with the development of sillimanite+almandine from the conditions where biotite+staurolite are stable initially. In high temperature paragenesis where cordierite is observed, with the development of this mineral, almandine and staurolite lose their stabilities. In the rocks having cordierite the development of muscovite in the last phase and chloritization of biotite indicates an additional retrograde phase. In the two mentioned samples, although they have different evolutionary paths, in the last phase of prograding metamorphism an increase in the temperature is expected.



Fig. 2 - The locked staurolite sticks in Almandines of the Gümüşler formation gneisses.

In Central Anatolian massif, around Kırşehir, it is known that the last stage of the prograding metamorphism is high T low P type. It is claimed that in this region pressure varies between 1.8-2 kb (Seymen, 1985) and 3 kb (Erkan, 1975, 1976) and temperature is approximately 700°C (Seymen, 1982; Erkan, 1975). The degree of metamorphism increases towards NW (Erkan, 1975). On the other hand, contrarily, in far SW of Akdağmadeni staurolite+disthene; in Ortaköy sillimanite; in Kümbet staurolite+sillimanite and in far NW end (İtıdağı) disthene are observed (Erkan, 1975,1980; Tülümen 1980; Özcan et al., 1980; Özer and Göncüoğlu, 1983). Considering the distribution of the critical minerals-instead of the presence of different metamorphism conditions stated by Erkan (1975)-it is

possible to think that regional metamorphism, in time, changes into low P/high T type from medium P/high T because of the rising thermal zones. Around Niğde, the transition of staurolite to metastable phase by the formation of sillimanite+almandine and the transition of almandine+staurolite to metastable phase by the formation of cordierite indicates such a change.

Üçkapılı granodiorite

The acidic intrusive rocks taking place in Niğde metamorphites were studied as Üçkapılı granodiorites which together with its aplites cuts Gümüşler formation, Kaleboynu formation, Aşığı formation and the overlying metamorphic ophiolitic complex. The distribution of the outcrops of granodiorite indicates the presence of a huge and shallow batholith in the center of the study area. In this region, within Üçkapılı granodiorite partially assimilated gneiss, amphibolite and marble xenoliths are seen. There is a narrow contact metamorphism zone between granodiorite and its border rocks. The determined paragenesis in the contact of granodiorite with gneiss, carbonate, and amphibolite and metagabbro are: cordierite+muscovite+garnet, diopside+hedenbergite+vesuvian+garnet (grossularite/andradite), and epidote+garnet+scapolite, respectively. These paragenesis are characteristic for hornblende-hornfels facies of the contact metamorphism (Winkler, 1976). The thickness of wall-rocks and contact metamorphic zone of the Üçkapılı granodiorite ranges from a few centimeters to decimeters.

Under microscope, granodiorite is seen as granoblastic textured and is fine-to-medium grained. Its modal composition is given in Table 2. The primary minerals forming granodiorite are K-feldspar, plagioclase, quartz and biotite. Muscovite, chlorite and rutile are seen as secondary minerals. Accessory minerals are zircon and opaque minerals. Plagioclase occurs as zoned hypidiomorph crystals. An-rich (An_{35-41}) central parts of the crystals are sericitized. On the edges fresh albite (An_{8-12}) is dominant.

Table 2 - Modal combination of Üçkapılı granodiorite

	<i>NM2a</i>	<i>NM2b</i>	<i>NM2c</i>	<i>NM4b</i>
Quartz	30.9	26.1	21.4	28.4
K-feldspar	32.1	28.4	25.5	21.2
Plagioclase	11.2	19.9	28.7	26.1
Biotite	17.6	20.3	18.2	15.4
Muscovite	3.6	2.9	2.7	4.2
Chlorite	4.2	2.1	3.3	4.4
Zircon	a	a	a	a
Apatite	a	0.2	a	0.1
Opaque	0.4	0.1	0.2	0.2

Quartz fills the space between the other minerals and is mostly xenomorphic. It contains reddish-brown idiomorphic biotite and plagioclase inclusions. There are K-feldspar crystals up to 1 cm and its boundaries with quartz and plagioclase are idiomorphic. In coarse blasts perthite formations are seen as bands or stains. K-feldspar has idiomorphic quartz, biotite and plagioclase inclusions. They, in some places, form zones and get coarser from center to the edges.

Biotite is observed as reddish-brown flakes and is 0.7 to 0.2 mm in size. When they are as inclusions in K-feldspar and quartz they are idiomorphic and less chloritized. Coarse biotite flakes

contain clear zircon inclusions elongated parallel to C-axis and apatite. There are paleochroic haloes around zircon inclusions. This kind of biotite crystals have been chloritized in a late hydrothermal stage. In the first stages of chlorite formation the paleochroic haloes have been preserved and on the edges of the grains ilmenite needles have been developed. In the last stage chlorite has replaced tetrahedral layers and has developed together with muscovite. In this kind of alteration products ilmenite has been concentrated on the cleavage planes of biotite.

Zircon, as mentioned above, has been concentrated in biotite and shows the characteristics of zircons crystallized from a solution. Apatite and magnetite can be found as accessory minerals.

The distribution of major and minor elements of Üçkapılı granodiorite is given in Table 3. According to Shand (1951) it is in «peraluminous» group. The average SiO_2 amount of the measured samples is 72.7 %. The samples numbered as NM2 a-b-c have uniform Na_2O and K_2O values. The sample numbered as NM4 b has greater values of SiO_2 and K_2O but less Fe_2O_3 and Na_2O than the samples numbered as NM2. The chemical characteristics and their interpretation will be given in detail in another paper (Göncüoğlu, in preparation).

Table 3 - Chemical combination of Üçkapılı granodiorite

	<i>NM2a</i>	<i>NM2b</i>	<i>NM2c</i>	<i>NM4b</i>
SiO_2	73.49	71.33	71.47	74.47
TiO_2	0.16	0.26	0.20	0.07
Al_2O_3	13.95	15.20	14.70	14.29
Fe_2O_3	1.23	1.64	1.27	0.52
MnO	0.04	0.04	0.04	0.04
MgO	0.26	0.50	0.38	0.16
CaO	0.91	1.71	1.35	1.05
Na_2O	4.07	4.26	4.16	3.69
K_2O	4.29	3.82	4.40	4.89
P_2O_5	0.05	0.08	0.07	0.04
LQI	1.00	0.70	1.50	0.60
Total	99.51	99.60	99.58	99.81
Nb (ppm)	12	11	8	14
Rb	206	166	159	153
Sr	65	165	133	80
Th	23	27	22	14
U	7	6	5	6
Y	28	13	13	26
Zr	110	144	118	62
Ba	412	489	477	236
Ce	32	53	24	39
La	27	33	16	10
V	7	16	12	4
Zn	14	44	33	0
Cr	8	12	7	5

GEOCHRONOLOGY

For the preliminary geochronological investigation, as a first step, Rb/Sr wholerock method has been used to determine the age of gneiss and granite and then by K/Ar and Rb/Sr method the age of micas have been determined.

Methods

The samples whose weight varies between 3 and 5.5 kg. were first broken by a jaw-crusher to sizes less than 5 cm and the altered parts were removed. Then the fragments separated for Rb/Sr wholerock analysis have been prepared according to Muller's (1979) method. Some of the prepared samples have been analyzed by x-ray fluorescence method in order to observe the distribution of the oxides and minor elements. The samples greater than 200 μ have been studied under microscope and it is determined that muscovite and biotite are suitable for mineral Rb/Sr and mineral K/Ar age determinations.

The BGR-Hannover method was applied for the Rb and Sr chemistry of the samples. For the analysis of Rb a spike ($Rb^{85}/Rb^{87}=0.007935$) which has been prepared in the same laboratory and for the analysis of Sr the spike SRM 988 was used. The Rb isotope ratios were measured by an «Aldermaston Micromass 30» type mass-spectrometer with double filament and the Sr isotope ratios were measured by an «Atlas CH4» type mass-spectrometer with a single filament.

The relative errors in measurements of Rb^{87}/Sr^{86} , Sr^{87}/Sr^{86} are 1.5 % and 0.1 %, respectively. Also, they are determined for wholerock isochrone and mineral isochrone calculations as $X^2=1.4$ and $X^2=0.9$, respectively. The constants for Rb/Sr were taken from Steiger and Jager (1977) and York's (1967) method has been used for isochrone calculations.

In K/Ar measurement, the K content of the micas comparing with the internal standard was measured by a double channel digital pipetted flame photometry of type EEL-170 which has Li-internal standard. The Ar isotope ratios were measured by the Ar-extraction system developed by H. Kreuzer through increasing the temperature up to 1500°C for biotite and 1460° for muscovite. In K/Ar measurements two series of different grain size from each sample have been measured and by grinding one of the biotite fractions cross-control has been provided. The acquired values and the model ages have been corrected by laboratory standards.

Rb/Sr wholerock systematics

In the rocks of Niğde group six samples have been measured to determine the Rb/Sr wholerock systematics. Two of these samples have been collected from the gneiss of Gümüşler formation and four of them have been collected from Üçkapılı granodiorite. The analytical data of the measured samples can be seen in Table 4. Plotting these data on Nicolaysen diagram (Fig. 3) isochrones of 460 ± 53 m.y. for gneiss and 95 ± 11 m.y. for granodiorite are obtained.

Table 4 - Rb/Sr wholerock analytical data of the samples of Niğde groups gneisses and Üçkapılı granodiorites

<i>Sample</i>	<i>Rock type</i>	<i>Rb⁸⁷</i> <i>ppm</i>	<i>Sr⁸⁶</i> <i>ppm</i>	<i>Rb⁸⁷/Sr⁸⁶</i>	<i>Sr⁸⁷/Sr⁸⁶</i>
NM1	Gneiss	31.30	11.03	2.805	0.72.464
NM4a	Gneiss	23.65	16.68	1.402	0.71.544
NM2a	Granodiorite	57.36	6.433	8.814	0.72.212
NM2b	Granodiorite	46.43	15.86	2.894	0.71.336
NM2c	Granodiorite	45.87	12.61	3.596	0.71.633
NM4b	Granodiorite	42.17	16.68	5.364	0.71.775

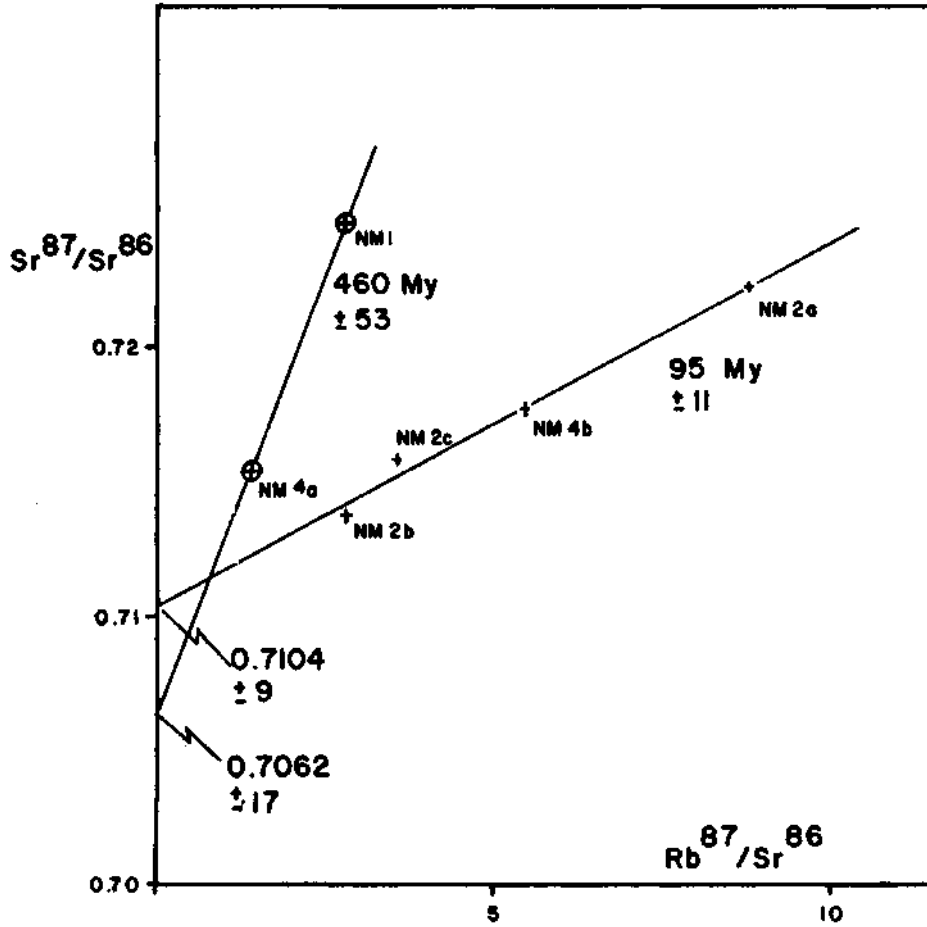


Fig. 3 - Niğde groups gneisses and the positions of Rb/Sr wholerock of Üçkapılı granodiorite samples in the Nicoloyesen diagram (Gümüşteler formation gneisses: NMI, NM4 a, Üçkapılı granodiorites: NM2 a, NM2 b, NM2c, NM4b).

The isochrone drawn from gneiss is not so important since it is represented only by two points. But it is the Pb^{207}/Pb^{206} model age calculated during the age determination of zircon fractions enriched from the sample numbered NMI (Göncüoğlu, 1982). Şengör et al. (1984) suggests that in various regions of Turkey this age corresponds to late Pan-African events. For this reason, it is necessary to sample the gneiss of Niğde group and determine its age by wholerock method and study its geological meaning.

The four samples collected from Üçkapılı granodiorite give an isochrone of 95 m.y. In unmetamorphosed granite, as known, wholerock isochrone age indicates the time by which Rb/Sr migration ends. This phenomena means, after the intrusion, material transportation in the solution was finished because of the crystallization. Then the calculated age, 95 m.y., corresponds to the crystallization age of Üçkapılı granodiorite.

On the other hand, the initial Sr^{87}/Sr^{86} Value of isochrone gives an important clue about the origin of Üçkapılı granodiorite. The calculated value ($Si=0.7104 \pm 0.0009$) indicates that the origin

of the granodiorite is continental crust or an extensive contamination of continental crust. This data, when considered with the presence of the sections where partial melting is reached locally in gneiss as mentioned in the introduction, may support the idea stating that the Üçkapılı granodiorite has been formed by the partial melting of continental crust.

Rb/Sr mineral analyses

In order to study the Rb/Sr distribution and Sr homogenization, biotite from the samples NM1 and NM4, biotite from the sample NM2b and muscovite and biotite from sample NM4b have been analyzed and the results were given in Table 5.

Table 5 - Rb/Sr mineral analytical data of the samples of Niğde groups gneisses and Üçkapılı granodiorites

Sample	Rb ⁸⁷ ppm	Sr ⁸⁶ ppm	Rb ⁸⁷ /Sr ⁸⁶	Sr ⁸⁷ /Sr ⁸⁶
BNM1	182.3	0.4644	387.8	1.1390
BNM4a	171.6	0.9269	183.0	0.9098
BNM2b	270.3	0.2395	115.5	1.9489
BNM4b	230.0	1.0673	213.0	0.9463
MNM4b	143.9	0.9419	151.0	0.8805

Evaluating the measured minerals and the samples together (Fig. 4), a certain mineral-wholerock isochrone which dates 77.8 ± 1.2 m.y. and gives an initial value of 0.7111 ± 0.0037 for Sr, is obtained. Then from the isochrone it is deduced that Sr homogenization for wholerock and has been realized. Isochrone line has less inclination than wholerock isochrone. This data which appears as the wholerock/mineral age of gneiss and granodiorite may be interpreted in two ways:

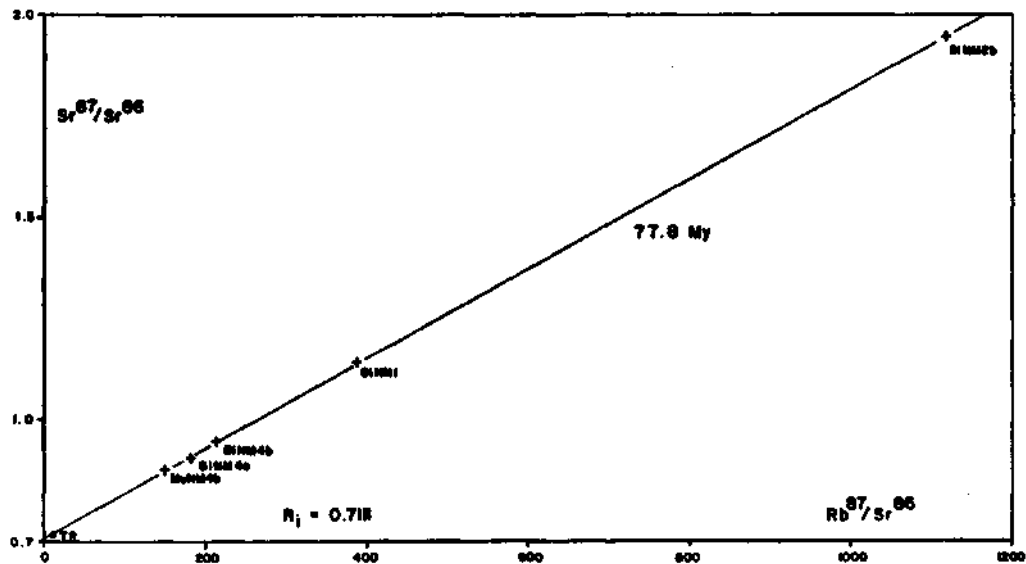


Fig. 4 - Distributions of mineral analysis of Niğde groups gneisses and Üçkapılı granodiorites in the Sr-evolution diagrams (B=biotite, M=muscovite, TR=wholerock, see figure 3 for the number of the samples).

a. The determined age indicates a metamorphism event which leads to Sr homogenization both in gneiss and granodiorite.

b. The determined age indicates a stage in which micas, at a certain temperature, have been blocked for Rb/Sr. In this case 77.8 ± 1.2 my is the cooling age of the measured samples for Rb/Sr. Considering the studies in the Alps (Dodson, 1973; Wagner et al., 1977) the above age is obtained by a decrease in the temperature of the measured samples down to $300 \pm 50^\circ\text{C}$.

The first interpretation may be eliminated since no trace of metamorphism or deformation is seen in Üçkapılı granodiorite. The second interpretation is especially supported by the wholerock-biotite-muscovite isochrone of the sample NM4b. From the structure of this isochrone, it is deduced that muscovite acted as an open system until biotite is blocked for Rb/Sr around 300°C . If it is considered that, in case of the formation of muscovite by metamorphism, the blocking temperature for Rb/Sr is around 500°C ($500 \pm 50^\circ\text{C}$) (Jager and Hunziker, 1979), because of the above stated reason, wholerock-muscovite-biotite isograd does not give metamorphism age. Another data supporting that 78 my reflects the cooling age is K-Ar mineral ages.

K-Ar mineral analyses

The following samples of Niğde group rocks have been analyzed for K-Ar: Two fractions from gneiss sample (NM1), biotite from gneiss (NM4a), ground biotite from granodiorite sample (NM2b), biotite and muscovite from granodiorite (NM4b). Analytical data is shown in Table 6. In this table biotites from gneisses and granodiorites give model ages varying between 74.9 ± 1 and 77.9 ± 1.2 m.y. These ages are consistent with Rb/Sr ages within error limits. Considering biotites have almost the same blocking temperatures for K-Ar and Rb/Sr (Jager and Hunziker, 1979), it is obvious that the acquired model ages reflect the cooling age, below 300°C ($\pm 50^\circ\text{C}$), as in Rb/Sr mineral ages. One of the muscovite sample taken from a granodiorite sample (NM4b) gives higher model age than that of biotites. This age, 78.5 ± 1.2 m.y. gives the blocking age of muscovite for K-Ar. Actually, the blocking temperature of muscovite is around 350°C for K-Ar and it blocks before biotites. Muscovite, therefore, must have a higher model age.

Table 6 - The mineral K-Ar analytical datas (B=biotite, M=muscovite) of Niğde groups gneisses and Üçkapılı granodiorites

Sample	Grain size	% K	$^{40}\text{Ar}/\text{rad}$	% rad/Ar	$^{40}\text{K}/^{36}\text{Ar}$	$^{40}\text{Ar}/^{36}\text{Ar}$	Model age (my)
BNM1	500-250	7.75	234.9	95.22	1357.9	6442	76.28 ± 1.2
BNM1	250-160	7.76	234.2	95.26	1448	6827	76.0 ± 1.0
BNM4a	400-160	7.66	235.3	97.11	2325	10972	77.4 ± 1.2
BNM2b	200-100	6.89	208.3	96.88	2216	10313	76.2 ± 1.2
BNM4b	500-160	6.27	186.3	94.93	1310	6115	74.9 ± 1.2
MNM4b	500-160	8.69	270.9	95.24	1413	6879	78.5 ± 1.2

When the blocking temperatures of muscovite and biotite and the acquired model ages are evaluated roughly together, a cooling rate of $15^\circ\text{C}/\text{m.y.}$ is obtained. This value may be considered as a preliminary data about the uplift of Niğde. group rocks after 75 my.

CONCLUSIONS

The Niğde group rocks consist of gneiss whose origin is possibly clastic and an overlying thick carbonate sequence. In the upper part of the massif is an ophiolitic complex which has undergone deformation and metamorphism together with the Niğde group rocks. The Niğde group rocks have been cut by Üçkapılı granodiorite and have undergone contact metamorphism. The oldest and unmetamorphosed unit which has relation with metamorphites contains fossils of Upper Maestrichtian.

When mineral paragenesis of Niğde group rocks have been studied it is noticed that the conditions of regional metamorphism, in time, changes from almandine-sillimanite medium grade to cordierite-almandine high grade. This change, especially in the pelitic originated rocks reach up to partial melting.

Gümüşler gneiss which forms the lowermost part of Niğde-group rocks, implies even if questionably, the existence of a Pan-African event in terms of Rb/Sr wholerock and zircon Pb^{207}/Pb^{206} model age.

The crystallization age of Üçkapılı granodiorite is determined as 95 ± 11 m.y. by Rb/Sr whole-rock isochrone. The initial Sr value (0.7104) obtained from isochrone shows that the granodiorite magma has been generated totally or extensively by the melting of the continental crust. This data supports the result reached by field observations and petrographic interpretation and indicates that the generation of granodiorite depends on the partial melting of the psammopelitic rocks situated in the lower parts of Niğde group. The ages 78 m.y. 78 m.y. and 75 to 78 m.y. determined from biotites and muscovites by mineral-wholerocks, from muscovites by K-Ar analysis and from biotites by K-Ar method, respectively, shows both the homogenization of gneiss and granodiorite together and the cooling of them together below $300 \pm 50^\circ C$ which is the blocking temperature for micas. Especially, the consistence of the mineral model ages of gneiss and granodiorite is interpreted to indicate that with granodiorite intrusion, in metamorphic rocks the Rb/Sr and K-Ar systems are opened below the formation temperatures of micas and closed during cooling. In order to determine the metamorphism ages of Niğde group metamorphites more analyses of gneiss by Rb/Sr wholerock method are needed.

The age determinations obtained from the gneiss and granodiorites of Niğde massif are slightly different than the ones obtained by Erkan and Ataman (1981) from the rocks of Kırşehir region and than the ones obtained by Ataman (1972) from the rocks of Cefalık Dağ region. Ataman concluded that the age is 71 m.y. by biotite-wholerock isochrone and stated that it is the cooling age of biotite. His suggestion about the age of the granite intrusion as 80 m.y. has no evidence. Erkan and Ataman (1981) states the K-Ar biotite age for amphibolites and micaschists of Kırşehir massif is 60 m.y. and the hornblende age for the same rocks is 74 m.y. They express these values as the «intrusion/cooling» age of granodiorite. Accepting these ages as cooling age, the evidences and age determinations of the writers are consistent with the ones obtained in Niğde massif.

In the Kırşehir, Akdağmadeni and Niğde regions of Central Anatolian massif similar rock series are seen (Seymen, 1981, 1985; Özcan et al., 1980; Tülümen, 1980; Göncüoğlu, 1977, 1981a). In these regions, from bottom to top, metaclastics, carbonate interbedded elastics and carbonates are dominant. At the top, -at least in Niğde and Akdağmadeni regions-together with the underlain platform type rocks, an ophiolitic complex which has undergone deformation and metamorphism can be seen. Granitic and granodioritic rocks cut both the metamorphics at the base and the ophiolitic rocks. Around Eskişehir-Sivrihisar region which is claimed to be in a different belt than Central Anatolian massif (Şengör and Yılmaz, 1981), there are great similarities in the sequence of metamorphism, position of ophiolitic complex and in age of the intrusives (91 m.y., Gautier, 1984).

Under such circumstances, in Central Anatolian Massif and probably around Sivrihisar region, granodiorite intrusion has taken place in Cenomanian (95-91 m.y.). Considering granodiorite cuts both the rocks at the base and ophiolite, it can be deduced that ophiolite emplacement must have been occurred in pre-Cenomanian times.

This idea is contradictory with Seymen's (1981, 1982, 1983, 1985) interpretations. Because, although Ataman (1972) states that the age determined in Cefalık Dağı granite mass (what Seymen calls «Barana Dağ Pluton»), 71 m.y., corresponds to the cooling age of granite and as a result the intrusion age must be older, Seymen (1985) puts forward that Uppermost Cretaceous-Lower Paleocene (69-63 m.y.) sediments were cut by the same granitic intrusions.

Görür et al. (1985) who are following Seymen's interpretations accept that the emplacement age of the ophiolitic mass overlying the Central Anatolian massif is Late Cretaceous and the age of the «arc plutonics» cutting them are Latest Cretaceous in age. In the geodynamic models of the authors it is suggested that, depending on Bergougnan (1975), the ophiolites of the northern branch of Neotethys have been thrust over the Central Anatolian massif in Upper Cretaceous. The magmatism cutting these ophiolites are thought to be related to the Andean type arc plutonism which is caused by the oceanic plate which subducts under Central Anatolian block along Inner Taurus suture. If the magmatism of the Central Anatolian massif is studied under the light of the data brought by this paper, it will be seen that it is necessary to review the geodynamic interpretations of Görür et al. (1985), at least for the time concerned.

ACKNOWLEDGEMENTS

The geochronological part of this study has been carried out in BGR laboratories and has been supported by CDG Institution of West Germany. I thank to Dr. P. Müller from Petrography Department and to Prof. Dr. I. Wendt, Dr. A. Hohndorf and Dr. H. Kreuzer from Geochronology Department for providing the laboratory facilities, and to Dr. Raschka for geochemical analyses and to S. Lenz for Rb/Sr measurements. I also thank to Dr. E. Sirel for paleontological determinations and to Asst. Prof. Dr. M. Satır for his valuable discussions of the results. İsmail Kuşçu kindly translated the paper.

Manuscript received December 12, 1985

REFERENCES

- Ataman, G., 1972, Ankara'nın güneydoğusundaki gronitik-granodiyoritik kütlelerden Cefalık Dağının radyometrik yaşı hakkında ön çalışma: Hacettepe Fen ve Müh. Bilimleri Derg., 2, 44-49.
- Ayan, M., 1963, Contribution a l'etude petrographique et geologique de la region situee au NE de Kaman: MTA Publ., 155, 332 p.
- Bergougnan, H., 1975, Relation entre les edifices pontique et taurique dans les Nord-Est de Anatolie: Bull. Soc. Geol. France, 7, 1045-1057.
- Dodsan, M.H., 1973, Closure temperature in cooling geochronological and petrological systems: Contrib. Mineral Petrol., 40, 459-474.

- Erkan, Y., 1975, Orta Anadolu Masifi güneybatısında (Kırşehir bölgesinde) etkili rejyonel metamorfizmasının petrolojik incelemesi: H.Ü. Thesis. 147 P.
- , 1976, Kırşehir çevresindeki rejyonel metamorfik bölgede saptanan izogradlar ve bunların petrolojik yorumları: *Yerbilimleri*, 2/1, 23-54.
- , 1980, Orta Anadolu Masifinin kuzeydoğusunda (Akdağmadeni, Yozgat) etkili olan bölgesel metamorfizmanın incelenmesi: *TJK Bull.*, 23, 213-218.
- and Ataman, G., 1981, Orta Anadolu Masifi (Kırşehir yöresi) metamorfizma yaşı üzerine K/Ar yöntemi ile bir inceleme: *H.Ü. Yerbilimleri*, 8, 27-30.
- Gautier, Y., 1984, Deformations et métamorphismes associées à la fermeture Téthysienne en Anatolie Central (Region de Sivrihisar, Turquie): Paris Univ., Ph.D. Thesis 151 p.
- Göncüoğlu, M.C., 1977, Geologie des westlichen Niğde Massivs: Bonn Univ., Ph.D. Thesis 181 p. (unpublished).
- , 1981a, Niğde Masifinin jeolojisi. İç Anadolu'nun Jeoloji Simpozyumu: *TJK Publ.*, 16-19.
- , 1981b, Niğde Masifinde viridin-gnaysm kökeni: *TJK Bull.*, 24/1, 45-51.
- , 1982, Niğde Masifi paragneyslarında zirkon U/Pb yaşları: *TJK Bull.* 25/1, 61-66.
- Görür, N.; Oktay, F.Y.; Seymen, İ. and Şengör, A.M.C., 1985, Paleotectonic evolution of the Tuzgölü basin complex, Central Turkey: sedimentary record of a Neo-Tethyan closure in: Dixon, J.E. ve Robertson, A.H.F. (ed.) 1985, *The Geological Evolution of the Eastern Mediterranean*, Spec. Pub. of the Geo. Soc. 17, Blackwell Sci. Pub., Oxford. 848 p.
- Jager, E. and Hunziker, K., 1979, *Introduction to Geochronology*: 329 p. Springer Verlag, New York.
- Ketin, İ., 1956, Yozgat bölgesinin jeolojisi ve Orta Anadolu Masifinin tektonik durumu: *TJK Bull.*, 6, 1-40.
- , 1966, Türkiye'nin tektonik birlikleri: *MTA Bull.*, 66, 20-34, Ankara.
- Müller, D., 1979, Erfahrungen bei der Mineraltrennung für radiometrische Altersbestimmungen: *Erzmetall*, 32/2, 232-263.
- Oktay, F.Y., 1982, Ulukış ve çevresinin stratigrafisi ve jeolojik evrimi: *TJK Bul.*, 25, 15-23.
- Özcan, A.; Erkan, E.; Keskin, A.; Keskin, E.; Oral, A.; Özer, S.; Sümengen, M. and Tekeli, O., 1980, Kuzey Anadolu Fayı Kırşehir Masifi arasının temel jeolojisi: *MTA Rap.*, 6722 (unpublished), Ankara.
- Özer, S. and Göncüoğlu, M.C., 1983, Orta Anadolu Masifi doğusunda (Akdağmadeni-Yıldızeli) ilginç metamorfik parajenezler: *MTA Bull.*, 95/96, 173-174, Ankara.
- Seymen, İ., 1981, Kaman (Kırşehir) dolayında Kırşehir Masifinin stratigrafisi ve metamorfizması: *TJK Bull.*, 24/2, 101-108.
- , 1982, Kaman dolayında Kırşehir Masifinin Jeolojisi: İTÜ Maden Fak. Thesis 164 p.
- , 1983, Tamadağ (Kaman-Kırşehir) çevresinde Kaman Grubunun ve onunla sınırdaş oluşukların karşılaştırılmalı tektonik özellikleri: *TJK Bull.*, 26, 89-98.
- , 1985, Kırşehir Masifi Metamorfitlelerinin Jeoloji Evrimi: Ketin Simpozyumu, *TJK Publ.*, 133-148.
- Shand, S.J., 1951, *Eruptive Rocks*: John Wiley, New York.
- Steiger, R.H. and Jager, E., 1977, Subcomission on geochronology: convention on the use of decay constants in geo- and cosmochronology: *Earth and Planet Sci. Letters*, 36, 359-362.
- Şengör, A.M.C. and Yılmaz, Y., 1981, Tethyan evolution of Turkey: a plate tectonic approach: *Tectonophysics*, 75, 181-241.
- , Satır, M. and Akkök, R., 1984, Timing of tectonic events in the Menderes Massif, Western Turkey: Implications for tectonic evolution and evidence for Pan-African basement in Turkey: *Tectonics*, 3/7, 693-707.
- Tülümen, E., 1980, Akdağmadeni (Yozgat) yöresinde petrografik ve metalojenik incelemeler: *KTÜ, Thesis*, 157 p.
- Wagner, G.A.; Reimer, G.M. and Jager, E., 1977, Cooling ages derived by apatite fission track, mica Rb/Sr and K/Ar dating: The uplift and cooling history of Central Alps: *Mem. Inst. Geol. Min. Univ., Padova*, XXX, Italy.
- Winkler, H.J.F., 1976, *Petrogenesis of metamorphic rocks*: Springerverlag, 4 Ed., 327 p.
- Yetiş, C., 1978, Çamardı yakın ve uzak dolayının jeolojisi ve Ecemiş yarılım kuşağının Maden Boğazı-Kamışlı arasındaki özellikleri: İ. Üniv., Ph.D. Thesis 164 p.
- York, D., 1967, The best isochrone: *Earth and Planet Sci., Letters*, 2, 479-482.

DETERMINING TWO DIMENSIONS OF A CONCEALED CHROMITE ORE BY MICRO-COMPUTER MODELLING OF MAGNETIC TOTAL FIELD INTENSITY PROFILE

Doğan AYDAL*

ABSTRACT. — Computer modelling, using Manik Talwani's method to determine the two dimensions of an ore body is described. It is shown that quite accurate determination of the two dimensions of ore body is possible with such application. It is suggested that such applications could be very useful for better programming of drilling and better estimation of ore bodies in chromite.

INTRODUCTION

During the research, so named «Searching unknown-unseen chromite ore deposits with a protonmagnetometer», which was supported by Turkish technical and research council, so called TÜBİTAK, some distinct anomaly were detected between chromite deposits and surrounding hostrock, after taking and evaluating some 4000 measurement in the 1.1 sq. km. Finally six probable ore deposition place and some 11 drillings on them were suggested.

As far as studied case concern, in one of the probable ore deposition area, two dimension of probable chromite ore deposit size was tried to be found, with the help of it's magnetic susceptibility and imagined ore shape in microcomputer.

The field research, including geophysical, geological and mineralogical work, has taken place in 1982 and 1983 summers period, whilst the laboratory work were done in 1983-1984 winters, so M.A.G. 617 TÜBİTAK project were completed within 3 years. Especially this study, which is based on, but not a part of mentioned project, was carried out some part of 1984 winter period.

The used path for research as follows; Five cross-section, so named as (C-D), (E-F), (G-H), (J-K), (L-M), were chosen over one of the probable ore deposition area, which is placed just NW of örnek ocak area and contoured on the 1:10.000 scaled total magnetic intensity map (Fig. 1). If it is noticed to mentioned cross sections (Fig. 3,4,5,6,7), that earth's total magnetic intensity as well as topografic condition were demonstrated on top another on the same page. At the end of rutin comparison of the topografic and magnetic sections together, it was realized, that high earth's total magnetic intensity values comes out on the high topografic part of sections in general, although it is not a rule.

On the contrary of this general view in the studied area, especially on the left part of the cross-section (L-M), some distinct earth's total magnetic intensity values were detected and all research diverted to find out this phenomena and cause of this unignorable magnetic value increases.

Before start the research, some other relevant studies were normally checked, but somehow there was no single study came cross, which is directly related with chromite reserve analysis with microcomputer. In fact, there are many studies, which were noticed, suggest some different methods of computer programme for evaluation of ore reserve in two or three dimension (see ref 1-to 15).

As a matter of fact, that the computer programme, was used in this studied case, was developed by Manik Talwani. In an other words, this present study's target is not a programme making for

computer, on the contrary, try to show a probability of a reserve analysis for chromite ore in the ultrabasic area, with a computer.

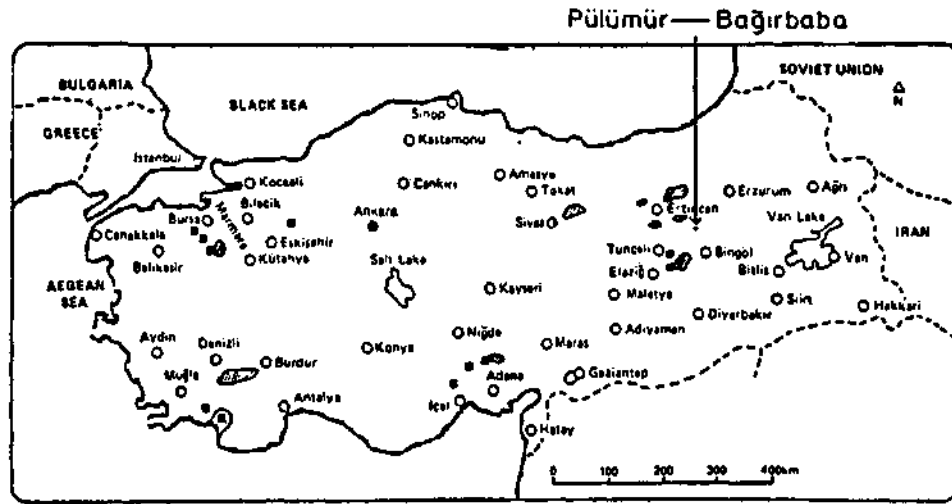


Fig. 1A - Location of the studied area in Turkey.

It is normally suggested, that some geologic 1 geophysical and the other suitable ways should be tried, before final reserve analysis is made in the studied area. As it is known, that even ore is thoroughly detected, the right outcropping and mining method should be decided carefully in advance of drillings.

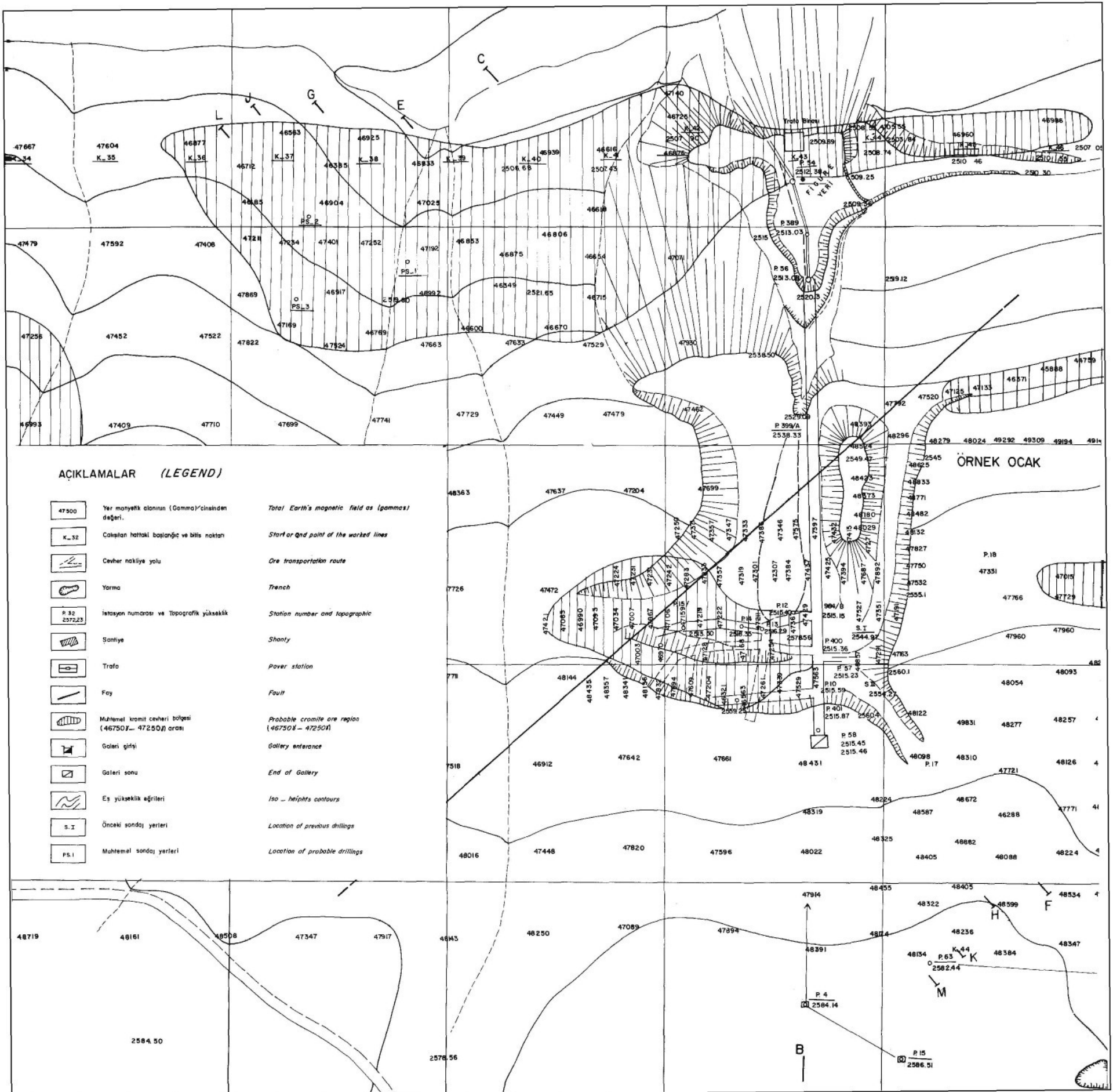
The present method is one of these ways, which may show the right economical path for mining. The specificity of this work is not only, that it was done by microcomputer, besides it was tried on chromite ores, in the low ferromagnetic ultrabasic area, which has no distinct ferromagnetic value, if it is compared with ferromagnetic Iron, thus the studied case was needed more sensitive care than usual.

MATERIAL AND METHOD

Earth's total magnetic intensity measurements were taken with 20 m. intervals at the field, whilst 4 m. intervals was used around örnek ocak ore deposition vicinity in order to improve trustability of measurements. As it was mentioned in advance that roughly 4000 measurement were taken within 1.1 sq. km.

The other maps was not included to this article just because, they have not got any direct relation with the present study. Thus, örnek ocak, where chromite deposits are still under mine, was chosen and all topographic and magnetic cross-section were taken over it in advance.

At first, bell-like anomaly on section (L-M) was drawn by computer with the help of 11 points (Fig. 2), than probable ore body's shape, which causes bell-like anomaly at the field, was tried to be found in two dimension. So that some 73 imaginary ore shapes were coded to computer in order to find out the most probable ore shape. Due to publishing problems, except some typical examples, most of them were not included to the present article.



AÇIKLAMALAR (LEGEND)

	Yer manyetik alanının (Gamma)'cinsinden değeri.	Total Earth's magnetic field as (gamma)
	Çalışılan hattaki başlangıç ve bitiş noktaları	Start or end point of the worked lines
	Cevher nakliye yolu	Ore transportation route
	Yarma	Trench
	İstasyon numarası ve Topografik yükseklik	Station number and topographic
	Şantiye	Shanty
	Trafo	Power station
	Fay	Fault
	Muhtemel kromit cevheri bölgesi (46750γ - 47250γ) arası	Probable chromite ore region (46750γ - 47250γ)
	Galeri girişi	Gallery entrance
	Galeri sonu	End of Gallery
	Eş yükseklik eğrileri	Iso - heights contours
	Önceki sondaj yerleri	Location of previous drillings
	Muhtemel sondaj yerleri	Location of probable drillings

ÖRNEK OCAK

In exception, Figure 8B, 9B, 10B and 11B were obtained with using same imagined shape (8A), but changing the real magnetic susceptibility value in between (0.0015-0.0025) emu (electro magnetic unity). At last of these trials (Fig. 13A, B; 14A, B; 15A, B; 16A, B), changing the real magnetic susceptibility values and imaginary ore shapes, the most probable ore shape and its anomaly were found, which can fit in to the anomaly, which was drawn according to earth's total magnetic intensity values, which were detected by proton magnetometer at the studied area (Fig. 17A, 17B).

If one would able to prepare some more cross-sections very close to section (L-M), than it may became possible to find out rough third dimension and more exact reserve analysis can be made.

Just before given one specific example to show followed path during model analysis, used constant and abbreviations should be explained.

On the microcomputer programme;

X — 1:500 scaled cross-section were placed on X abscissa as (m)

F = Measured total magnetic intensity of earth at the studied area placed on Y ordinate as gammas (g)

A = Inclination angle, 58° at the studied area

B = Denclination angle, 2° at the studied area

C = Cross-section strike's angle from north
At the studied area, it is 40° for all
(C-D), (E-F), (G-H), (J-K), (L-M) sections

K = The real magnetic susceptibility values for chromite ore, which were found at the laboratory in between (0.0015-0.0025) emu

The earth's total magnetic intensity's background of studied area is 46 500 g, but for this present study, above 47 000 g level was accepted as «fit in» part, for obtained computer graphic and graphic obtained from field measurement.

It can be seen easily, if it is noticed the first 5 cornered imagined ore shape (8A), which is 1:1000 scaled on the Y ordinate, 1:500 scaled on the X abscissa and computed, with found susceptibility value.

At the first trial, the real magnetic susceptibility value of chromite ore is accepted as $K=0.0017$ emu, but after trial, it was seen that the graph obtained, did not fit in to bell-like anomaly, which was obtained from (L-M) cross-section of field measurement.

Than for the same shape, different susceptibility values (0.0019, 0.0022, 0.0024 emu) were tried, but still «fit in» graph could not have been obtained (Fig. 9B, 10B, 11B). Later on, imagined ore shape was changed and 6 cornered shape in different coordinate and position were tried with different k values.

At the end of 73 trials, the most probable ore shape and the most «fit in» position were obtained (Fig. 17 A,B).

According to this final ore shape, the probable ore, with 85 m. depth and roughly 30 m. width, situated roughly 15 m. from surface level.

Tunceli Pülümür

<i>Point</i>	<i>X</i>	<i>Z</i>	<i>V</i>
1	0	52	-5.00000E+002
2	10	47	-5.20000E+002
3	25	40	-4.30000E+002
4	37	35	-2.00000E+002
5	50	30	3.00000E+001
6	69	23	2.00000E+002
7	81	22	5.00000E+001
8	90	21	-2.00000E+002
9	100	21	-3.50000E+002
10	115	17	-4.10000E+002
11	130	10	-3.00000E+002

F = 46500
 A = 58
 C = 40
 B = 2

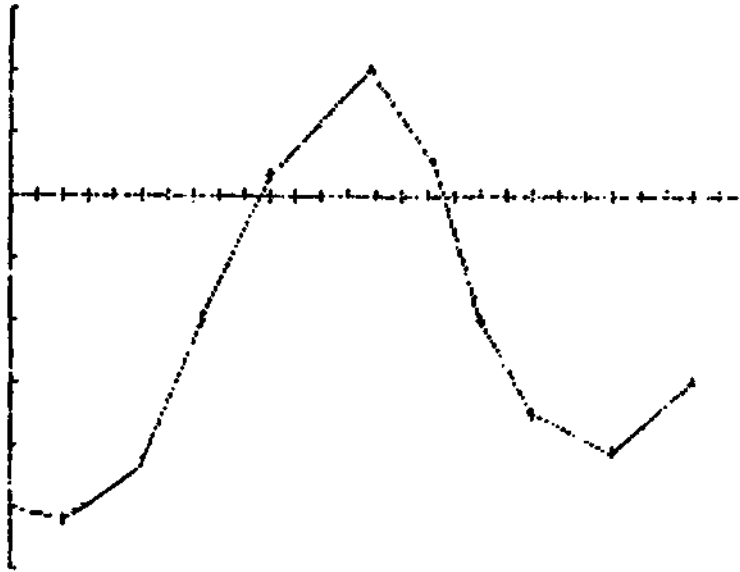


Fig. 2 - Bell-like anomaly from the section (L-M) was drawn with the help of 11 points by micro computer.

DISCUSSIONS AND RESULTS

The main weakness of the suggested method is that not being managed to prove it with drillings. The studied vicinity's concession right belong to private bodies and naturally managed by them, therefore neither TÜBİTAK, nor any other relevant government establishment, such as MTA, Etibank, would have been able to support these suggested drillings. Besides, it was seen very difficult to persuade private miners for such heavy investment.

A part of this main weakness, there is another important point was that, surrounding host-rock interference, either positive or negative direction was not being able to calculated in the computer programme. But even than, it was found quite useful to try as it is.

After working some other places with the same method and seeing the result of drillings, than ore can search, in what condition and how, the surrounding rocks magnetic susceptibility interference, add or deduct from calculation in the computer programme.

Besides all, one must be careful, while collecting hand samples. Naturally more sample collection would improve the sensitivity of the results, which would be obtained at the laboratory.

Susceptibility measurement should be repeat as much as one can, in order to minimize faulty measurement probability.

During the magnetic susceptibility analysis, samples were grinded into a rice and/or cracked-wheat size, than measurement took place. But, samples can be grinded in to a different mesh size and compare the results respectively. Finally, if all results would have come out to be affirmative to the present method, it can be said that, in the studied part of the searched area, some 85 m. depth, and roughly 30 m. width chromite deposit was detected. Even the thickness of ore is accepted only as 10 m. and tenore of chromite is accepted as 40-42 % Cr_2O_3 , than roughly 50.000 tons of pure chromite supposed to be found. If one would like to find out exact thickness of ore, instead of 10 m. estimation, than should try to prepare topographic and magnetic cross-sections very close to (L-M) section, and do exactly same process for each.

As it is known, that for the time being in Turkey, either government managed mining companies or rich private companies have computer facilities, so that it is worth to try this type of advance work before drillings, in order to spare time and money.

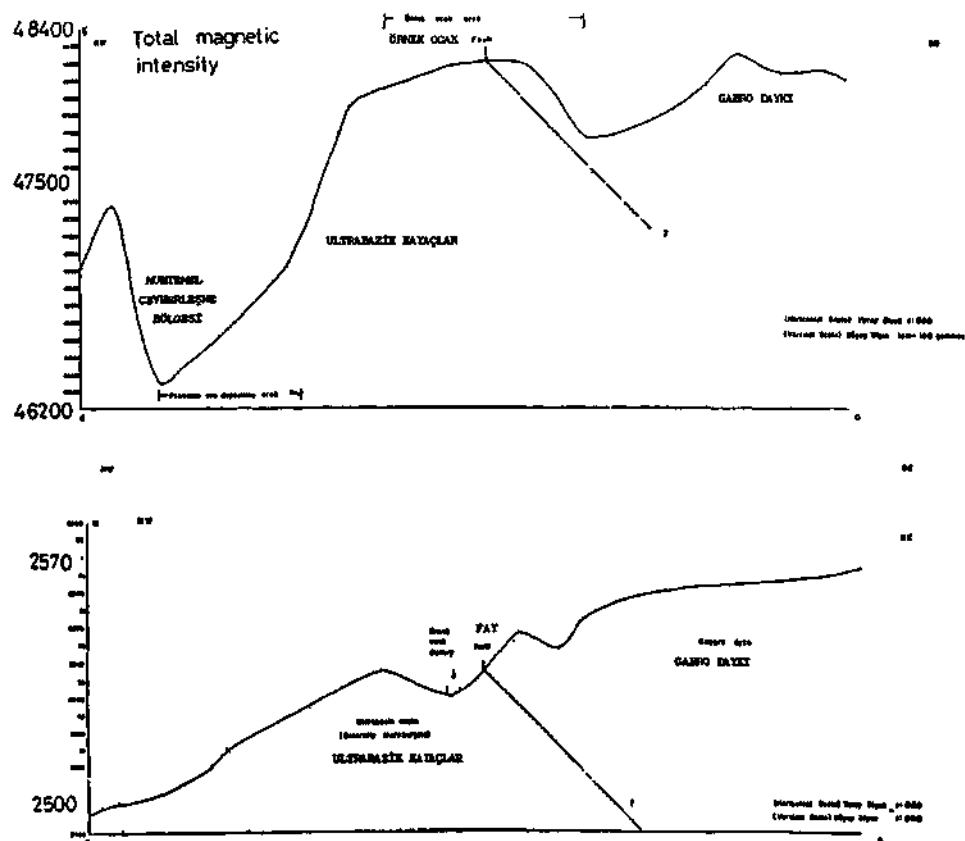


Fig. 3 - The cross-section (C-D).

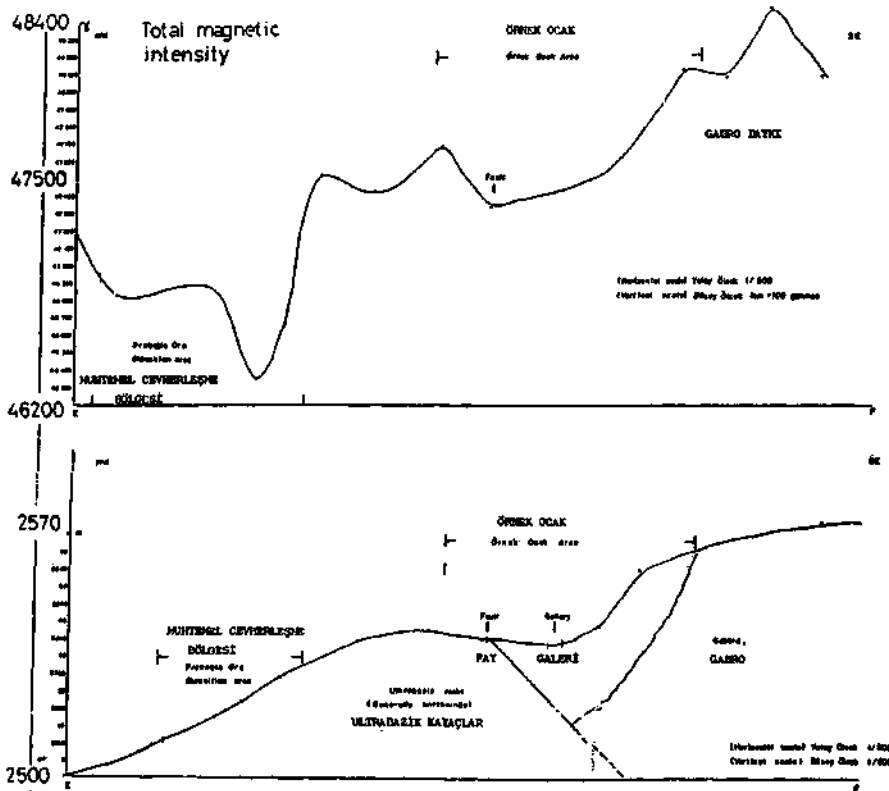


Fig. 4 - The cross-section (E-F).

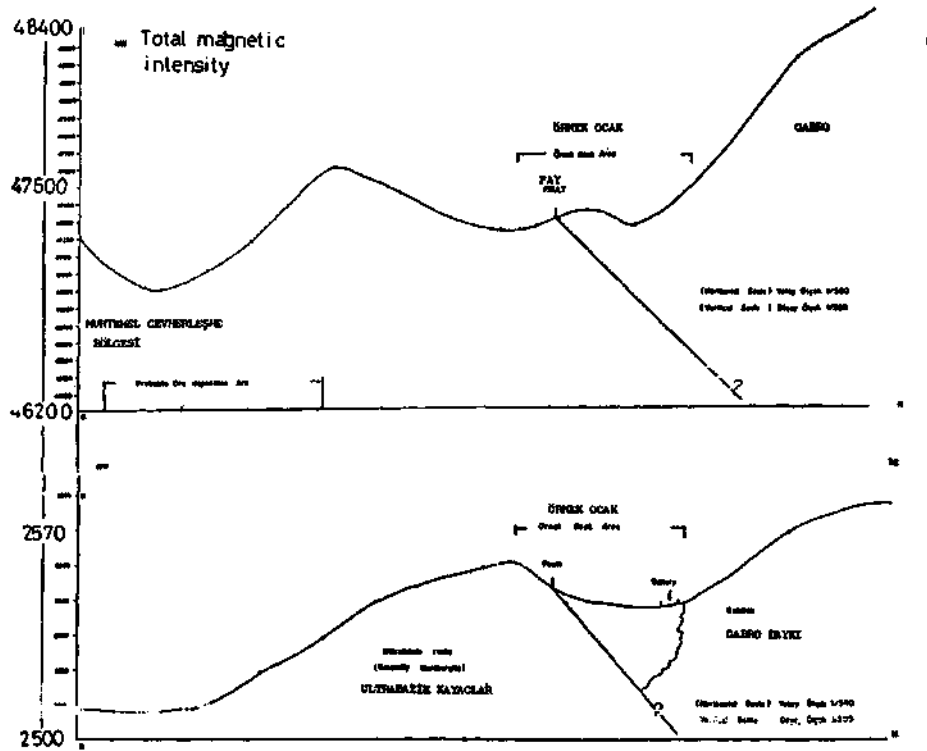


Fig. 5 - The cross-section (G-H).

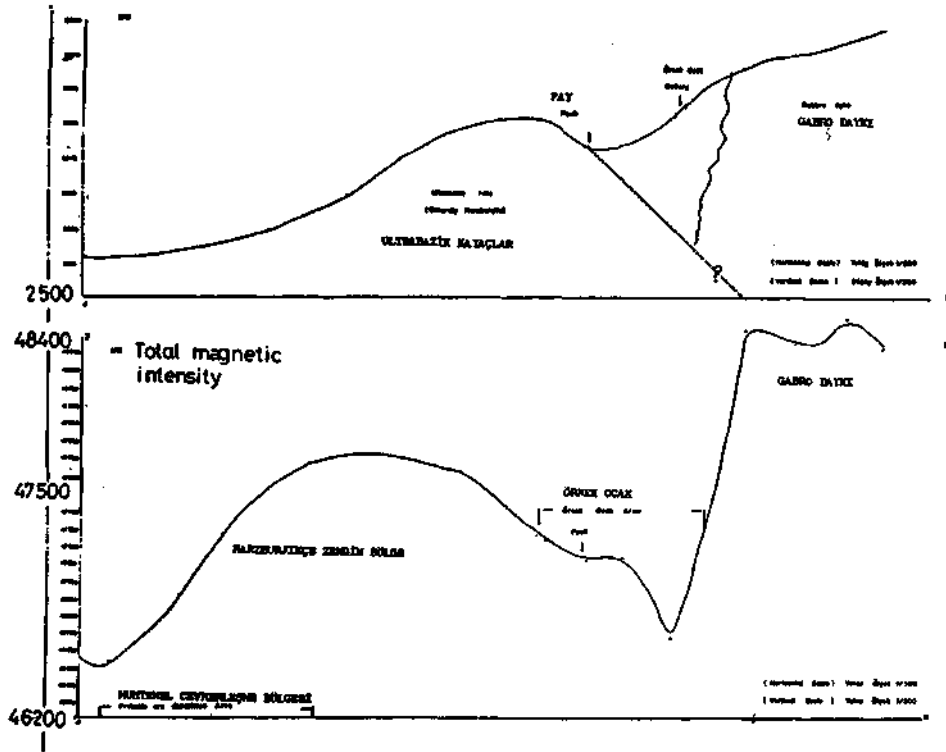


Fig. 6 - The cross-section (J-K).

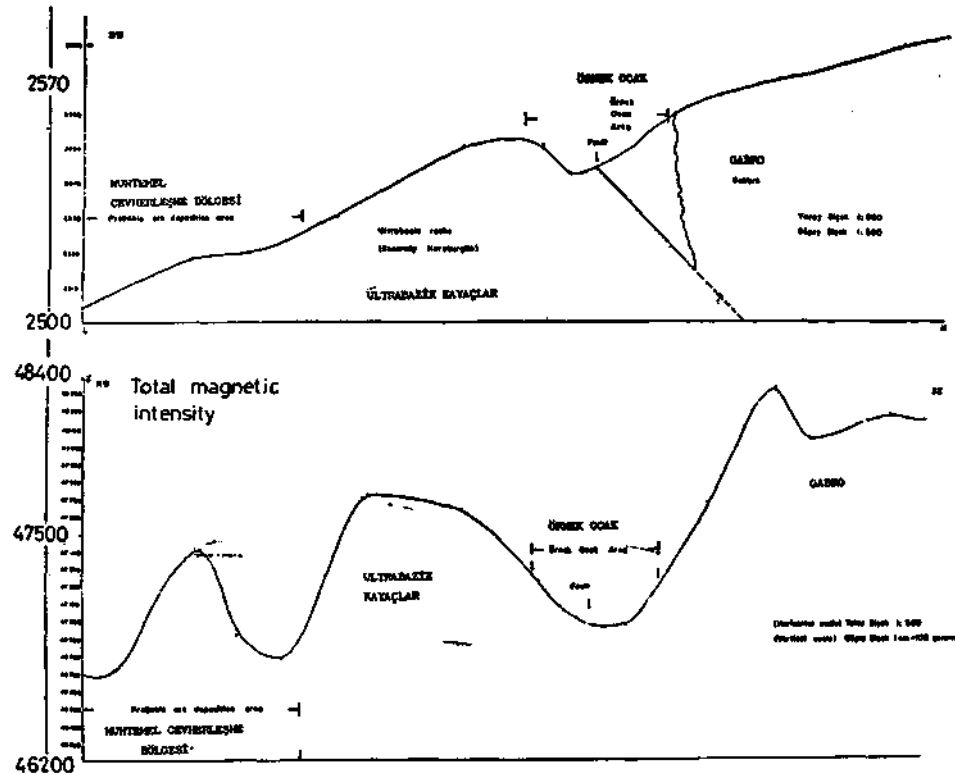


Fig. 7 - The cross-section (L-M).

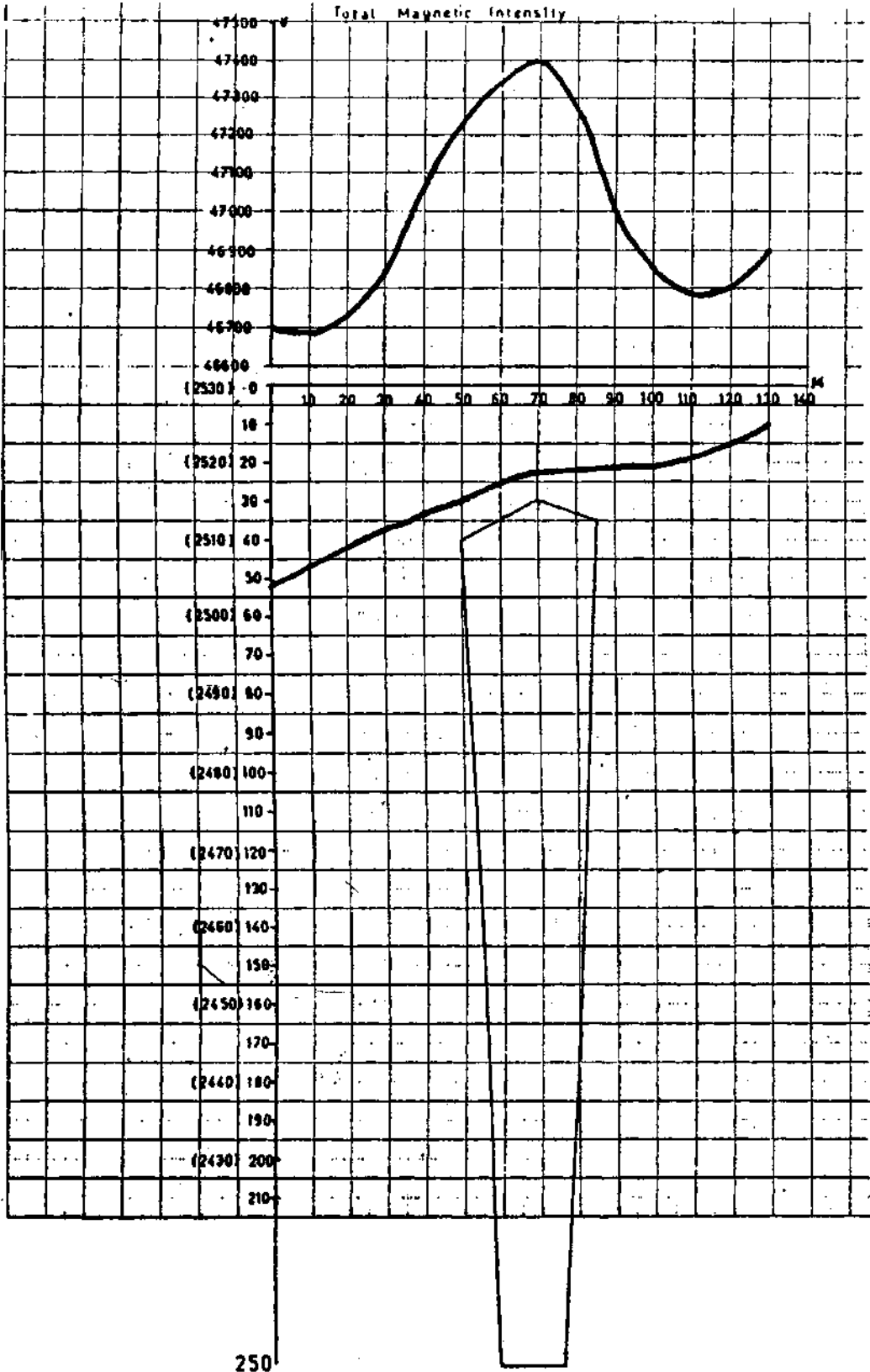


Fig. 8A - The first suggested ore shape.

$K = 0.0017$

Corner numbers of the polygon : 5

Corner coordinates of the polygon

Corner no.	Coordinates
1	(70,30)
2	(50 , 40)
3	(60 , 250)
4	(75 , 250)
5	(85 , 35)

Tunceli Pülümür

Magnetic anomaly calculation of tuwo dimensional prisms by Talwani method

<i>I</i> Point no.	<i>X</i> Horizontal distance	<i>Z</i>	<i>T</i> Calculated gamma values
1	0	32	-4.35878E+001
2	10	47	-4.65745E+001
3	25	40	-4.82039E+001
4	37	35	-3.26673E+001
5	50	30	1.01703E+002
6	69	23	2.87616E+002
7	81	22	1.83513E+002
8	90	21	8.48207E+001
9	100	21	2.77355E+001
10	115	17	6.11447E+000
11	170	10	1.87876E+000

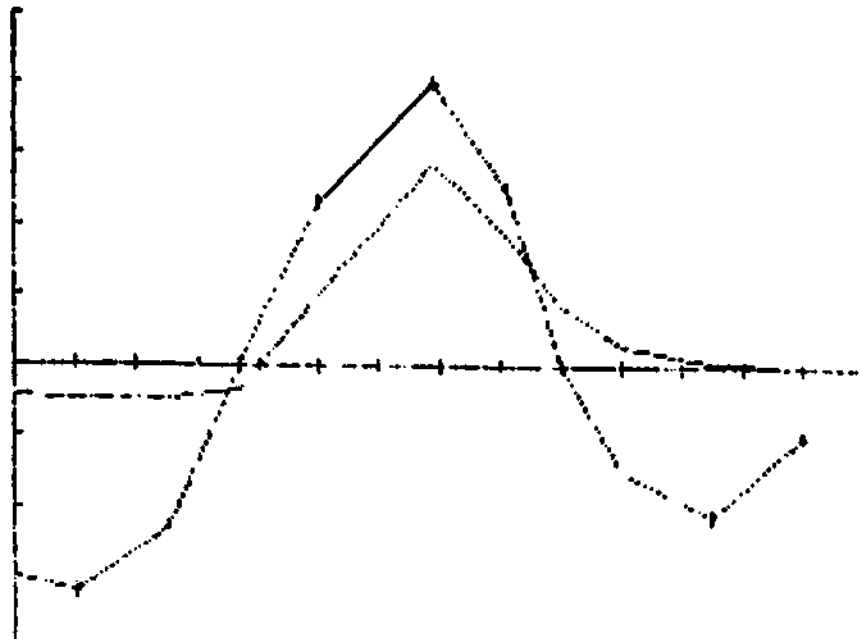


Fig. 8B - The graph is drawn by microcomputer with the help of shape 8 A and $K=0.0017$ emu real susceptibility value of chromite sample.

$$K = 0.0019$$

Corner numbers of the polygon : 5

Corner coordinates of the polygon

Corner no.	Coordinates
1	(70 , 30)
2	(50 , 40)
3	(60 , 250)
4	(75 , 250)
5	(85 , 35)

Tunceli Pülümür

Magnetic anomaly calculation of two dimensional prisms by Talwani method

<i>I</i> Point no.	<i>X</i> Horizontal distance	<i>Z</i>	<i>T</i> Calculated gamma values
1	0	52	-4.87158E+001
2	10	47	-5.20539E+001
3	25	40	-5.38750E+001
4	37	35	-3.65329E+001
5	30	30	1.13668E+002
6	69	23	3.20782E+002
7	81	22	2.05103E+002
8	90	21	8.47996E+001
9	100	21	3.09985E+001
10	115	17	6.83382E+000
11	130	10	2.09980E+000

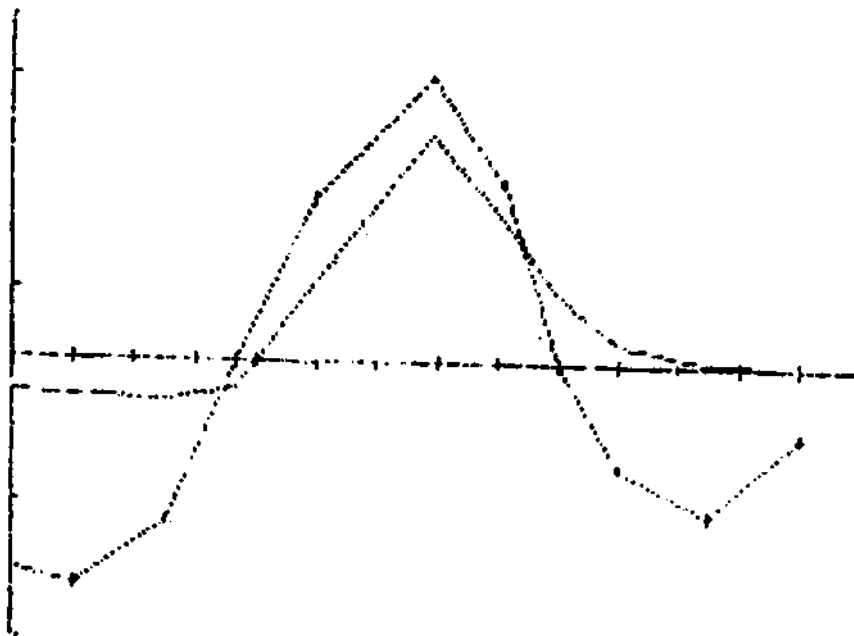


Fig. 9B - The graph is drawn by microcomputer with the help of shape 8 A and $K=0.0019$ emu real susceptibility value of chromite sample.

$K = 0.0022$

Corner numbers of the polygon : 5

Corner coordinates of the polygon

<i>Corner no.</i>	<i>Coordinates</i>
1	(70 , 30)
2	(50 , 40)
3	(60 , 250)
4	(75 , 250)
5	(85 , 35)

Tunceli Pülümür

Magnetic anomaly calculation of two dimensional prisms by Talwani method

<i>I</i>	<i>X</i>	<i>Z</i>	<i>T</i>
<i>Point no.</i>	<i>Horizontal distance</i>		<i>Calculated gamma values</i>
1	0	52	-5.64077E+001
2	10	47	-6.02729E+001
3	25	40	-6.23816E+001
4	37	35	-4.23012E+001
5	50	30	1.31616E+002
6	69	23	3.71432E+002
7	81	22	2.37487E+002
8	90	21	1.09768E+002
9	100	21	3.68930E+001
10	115	17	7.91284E+000
11	130	10	2.43134E+000

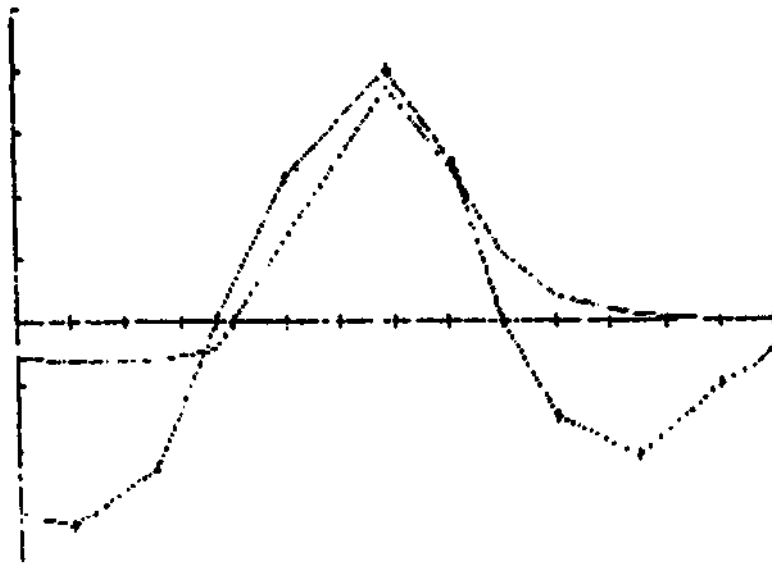


Fig. 10B - The graph is design by microcomputer with the help of 'shape 8 A and $K=0.0022$ emu real susseptibility value of chromite sample.

$$K = 0.0024$$

Corner numbers of the polygon : 5

Corner coordinates of the polygon

<i>Corner no.</i>	<i>Coordinates</i>
1	(70 , 30)
2	(50 , 40)
3	(60 , 250)
4	(75 , 250)
5	(85 , 35)

<i>Corner no.</i>	<i>Coordinates</i>
1	(70 , 30)
2	(50 , 40)
3	(60 , 250)
4	(75 , 250)
5	(85 , 35)

Tunceli Pülümür

Magnetic anomaly calculation of two dimensional prisms by Talwani method

<i>I</i>	<i>X</i>	<i>Z</i>	<i>T</i>
<i>Point no.</i>	<i>Horizontal distance</i>		<i>Calculated gamma values</i>
1	0	52	-6.15357E+001
2	10	47	-6.57522E+001
3	25	40	-6.80526E+001
4	37	35	-4.61468E+001
5	50	30	1.43581E+002
6	69	23	4.05198E+002
7	31	22	2.59077E+002
8	90	21	1.19747E+002
9	100	21	3.91560E+001
10	115	17	8.63219E+000
11	130	10	2.65237E+000

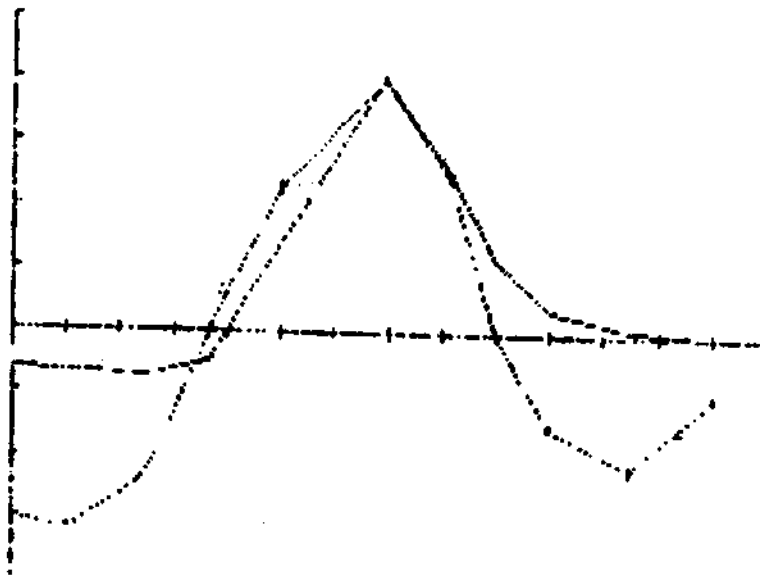


Fig. 11B - The graph is drawn by microcomputer with the help of shape 8 A and $K=0.0024$ emu real susceptibility value of chromite sample.

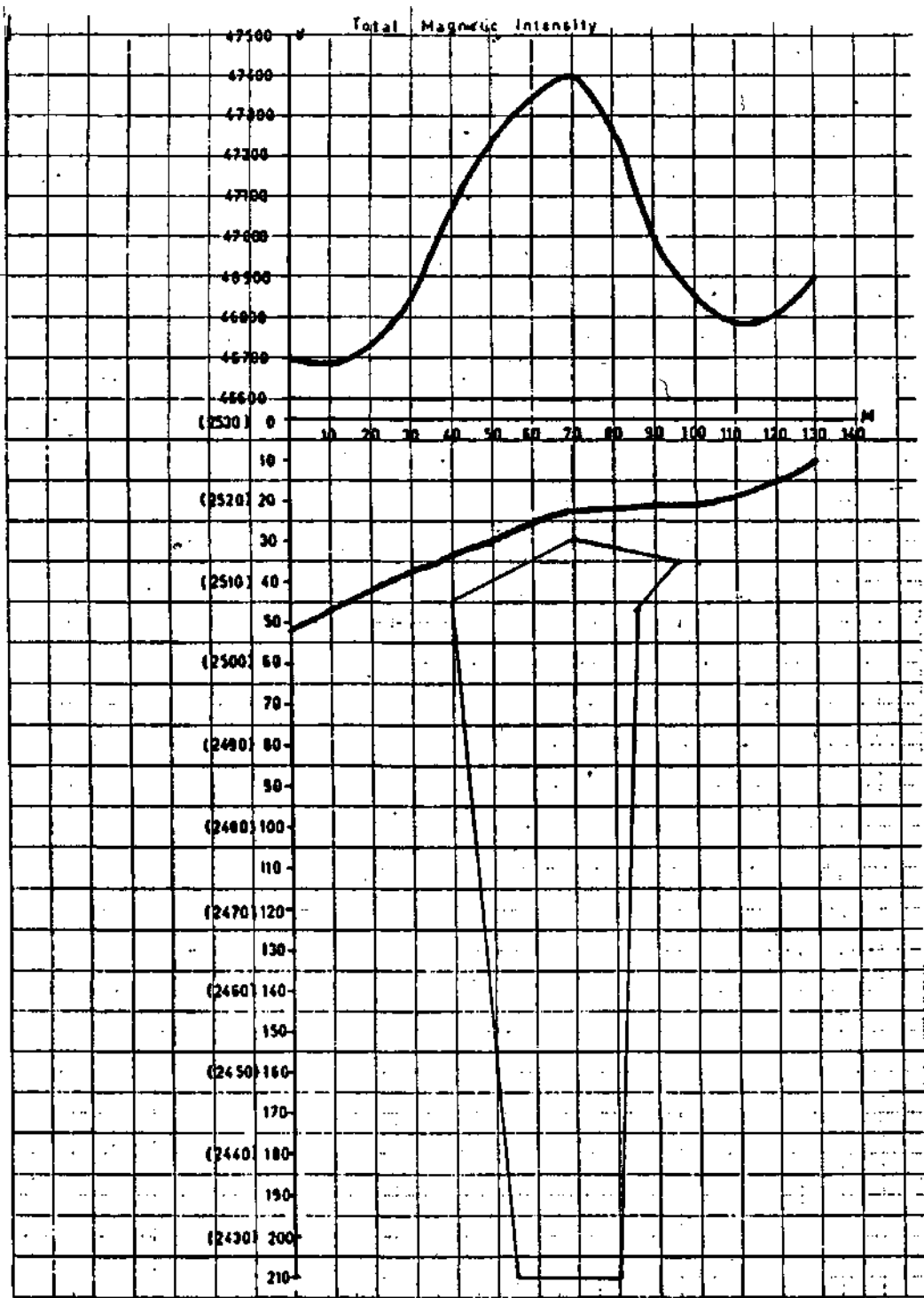


Fig. 12A - The new suggested ore shape.

$K = 0.0025$

Corner numbers of the polygon : 6

Corner coordinates of the polygon

Corner no.	Coordinates
1	(70 , 30)
2	(40 , 45)
3	(55 , 210)
4	(80 , 210)
5	(85 , 47)
6	(95 , 35)

Tunceli Pülümür

Magnetic anomaly calculation of two dimensional prisms by Talwani method

<i>I</i>	<i>X</i>	<i>Z</i>	<i>T</i>
Point no.	Horizontal distance		Calculated gamma values
1	0	52	-9.58305E+001
2	10	47	-1.02363E+002
3	25	40	-9.11875E+001
4	37	35	3.86762E+001
5	50	30	2.64409E+002
6	69	23	4.48427E+002
7	81	22	3.35426E+002
8	90	21	1.86521E+002
9	100	21	5.49421E+001
10	115	17	4.03052E+000
11	130	10	-1.85880E+000

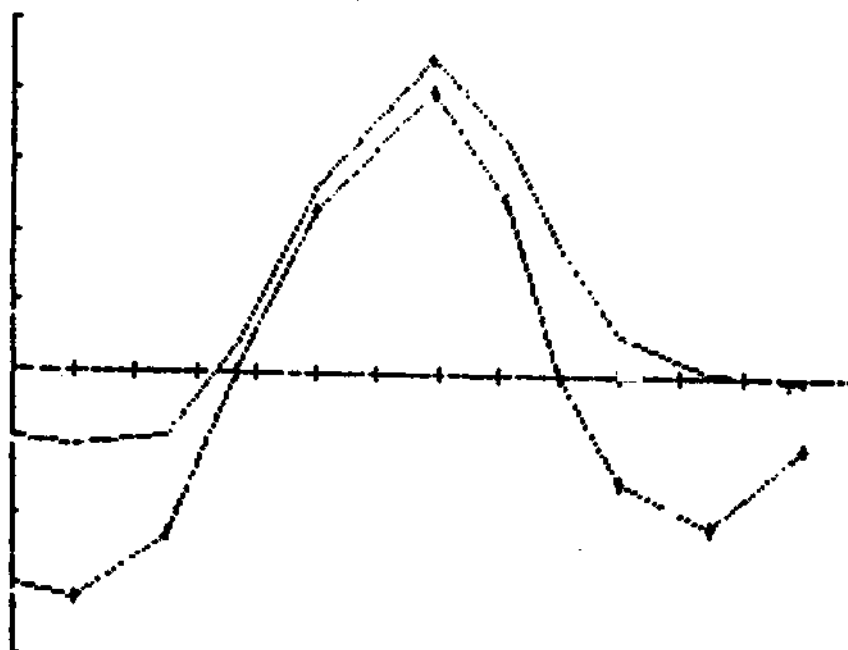


Fig. 12B - The graph is drawn by microcomputer with the help of shape 12 A and $K=0.0025$ emu the real susceptibility value of chromite sample.

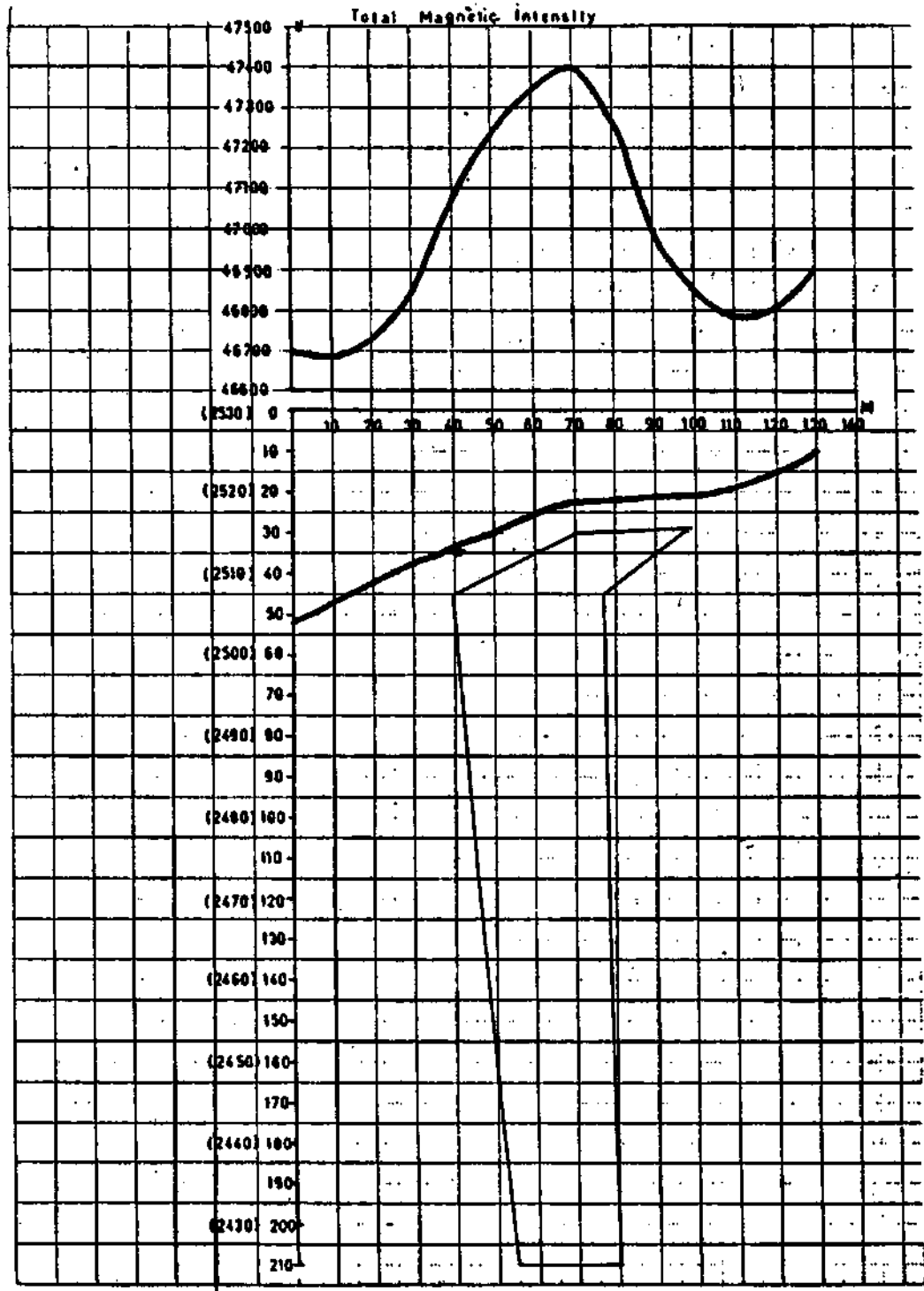


Fig. 13A - The suggested ore shape.

$K = 0.0025$

Corner coordinates of the polygon

Corner no.	Coordinates
1	(70 , 30)
2	(40 , 45)
3	(55 , 210)
4	(80 , 210)
5	(77 , 45)
6	(98 , 29)

Tunceli Pülümür

Magnetic anomaly calculation of two dimensional prisms by Talwani method

<i>I</i>	<i>X</i>	<i>Z</i>	<i>T</i>
Point no.	Horizontal distance		Calculated gamma values
1	0	52	-8.58624E+001
2	10	47	-9.19589E+001
3	25	40	-8.16611E+001
4	37	35	4.44529E+001
5	50	30	2.56747E+002
6	69	23	3.94203E+002
7	81	22	3.11761E+002
8	90	21	1.77768E+002
9	100	21	1.97633E+001
10	115	17	-1.10789E+001
11	130	10	-7.34844E+000

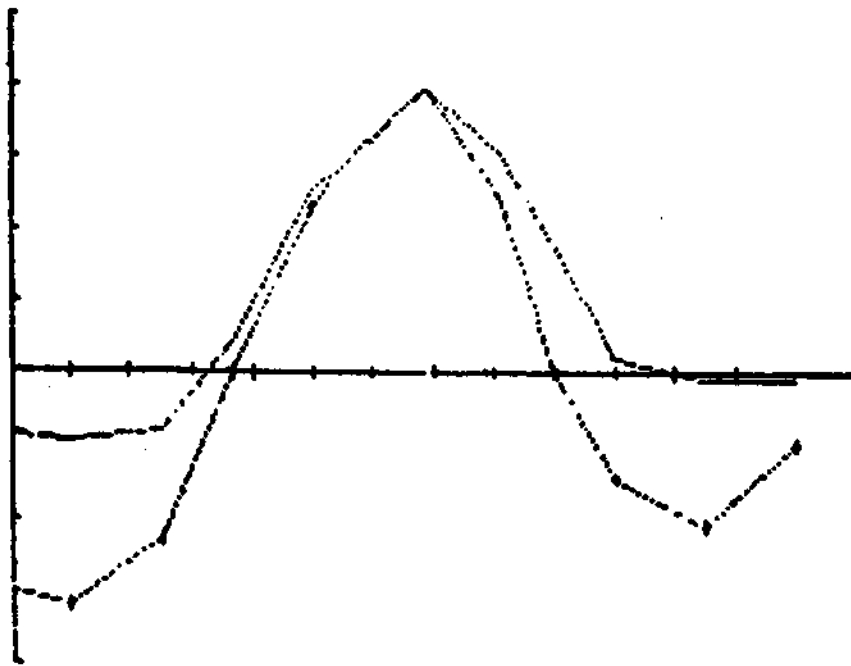


Fig. 13B. - The graph is drawn by microcomputer with the help of shape 13 A and $K=0.0025$ emu the real susceptibility value of chromite sample.

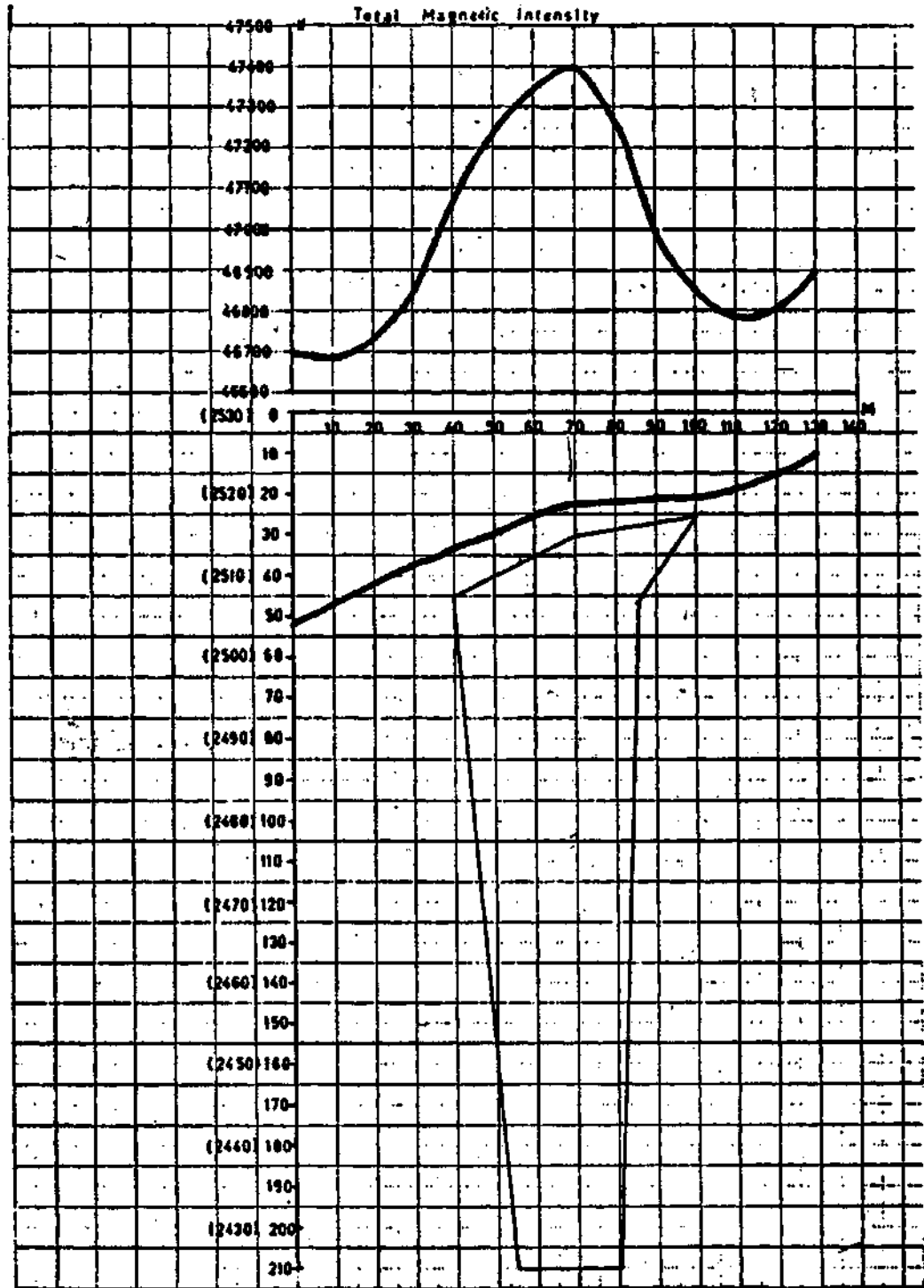


Fig. 14A - The suggested ore shape.

$$K = 0.0025$$

Corner numbers of the polygon : 6

Corner coordinates of the polygon

<i>Corner no.</i>	<i>Coordinates</i>
1	(70 , 30)
2	(40 , 45)
3	(55 , 210)
4	(80 , 210)
5	(85 , 47)
6	(100 , 25)

Tunceli Pülümür

Magnetic anomaly calculation of two dimensional prisms by Talwani method

<i>I</i>	<i>X</i>	<i>Z</i>	<i>T</i>
<i>Point no.</i>	<i>Horizontal distance</i>		<i>Calculated gamma values</i>
1	0	52	-9.85706E+001
2	10	47	-1.05905E+002
3	25	40	-9.71108E+001
4	37	35	2.88970E+001
5	50	30	2.44920E+002
6	69	23	4.13660E+002
7	81	22	4.09930E+002
8	90	21	3.27209E+002
9	105	21	8.33651E+001
10	115	17	-1.46027E+001
11	130	10	-9.40075E+000

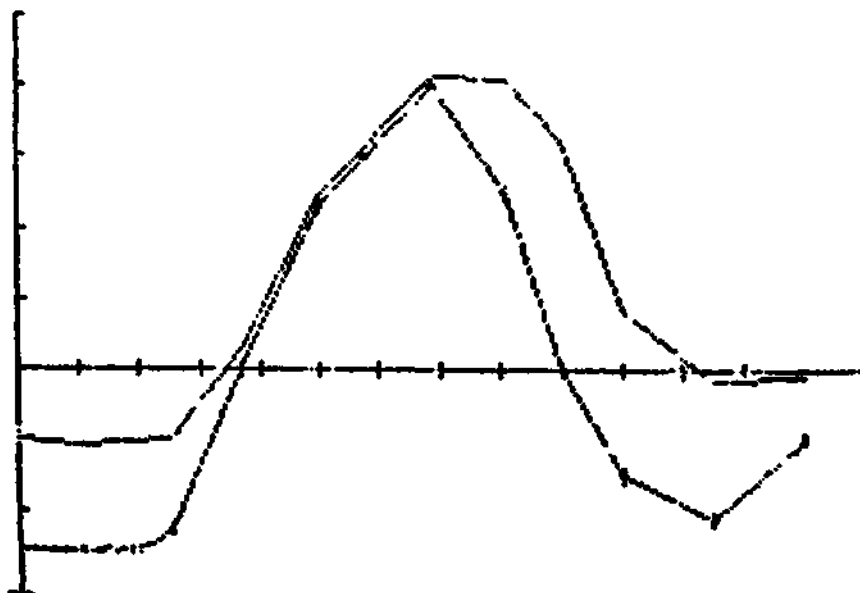


Fig. 14B - The graph is drawn by microcomputer with the help of shape 14 A and $K=0.0025$ emu the real susceptibility value of chromite sample.

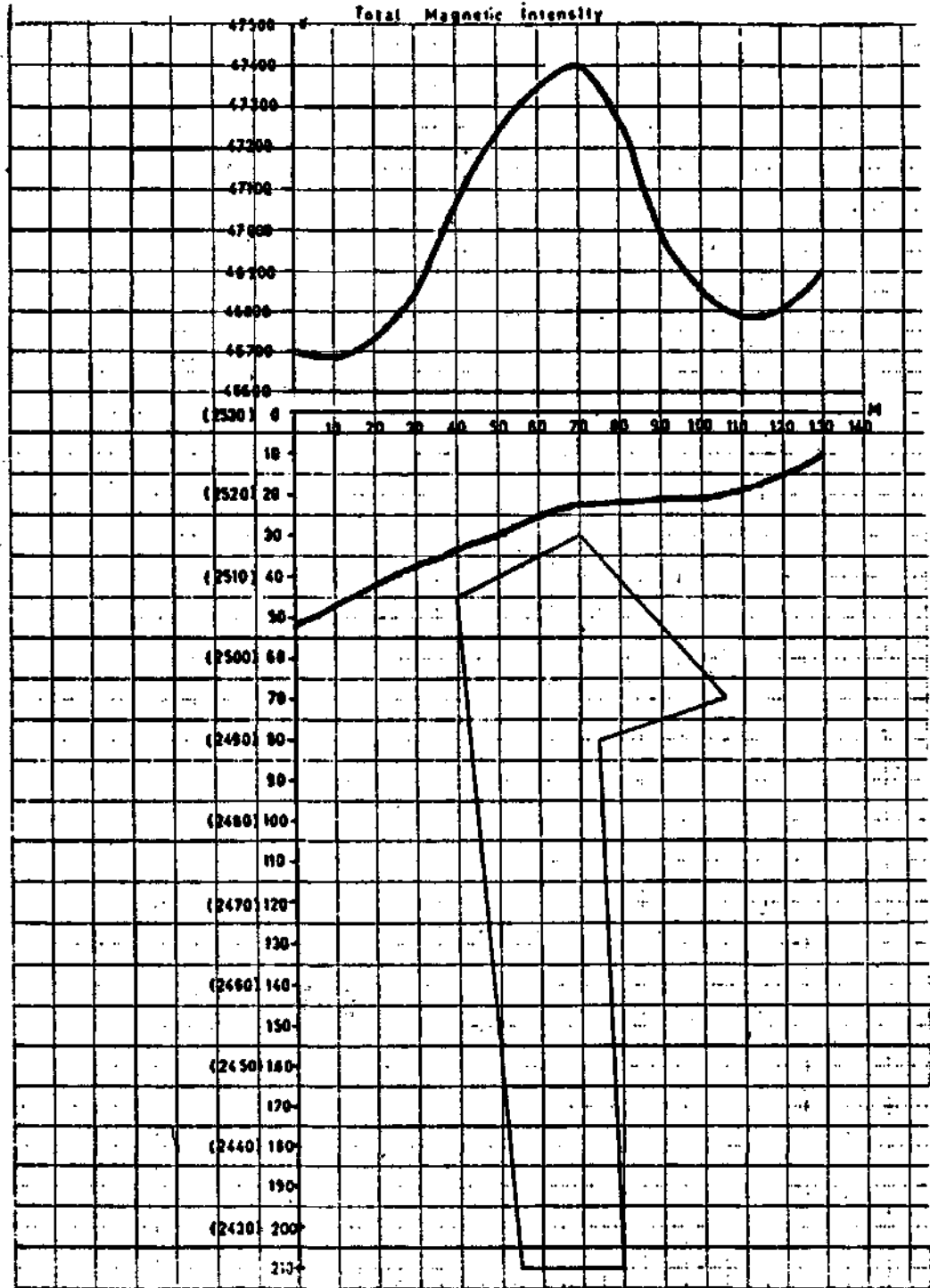


Fig. 15A - The suggested ore shape.

$$K = 0.0025$$

Corner numbers of the polygon : 6

Corner coordinates of the polygon

<i>Corner no.</i>	<i>Coordinates</i>
1	(70 , 30)
2	(40 , 45)
3	(55 , 210)
4	(80 , 210)
5	(75 , 80)
6	(105 , 70)

Tunceli Pülümür

Magnetic anomaly calculation of two dimensional prisms by Talwani Method

<i>I</i>	<i>X</i>	<i>Z</i>	<i>T</i>
<i>Point no.</i>	<i>Horizontal distance</i>		<i>Calculated gamma values</i>
1	0	52	-9.47469E+001
2	10	47	-1.02405E+002
3	25	40	-9.23563E+001
4	37	35	4.00534E+001
5	50	30	2.79975E+002
6	69	23	4.26836E+002
7	81	22	2.33643E+002
8	90	21	1.34899E+002
9	100	21	6.59235E+001
10	115	17	1.82314E+001
11	130	10	3.35604E+000

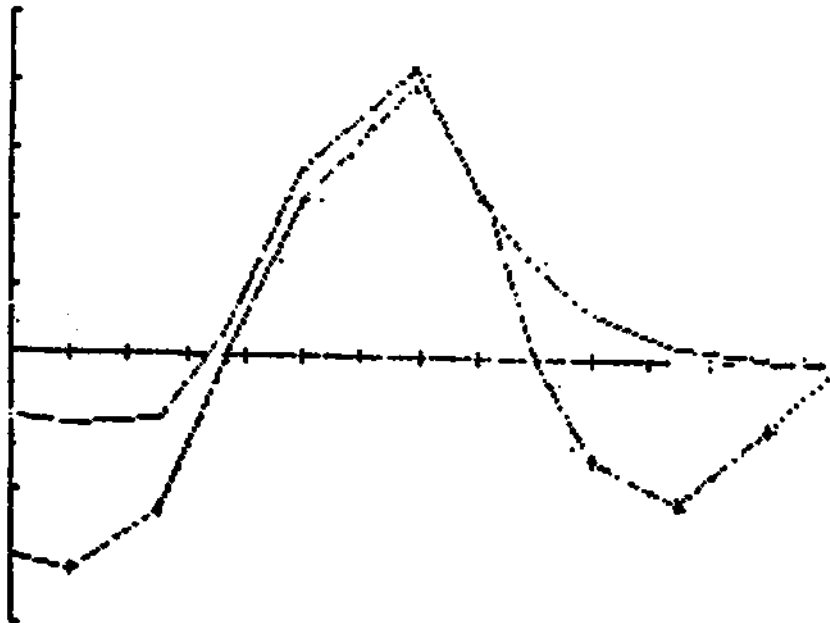


Fig. 15B - The graph is drawn by microcomputer with the help of shape 15 A and $K=0.0025$ emu the real susceptibility value of chromite sample.

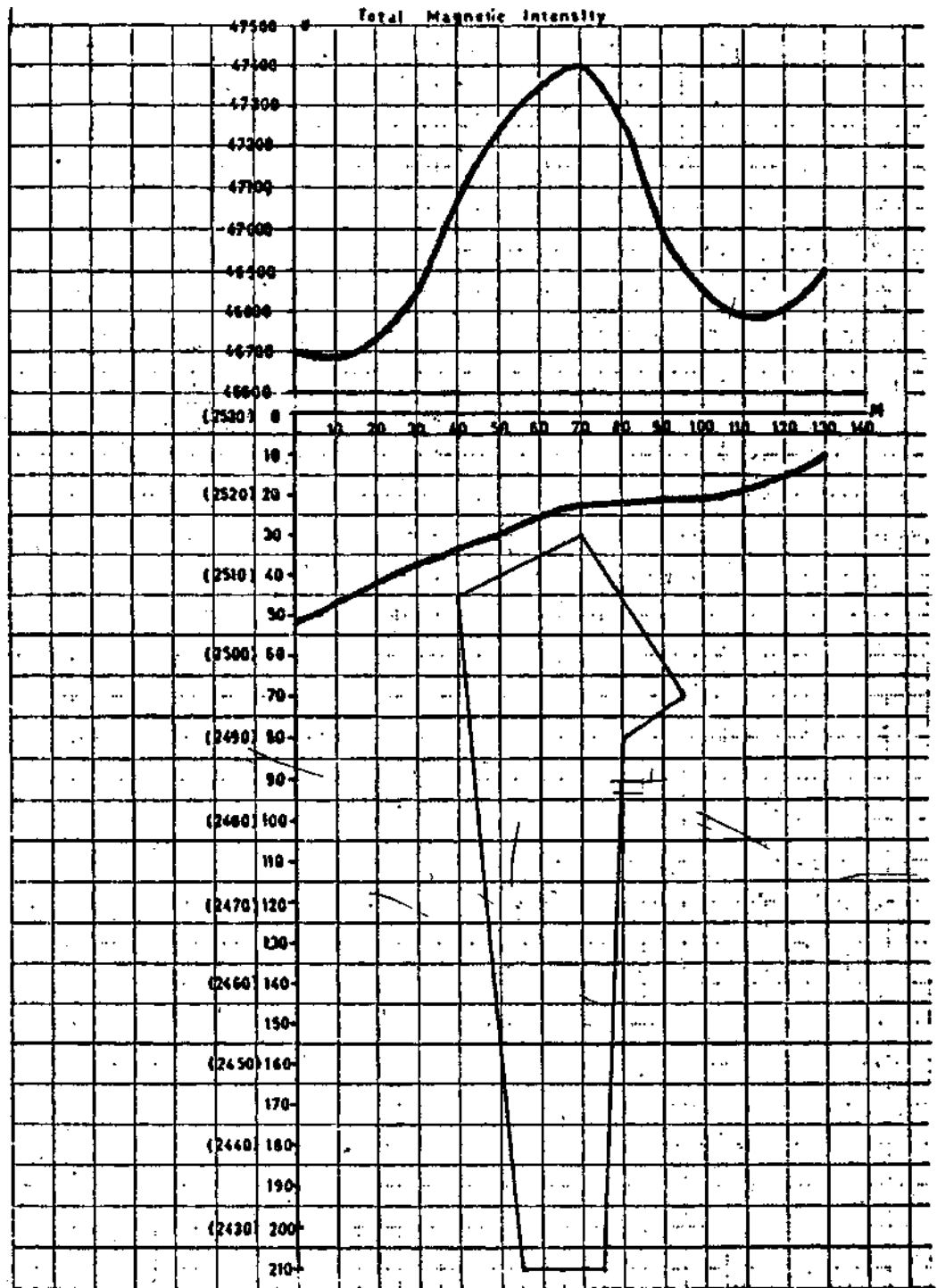


Fig. 16A - The suggested ore shape.

$K = 0.0025$

Corner numbers of the polygon : 6

Corner coordinates of the polygon

Corner no.	Coordinates
1	(70 , 30)
2	(40 , 45)
3	(55 , 210)
4	(75 , 210)
5	(80 , 80)
6	(95 , 75)

Tunceli Pülümür

Magnetik anomaly calculation of two dimensional prisms by Talwani method

<i>I</i>	<i>X</i>	<i>Z</i>	<i>T</i>
Point no.	Horizontal distance		Calculated gamma values
1	0	52	-9.08993E+001
2	10	47	-9.65380E+001
3	25	40	-8.19111E+001
4	37	35	5.51905E+001
5	50	30	2.97188E+002
6	69	23	3.99885E+002
7	81	22	1.90296E+002
8	90	21	1.03186E+002
9	100	21	4.71294E+00
10	115	17	1.28561E+001
11	130	10	2.49310E+000

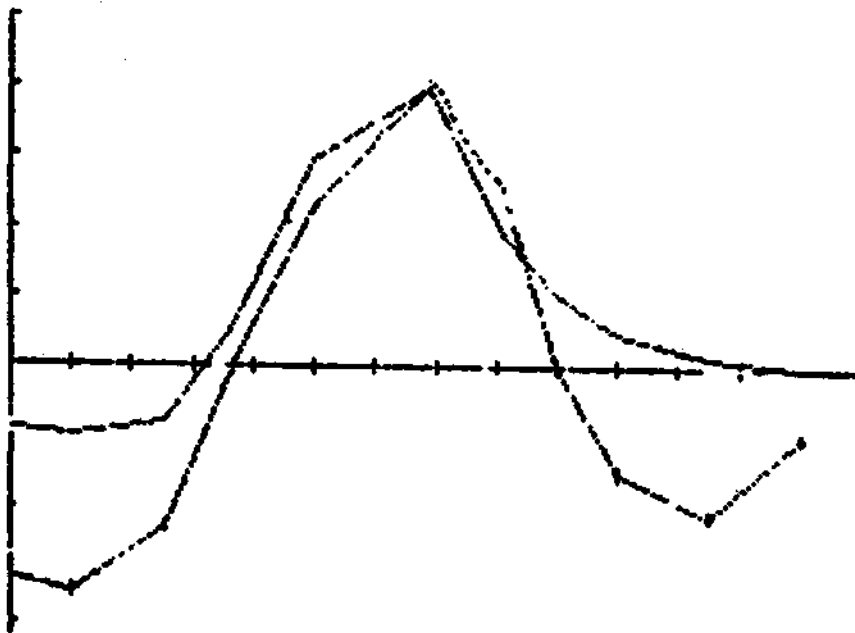


Fig. 16B - The graph is drawn by microcomputer with the help of shape 16 A and $K=0.0025$ emu the real susseptibility value of chromite sample.

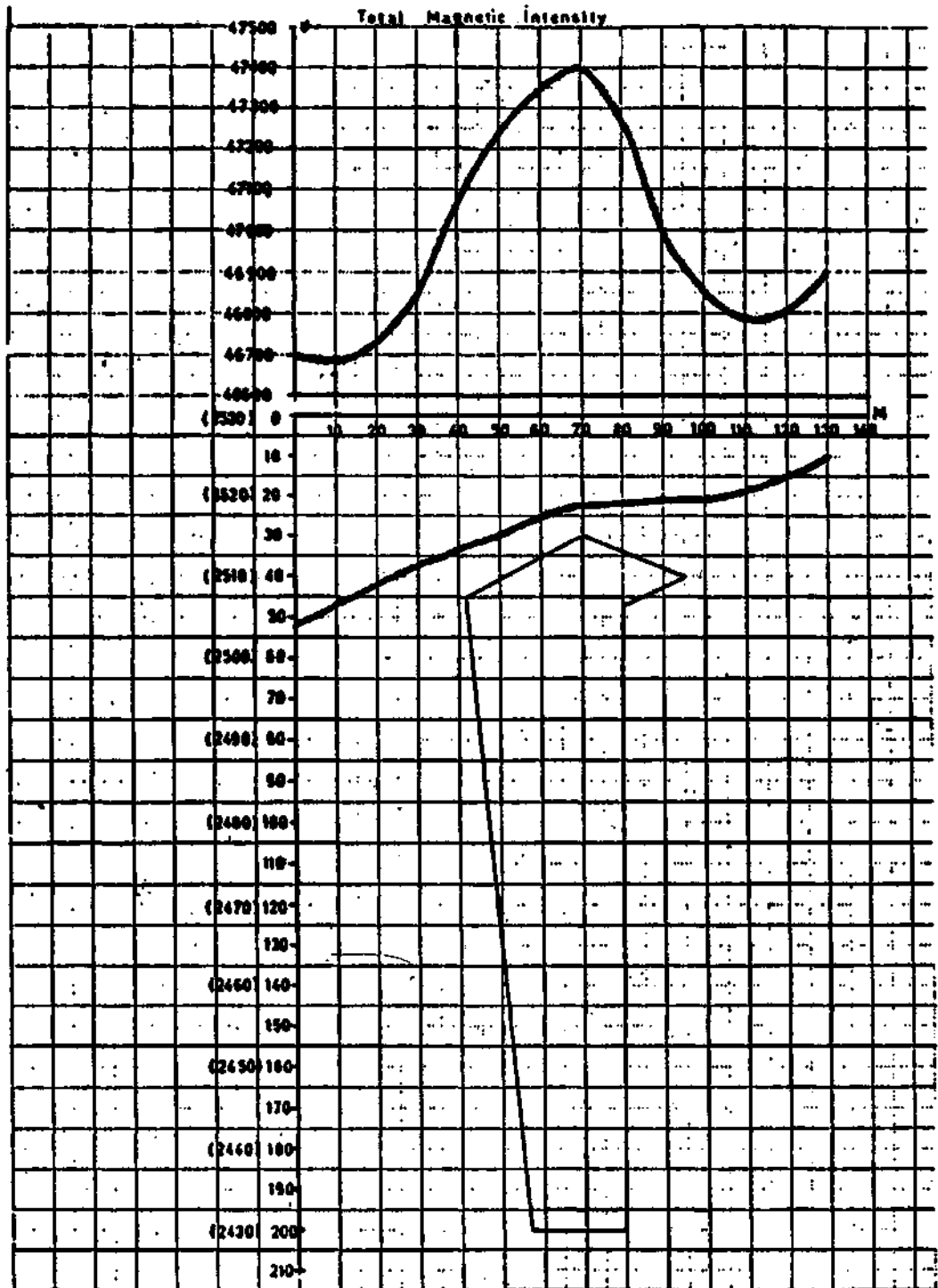


Fig. 17A - The most ideal ore shape which is found after 73 trial.

$K = 0.0024$

Corner numbers of the polygon : 6

Corner coordinates of the polygon

<i>Corner no.</i>	<i>Coordinates</i>
1	(70 , 30)
2	(42 , 45)
3	(57 , 200)
4	(80 , 200)
5	(80 , 47)
6	(95 , 40)

Tunceli Pülümür

Magnetic anomaly calculation of two dimensional prisms by Talwani method

<i>I</i>	<i>X</i>	<i>Z</i>	<i>T</i>
<i>Point no.</i>	<i>Horizontal distance</i>		<i>Calculated gamma values</i>
1	0	52	-8.09269E+001
2	10	47	-8.67043E+001
3	25	40	-8.00498E+001
4	37	35	1.37344E+001
5	50	30	2.27617E+002
6	69	23	4.01627E+002
7	81	22	2.50349E+002
8	90	21	1.22763E+002
9	100	21	3.41601E+001
10	115	17	5.04258E+001
11	130	10	-3.13139E+000

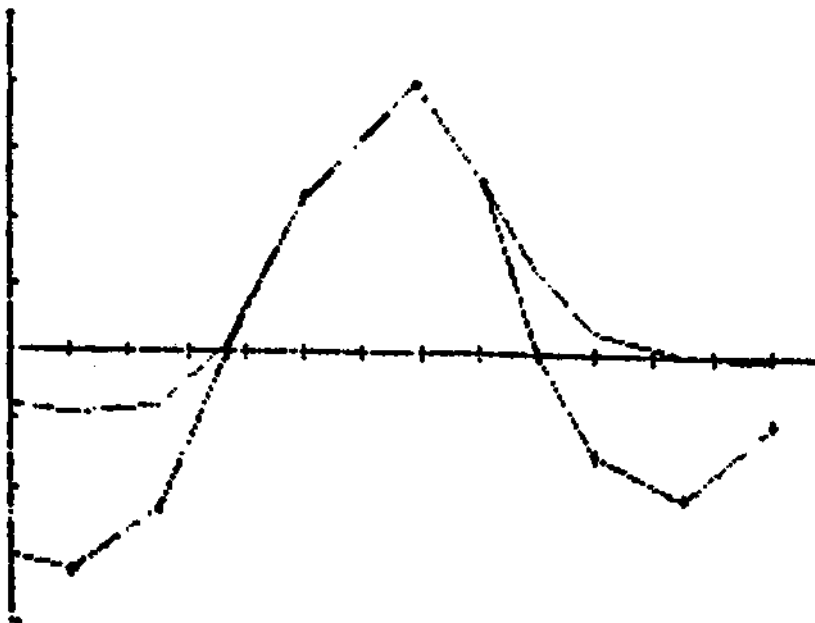


Fig. 17B - The graph is drawn by microcomputer with the help of the most ideal shape 17 A and $K=0.0024$ emu the real susceptibility value of chromite sample.

ACKNOWLEDGEMENTS

The author would like to express his great appreciation and thanks to geophysical department of Mineral Research and Exploration Institute, especially to Mr. Aydok Çalım, Fikret Özkazanç, Tankut Kılınç and Seyit Tosun who gave great support and facilities during susceptibility measurements and computer modelling.

Manuscript received January 14, 1986

REFERENCES

- 1 — Affleck, J., 1958, Interrelationships between magnetic anomaly components: *Geophysics*, 23, 738-748.
- 2 — Bott, M.H.P., 1963, Two methods applicable to computer for evaluating magnetic anomalies due to finite three dimensional bodies: *Geophys. Prosp.*, 11, 292-299.
- 3 — Gay, S.P., Jr., 1963, Standard curves for interpretation of magnetic anomalies over long tabular bodies: *Geophysics*, 28, 161-200.
- 4 — Henderson, R. G. and Allingham, J. W., 1964, Magnetization of an inhomogeneous laccolith calculated on a digital computer, in computers in the mineral industries, part 2: Stanford University publications, *Geol. Sciences*, 9, 481-497.
- 5 — Hersey, J. B., 1962, Findings made during the June 1961 cruise of Chain to the Puerto Rico Trench and Caryn Seamount: *Jour. Geophys. Res.*, 67, 1109-1116.
- 6 — Miller, E.T. and Eving, M., 1956, Geomagnetic measurements in the Gulf of Mexico and in the vicinity of Caryn Peak: *Geophysics*, 21, 406-432.
- 7 — Steenland, N.C., 1962, Gravity and aeromagnetic exploration in the Paradox Basin: *Geophysics*, 27, 73-89.
- 8 — Talwani, M. and Heirtzler, J.R., 1964, Computation of magnetic anomalies caused by two dimensional structures of arbitrary shape, in computer in the mineral industries, part 1: Stanford University publications, *Geol. Sciences*, 9, 464-480.
- 9 — Thyssen Bornemisza, S. and Stackler, W. F., 1956, Observing vertical gravity gradient: *Geophysics*, 21, 771-779. 1962, The average horizontal gravity gradient: *Geophysics*, 27, 714-715.
- 10 — Vacquier, V., 1963, A machine method for computing the magnitude and the direction of magnetization of a uniformly magnetized body from its shape and a magnetic survey: *Proc. Benedum Earth Magnetism Symposium 1962*, University of Pittsburgh press.
- 11 — ———; Steenland, N.C.; Henderson, R.G. and Zietz, I., 1951, Interpretation of aeromagnetic maps: *Geol. Soc. Amer., Mem.*, 47.
- 12 — Vogel, A., 1963, The application of electronic computers to the calculation of effective magnetization: *Geophys. Prosp.*, 11, 51-58.
- 13 — Werner, S., 1953, Interpretation of magnetic of anomalies at shectlike bodies: *Sveriges Geologiska Undersockning, Arsbok*, 43.
- 14 — Worzel, J. L., 1959, Continuous gravity measurements on a surface ship with the Graf Sea Gravimeter: *Jour. Geophys. Res.*, 64, 1299-1315.
- 15 — Zietz, I. and Henderson, R.G., 1956, A preliminary report on model studies of magnetic anomalies of three dimensional bodies: *Geophysics*, 21, 794-814.
- 16 — Talwani, M., 1965, Computation with the help of a digital computer of magnetic anomalies caused by bodies of arbitrary shape: *Geophysics*, xxx, 5 (October, 1965), 797-817, 11 figs.

LACAZINA OEZTEMUERI SİREL 1981 RENAMED AS *PSEUDOLACAZINA OEZTEMUERI* (SİREL)» FROM THE THANETIAN LIMESTONE (CENTRAL TURKEY)

Ercüment SİREL*

ABSTRACT. — In 1981, *Lacazina oeztemueri* Sirel was first described and figured by the present author from the Paleocene (Thanetian) of the different regions in central Turkey; Aksaray (southeast of Tuz lake), Kırıkkale (southeast of Ankara), Ereğli (northwest of Bolkar mountains), and Örencik, Demircilik (southeast of Sivas). In this paper, *Lacazina oeztemueri* is reviewed on well preserved material of this species. Because of the following characters, *Lacazina oeztemueri* Sirel is renamed as *Pseudolacazina oeztemueri* (Sirel); all the chambers of the form A are arranged in biloculine mode; the growth stages of the form B are composed of quinqueloculine with proloculus, biloculine and monoloculine chambers; the septula are arranged in continuous rows in both generations (form A, B).

INTRODUCTION

During an investigation of Paleocene strata of the Aksaray, Kırıkkale, Ereğli, Örencik and Demircilik regions (central Turkey) (Fig. 1) carried out in 1981; a «fabularid» species resembling *Lacazina* «*Lacazina oeztemueri*» was observed and described from limestone regarded as of Thanetian age. The four trematophorid foraminifers (*Lacazina* Munier-Chalmas 1882, *Fabularia* Defrance 1820, *Periloculina* Munier-Chalmas and Schlumberger 1885 and *Pseudolacazina* Caus 1979) are globular to ovoid in general shape, porcellaneous form and the same subdivision of the chambers with chamberlets. When studying on only one of the generations (form A,B) of these trematophorid forms, they can be confuse with each other, even in thin sections examination. It is obvious that all observable features of both generations (form A,B) must be taken into consideration when studying on trematophorid foraminifers such as *Fabularia*, *Periloculina*, *Lacazina* and *Pseudolacazina*.

In this study, the some diagnostic characters of the genus *Pseudolacazina* have been obtained from the both generations (form A,B) of the *Lacazina oeztemueri* which is reviewed on well preserved materials of this species. For this reason, *Lacazina oeztemueri* is transferred to genus *Pseudolacazina* Caus. The figured samples are deposited at the Museum d'Histoire naturelle, Geneve, Suisse (86-10019—86-10033).

SYSTEMATIC DESCRIPTION

Order : Foraminiferida Eichwald, 1830
Superfamily : Miliolacea Ehrenberg, 1839 .
Family : Fabulariniidae Ehrenberg, 1839, emend Drobne, 1984
Genus : *Pseudolacazina* Caus, 1979 -
Type species : *Pseudolacazina hottingeri*, 1979

Pseudolacazina oeztemueri (Sirel), 1981
(Plate I, fig. 1-6; Plate II, fig. 1-10 ; Plate III)

1981 *Lacazina oeztemueri* Sirel, Pl. 4, fig. 1-6; Pl. 5, fig. 1-6.

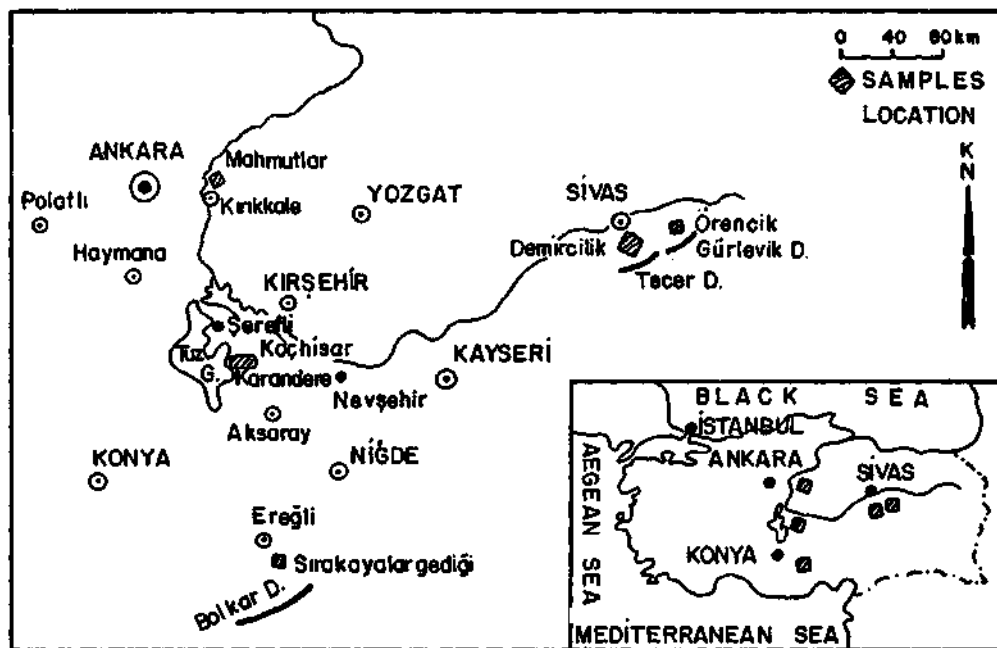


Fig. 1 - Location map.

Diagnosis. — Test large, ovoid, slightly elongate in the direction of the apertural axis, imperforate porcellaneous shell with thick wall. All the chambers except 4-6 undivided chambers around the proloculus of the form A are arranged in biloculine mode, all the chambers of the form B are quinqueloculine to monoloculine; 3 cycles undivided quinqueloculine chambers completely embracing mikrospheric embryo, the first 4-5 chambers which follow the quinqueloculine cycles are arranged in biloculine pattern, all later 7-11 chambers are monoloculine; the cavities of the biloculine and monoloculine chambers are subdivided by the continuous thick septula in parallel tooth-like chamberlets, the aperture is trematophore at one end of the apertural axis.

Description

Microspheric form: Test is large, ovoid, slightly elongated in the direction of the poles (apertural region). The wall (outer wall and basal layer) is porcellaneous calcite. The equatorial diameter varies between 2.7-4.9 mm, axial diameter reaches 3.4 mm, index of elongation (ratio of the equatorial diameter to the axial diameter) is 1.15-1.44 but the mean values are around 1.3. The microsphere is spherical (Pl.I, fig. 1,2,4,6) its diameter varies between 22 μ -25 μ . The first 3 cycles which follow the microsphere are arranged in quinqueloculine pattern and coiled very tightly, their diameter varies from 248 μ to 266 μ . They are followed by 4-5 whorls of biloculine mode with a diameter 719-892 μ . All the later 7-11 chambers are monoloculine. The cavities of the biloculine and monoloculine are subdivided by the septula into parallel chamberlets. The thick septula join the outer wall of the chamber together with the septum; they are arranged in continuous rows from one chamber to the next. The continuous pattern in the arrangement of the septula is recognized best in the tangential sections. The basal layer of the biloculine and monoloculine chambers are thick compared to the chamber spaces. The chamberlets are small, their cross-sections are generally tooth-like in shape.

The trematophores are alternating from one pole to the other in successive biloculine and monoloculine chambers.

Macrospheric form: The shell is very small, ovoid, rather elongated in the direction of the apertural axis. The equatorial diameter is 1.6-1.8 mm, axial diameter 1.29-1.35 mm and index of elongation around 1.6; it is counted 5 chambers for an axial diameter of 1.3 mm. The proloculum is ovate and very large compared to the size of the shell. The diameter of the megalosphere varies between 235 μ , and 310 μ . There is the thick goulot as the in alveolid genus. There are 4-6 undivided chambers around the proloculus. All the later chambers of the form A are arranged in biloculine pattern. The biloculine arranged chambers are subdivided by the septula into parallel very small chamberlets. The shape of the cross-section of the chamberlets is subspheric. The trematophore plate is often positioned out of the pole in the form A.

Comparisons and remarks. — It is accepted by the present author that the foraminifer found in Lower Part of Thanetian limestone described and figured as *Lacazina oeztemueri* in Sirel (1981) from the central Turkey, belongs to *Pseudolacazina* Caus: when restudying on well preserved materials of *L. oeztemueri* the some some diagnostic characters of *Pseudolacazina* have been obtained from the form A,B, and because of the following some diagnostic characters, *L. oeztemueri* is renamed as «*Pseudolacazina oeztemuerh*»:

1. All the chambers (except 4-6 undivided chambers around the macrospheric embryo) of the form A are arranged in biloculine pattern (Pl. II, fig. 4,5,8).
2. The chambers of the growth stages of the form B as the follow:
 - a. The first 3 cycles which follow the microsphere are arranged in quinqueloculine mode (Pl. I, fig. 1,2,4,6).
 - b. The quinqueloculine chambers are followed by 4-5 whorls of biloculine mode (Pl. I, fig. 1,2,3,4,6; Pl. II, fig. 1,2,6,7,10).
 - c. The later 7-11 chambers (average 7 chambers) are monoloculine (Pl. I, fig. 1,3,4,6; Pl. II, fig. 1,3,6,7,10).
3. The septula are arranged in continuous rows in both generations (form A,B) (Pl. I, fig. 5; Pl. II, fig. 4; Pl. III).

The first occurrence of the genus *Pseudolacazina* Caus reported by the Drobne (1974); in her study on the specimens of form A and form B (without equatorial sections) from Yugoslavia, described as «*Fabularia donatae*» Drobne. This fabularid species is transferred to *Pseudolacazina* by the Caus (1979).

Pseudolacazina donatae (Drobne) differs from *Pseudolacazina oeztemueri* (Sirel) by having delicate internal structure (very tightly coiled); it has 11 whorls (biloculine and monoloculine chambers) in an axial section of 2 mm; Drobne (1974) Pl. 4, fig. 21; Pl. 9, fig. 1; whereas, *P. oeztemueri* has 11 whorls (biloculine and monoloculine chambers) in an axial section of 3.26mm; Pl. II, fig. 1, also the form A of *P. donatae* has 6 whorls (in biloculine pattern) in an axial section of 1-1.15 mm; Drobne (1974), Pl. 3, fig. 1,4; but, form A of *P. oeztemueri* has 4-5 whorls (in biloculine mode) in an axial section of 1.35 mm; Pl. II, fig. 8. The form A of *P. oeztemueri* has more chamberlets per whorl than form A of *P. donatae*.

P. oeztemueri Distinguished from the *Pseudolacazina hottingeri* Caus by having external shape, larger size, loosely coiling and well development quinqueloculine and biloculine stages.

Stratigraphic level and geographic distribution. — The detail stratigraphic level and geographic distribution of *P. oeztemueri* were reported by the present author Sirel(1981). In the Haymana (south of Ankara), Polatlı (southwest of Ankara), Kırıkkale (west of Ankara), Aksaray (southeast of Tuz lake), Ereğli (northwest of Bolkar mountains), Demircilik and Örencik (southeast of Sivas) regions, *P. oeztemueri* is abundant restricted shelf-back reef environments where it is accompanied by *Solkarina aksarayi* Sirel, *Laffiteina mengaudi* (Astre) (only three specimens are observed in about 150 thin section), *Keramosphaera* cf. *iranica* Rahaghi, *Pseudolacazina* aff. *donatae* Drobne, *Idalina* cf. *sinjarica* Grimsdale, *Peneroplidae* (*Hottingerina*), *Miliolidae*.

P. oeztemueri occurs in the Upper most Part of the biozone *L. mengaudi* and reaches to the lower boundary of the biozone *Aheolina* (*Glomaheolina*) *primaeva*. Up to now, *P. oeztemueri* has not found together with *A. (Glomaheolina) primaeva* Reichel.

Manuscript received, December 23, 1985

REFERENCES

- Caus, E., 1979, *Fabularia roselli* n.sp.et *Pseudolacazina* n.gen., Foraminiferes de l'Eocene moyen du Nord-Est de l'Espagne: Geobios, Lyon, 12, 29-45.
- Drobne, K., 1974, Les grandes Miliolides des couches Paleocenes de la Yougoslavie du Nord-Ouest (*Idalina*, *Fabularia*, *Lacazina*, *Periloculind*): Razprave 4. razr. Sazu, Ljubljana, 17, 125-184.
- Sirel, E., 1981, *Bolkarina*, new genus (Foraminiferida) and some associated species from the Thanetian limestone (Central Turkey): Eclogae Geol. Helv., 74/1, 75-95.

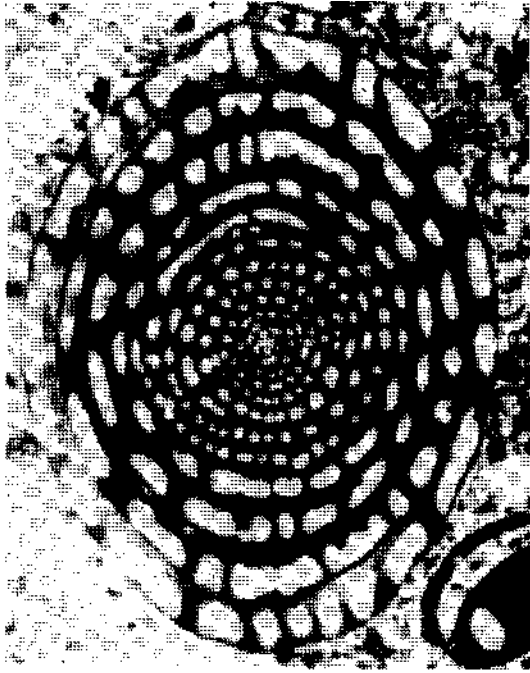
PLATES

PLATE - I

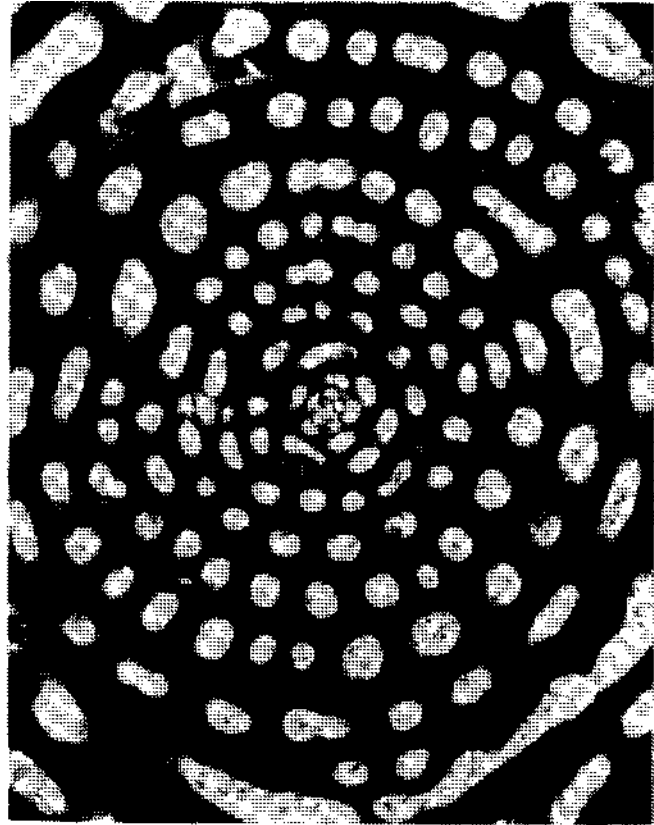
Pseudolacazina oeztemueri (Sirel) 1981

Form B

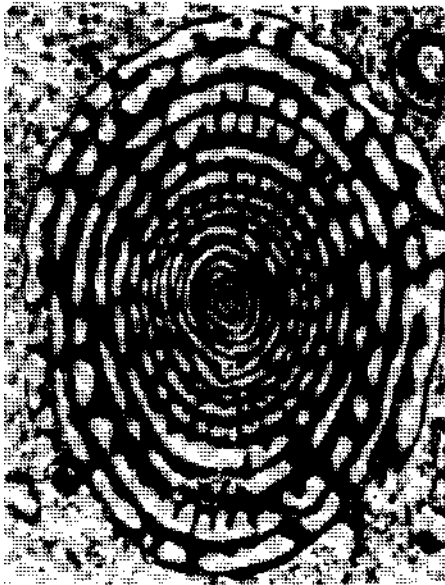
- Fig. 1 - Oblique section, slightly inclined to axial section, all the stages of the growth (86-10019), X 18.
- Fig. 2 - The quinqueloculine and the biloculine stages, magnification from figure 1, (86-10019), X 91.
- Fig. 3 - Oblique section, slightly inclined to axial section (it is figured in Sirel, 1981; Pl. 4, fig. 5 (86-10020), X 17.
- Fig. 4 - Axial section, microsphere and all growth stages (86-10021), X 18.
- Fig. 5 - Tangential section, showing continuous septula (figured in Sirel, 1981, Pl. 5, fig. 2) (86-10022), X 15.
- Fig. 6 - Axial section, showing microsphere, quinqueloculine, biloculine and monoloculine chambers, magnification from Fig. 4 (86-1002!), X 56.



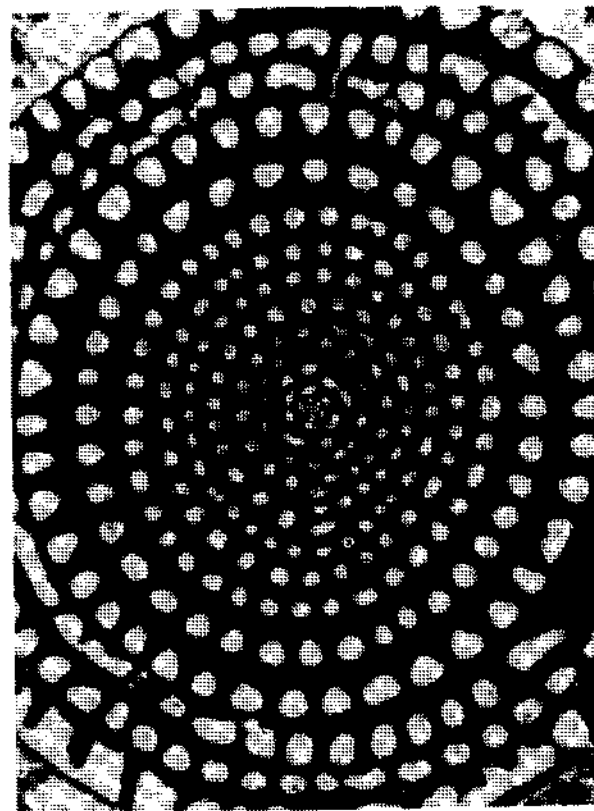
1



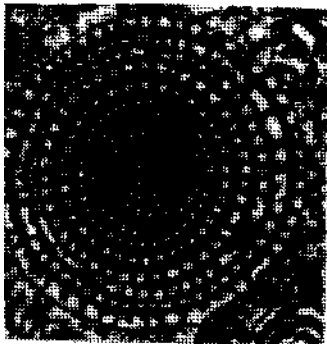
2



3



4



5

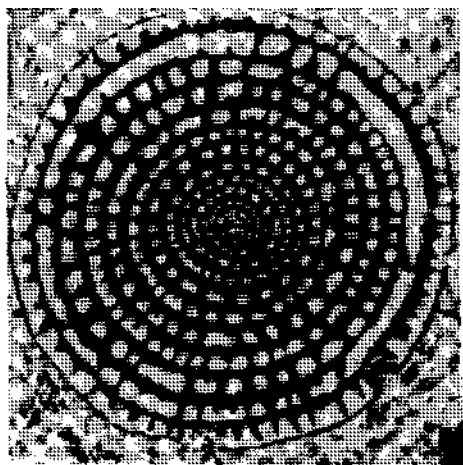


6

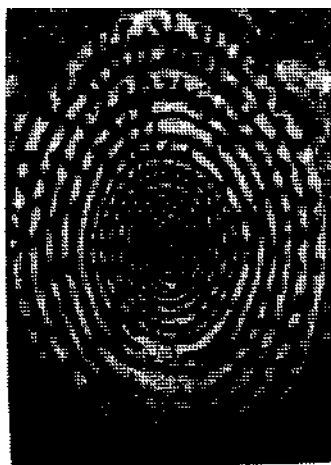
PLATE - II

Pseudolacazina oeztemueri (Sirel) 1981

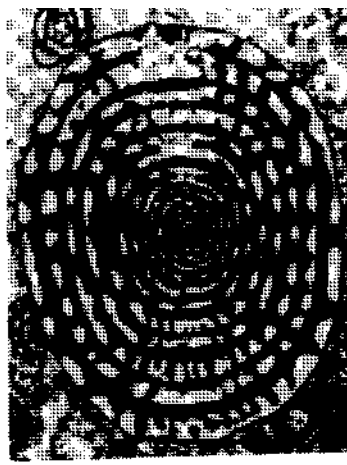
- Fig. 1 - Form B, axial section, all growth stages; figured in (Sirel) 1981, Pl. 4, fig. 6 (86-10023) X 18.
- Fig. 2 - Form B, oblique section, largest specimen, (86-10024), X 12.
- Fig. 3 - Form B, oblique section (86-10025), X 14.
- Fig. 4 - Form A, axial, equatorial and tangential sections (86-10026), X 22.
- Fig. 5 - Form A, equatorial section, showing 6 undivided chambers around the macrosphere and bicoline chambers (86-10027), X 34.
- Fig. 6 - Form B, equatorial section, trematophore with tooth (86-10028), X 18.
- Fig. 7 - Form B, oblique section (86-10029), X 17.
- Fig. 8 - Form A, axial section, figured in Sirel 1981 as *Fabulana donatae* Drobne, Pl. 5, fig. 7 (86-10030), X 23
- Fig. 9 - Form B, parallel section to the axial plane, passing close the trematophore; figured in Sirel 1981, Pl. 5, fig. 6 (86-10031), X 18.
- Fig. 10 - Form B, slightly oblique section to the equatorial section, figured in Sirel 1981, Pl. 5, fig. 4 (86-10032), X 19.



1



2



3



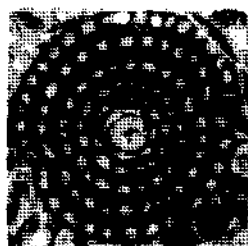
4



5



6



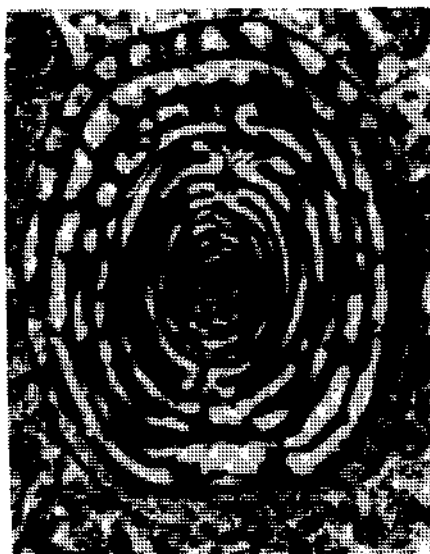
8



7



9



10

PLATE - III

Microfacies, Algal limestone with foraminiferal association (86-10033), X 6.

PB - *Pseudolacazina oeztemueri* (Sirel), form B.

PA - *Pseudolacazina oeztemueri* (Sirel), form A.

B - *Bolkarina aksarayi* Sirel, form B.

La₁ - *Laffitteina mengaudi* (Astre), form B.

La₂ - *L. mengaudi* (Astre), magnification from La₁. X 26.

I - *Idalina*

C - Corals

A - Algae

